

Final Report

Project:

Paleoseismic investigation of northern Germany

Paläoseismische Untersuchung Norddeutschlands

October 2016 - October 2018

28th November 2019

Report authors

Katharina Müller
Christian Brandes
Jutta Winsemann

Institut für Geologie
Leibniz Universität Hannover
Callinstraße 30
30167 Hannover

Federal Institute for Geosciences and Natural Resources (BGR)

Stilleweg 2
30655 Hannover

Contract 201-10079313

How to cite this report:

Müller, K., Brandes, C., Winsemann, J. (2019). Paleoseismic investigation of northern Germany – Final Report. *Gottfried Wilhelm Leibniz Universität Hannover*, p. 155.

List of contents

List of contents	3
List of figures	6
List of tables	10
Abstract	13
Zusammenfassung	15
1. Introduction	17
1.1. Background	17
1.2. Paleoseismic studies in northern Germany	17
1.3. Aim of the paleoseismic project in northern Germany	18
1.4. Project approach	18
2. Geological setting	21
2.1. Geological evolution of the study area	21
2.2. Recent stress field and glacial-isostatic adjustment (GIA)	25
2.3. Harz Boundary Fault	28
2.4. Osning Thrust	29
2.5. Halle Fault system	29
2.6. Aller Valley Fault	30
2.7. Gardelegen Fault	31
2.8. Steinhuder Meer Fault	31
2.9. Elbe Lineament	32
3. Deformation structures	33
3.1. Deformation processes	33
3.1.1. Neotectonic deformation processes	33
3.1.2. Glaciotectonic deformation processes	34
3.1.3. Cryoturbation deformation processes	34
3.2. Deformation mechanisms	34
3.2.1. Seepage	35
3.2.2. Liquefaction	35
3.2.3. Fluidization	36
3.3. Driving mechanisms for soft-sediment deformation structures	37
3.3.1. Depositional loading	37
3.3.2. Neotectonic activity	37

3.3.3. Ice loading and unloading	41
3.3.4. Freeze and thaw cycles	45
3.4. Summary.....	50
4. Methods	52
4.1. Selection of outcrops and fault systems	52
4.2. Fieldwork.....	53
4.2.1. Sedimentological analysis	53
4.2.2. Structural analysis.....	54
4.3. Luminescence dating	56
4.3.1. Sample collection and preparation	57
4.3.2. Dose rate determination.....	58
4.3.3. Luminescence dating	59
4.4. Further analyses	62
5. Seismic database and Environmental Seismic Intensity scale (ESI).....	62
5.1. Important catalogue of historic earthquakes	62
5.2. The ESI scale.....	62
5.3. The paleoseismic database of Germany and adjacent regions (PalSeisDB) ..	63
6. Results	65
6.1. Harz Boundary Fault	66
6.2. Osning Thrust	73
6.3. Halle Fault system.....	77
6.4. Aller Valley Fault	80
6.5. Gardelegen Fault	85
6.6. Steinhuder Meer Fault.....	86
6.7. Elbe Lineament	91
6.8. Summary of results	92
7. Discussion.....	95
7.1. Synthesis of the tectonic structures and the distribution of fault activity.....	95
7.2. The Soltau 1977 and Rotenburg 2004 earthquakes	96
7.3. Limitations of the sand and gravel pit analysis	97
7.4. Limitations of soft-sediment deformation structures for identifying paleo-earthquakes	98
7.5. Indicators for neotectonic movements	101

7.6. Characterization of deformation structures with the ESI scale and the PalSeisDB	102
7.7. Summary of evidence for movement at the basement faults	103
8. Conclusions.....	109
9. Outlook.....	110
Appendix	112
References.....	125

List of figures

Fig. 1: Geological evolution of northern Germany. (Drawing by C. Brandes according to Gast and Gundlach 2006; Kley and Voigt 2008; von Raumer et al. 2013).	22
Fig. 2: Geological setting. a) Overview of the sedimentary basins in the study area; BFB: Broad Fourteens Basin; LSB: Lower Saxony Basin; SB: Subercynian Basin; WNB: West Netherlands Basin, (modified according to Scheck-Wenderoth and Lamarch, 2005); b) northern Germany with the maximum extent of the Elsterian (green), Saalian (dark and light blue) and Weichselian (yellow) ice sheets (modified according to Ehlers et al., 2011); c) fault map of northern Germany, the faults analysed are shown in red (based on Kley and Voigt, 2008). The grey strip marks the area in which sand and gravel pits were investigated.....	23
Fig. 3: Chronostratigraphy of the Pleistocene in northern Central Europe. The blue arrows represent ice advances. Two different stratigraphic charts exist for NW Europe and Central Europe.	24
Fig. 4: Schematic sketch of the north Atlantic ridge push and the N-S-directed force caused by Alpine collision (modified according to Grünthal and Stromeyer, 1992). ..	26
Fig. 5: Conceptual model for stresses during a glaciation. Lithosphere deflection causes bending stress in the lithosphere. A glacial forebulge develops in front of the ice sheet due to the flexure of the lithosphere. The forebulge area is characterized by uplift and extension. The faults parallel to the ice margin have a high reactivation potential (modified according to Stewart et al., 2000).	27
Fig. 6: The position of the Late Pleistocene glacial forebulge (shaded area) (according to Kiden et al., 2002).	27
Fig. 7: A model for the gradual development of convolute bedding, ball-and-pillow structures, dish structures, pillar structures and sheet dewatering. Excess pore fluid pressure drives the escape of sediment and water upwards. Gravity assists the downward movement of larger intact blocks (modified according to Cheel and Rust, 1986; Collinson et al., 2006).	36
Fig. 8: Kinematic classification of deformation bands. T, thickness; D, displacement (from Fossen, 2010a)	40
Fig. 9: The principal types of deformation bands according to the deformation mechanism (from Fossen, 2010a).	40
Fig. 10: Classification of glacial deformation mechanisms due to ice sheet-related stress field variations (modified according to Feeser, 1988).	42
Fig. 11: Glaciotectonic complex. Subglacial deformation is highly variable in style and intensity and can result in normal faulting and the formation of horst and graben structures as well as heterogeneous folds, soft-sediment deformation structures and ductile shearing. Proglacial deformation leads to the formation of large-scale contractional structures such as folds, reverse and thrust faults. Cryoturbation features can occur in the periglacial environment (based on Aber and Ber, 2007; Müller et al., <i>in press c</i>).	43
Fig. 12: Deformation model showing the development of different deformation structures in a subglacial shear zone (modified according to Lee and Phillips, 2008).	44

Fig. 13: Examples of typical soft-sediment deformation structures in the study area. a) Pit 48, Groß Eilstorf. The remnants of two sand volcanoes in meltwater deposits that developed as a result of fluidization processes; b) pit 64, Scheuen. Glaciotectonic deformation structures in meltwater deposits. Large-scale thrust sheets as a result of proglacial compressional deformation; c) pit 44, Filterberg. Glaciotectonic deformation structures in meltwater sediments. Shear-deformation bands with normal and reverse displacement. The shear-deformation band with normal displacement is offset by a 45 younger shear-deformation band with reverse displacement; d) pit 72, Dolle. Glaciotectonic deformation structures in meltwater deposits. Shear-deformation band with normal displacement overlain by a till bed. The shear-deformation band developed subglacially due to ice loading; e) pit 80, Ferbitz. Glaciotectonic deformation structures in meltwater deposits. Overview image with large scale folds.....45

Fig. 14: Model of permafrost in a periglacial climate environment (modified according to Dobinski, 2011).46

Fig. 15: Different cryoturbation structures (modified according to Vandenberghe, 2013). Type 1 cryoturbation features are undulations or small folds with low amplitude (dm) and large wavelength (m). Type 2 cryoturbations include a series of closely spaced symmetrical (amplitude 0.5 and 2 m) intensively folded forms. The lower parts are sometimes flat. The size varies with the lithology and the thickness of the sediment. Type 3 is very similar to type 2 but smaller in size (cm - dm). Type 4 cryoturbation structures have symmetrical geometries (very similar to types 2 and 3) but with individual geometries and different amplitudes. Type 5 looks similar to type 2 but, unlike type 3, the lower sediment has risen along platy dykes. The upper sediment of type 5 has subsided sack-wise. Type 6 is classified as having structures of irregular shape and all dimensions.46

Fig. 16: Periglacial ice wedges and ice wedge casts in different sediments (modified according to Van Vliet-Lanoë et al., 2004).48

Fig. 17: Examples of typical cryoturbation structures. a) Pit 90, Bolsehle. Ice wedge cast in glaciolacustrine deposits; b) pit 45, Garßen. Ice wedge casts in the upper part of a 3.5-m-thick till bed; c) pit 54, Hülsenberg. Periglacial involutions in meltwater sand and silt.....49

Fig. 18: Formation of soft-sediment deformation structures by different mechanisms and drivers (modified according to Müller et al., *in press c*).51

Fig. 19: Schematic representation of the 20-km-wide study area along a major basement fault. The yellow dots represent sand and gravel pits (X marks the number of the pit) within this strip that are feasible for further analyses. Increasing distance from the major basement fault decreases the likelihood of earthquake indicators expected in this intraplate setting.52

Fig. 20: Flow chart of the different working steps for finding evidence of neotectonic movements, especially paleo-earthquakes along major basement faults. The steps not connected with arrows (shear wave seismic profiles, electrical resistivity tomography profiles and trenching) were not part of the project, but constitute key methods for further analysis.....54

Fig. 21: Example of a stereographic projection of a plane that dips 80° SE (modified according to Möbus, 1989).55

Fig. 22: Accumulation of the luminescence signal through time (modified according to Aitken, 1998).57

Fig. 23: The Environmental Seismic Intensity scale (ESI 2007) is a seismic scale used for measuring the intensity of earthquakes on the basis of their effects on the natural environment (from Michetti et al., 2007).64

Fig. 24: Map of the seven major fault zones in northern Germany with the location of sand and gravel pits analyzed. Only the sand and gravel pits are shown in which deformation structures are exposed in this figure. Fault traces are taken from Baldschuhn and Kockel (1987, 1996), Martiklos et al. (2001), Lohr et al. (2007), Kley and Voigt (2008). Red marks the section of the fault analyzed (see also Fig. 2c)65

Fig. 25: Geological map of the study area with geological cross-section (modified according to Schröder et al. 1927; from Müller et al., *in press a*).....67

Fig. 26: Fault zone exposed in a sinkhole near Benzingerode (outcrop 5) showing a two-fault evolution with normal and reverse components. The fault follows the trend of the Harz Boundary Fault. This indicates a close relation between the Harz Boundary Fault and the fault in the sinkhole. The stereoplot shows the data from the outcrop in the sinkhole (fault traces according to Martiklos et al. 2001).69

Fig. 27: Faulted debris-flow deposits exposed in a sinkhole near Benzingerode. a) Fault plane in Lateglacial debris-flow deposits and location of OSL and IRSL samples; b) stereographic projections of the normal fault component; c) stereographic projections showing normal and reverse fault kinematic components (modified according to Müller et al., *in press a*).....70

Fig. 28: Osning Thrust. Shear-deformation bands with normal displacement in pit 19 near Augustdorf with stereographic projection of the deformation band orientation (fault traces according to Baldschuhn and Kockel 1999).74

Fig. 29: Osning Thrust. a) Pit 19, Augustdorf. Shear-deformation bands in alluvial-fan and aeolian deposits; b) interpretation of image a) and related stereographic projection of the band orientation, trowel for scale; c) pit 22, Oerlinghausen. Low-angle deformation band with reverse displacement and anticline in the hanging wall developed in mixed alluvial-aeolian deposits; d) interpretation of image c).....76

Fig. 30: Halle Fault system. Shear-deformation bands with normal displacement in meltwater sand in pit 25 near Könnern with stereographic projections of the deformation band orientation. The orientation of the shear-deformation bands is similar to the minor fault near Könnern and the Halle Fault (fault trace according to Martiklos et al. 2001).78

Fig. 31: Shear-deformation bands in meltwater deposits in pit 25 near Könnern. a) Shear-deformation band and interpreted trace together with stereographic projections of the deformation band orientation (n=14); b) shear-deformation band with normal displacement (n=6); c) conjugate shear-deformation bands with interpreted trace and stereographic projections (n=9).80

Fig. 32: Aller Fault zone. Shear-deformation bands with normal displacement in meltwater sand in pit 42 near Eitze with stereographic projection of the deformation band orientation. Small map based on Lohr et al. (2007); fault traces modified according to Baldschuhn and Kockel (1996).82

Fig. 33: Deformation structures in Middle Pleistocene Saalian meltwater deposits near Eitze. a) Overview image of the pit near Eitze. The deformation bands penetrate the entire succession. A stereographic projection shows the orientation of the deformation bands (n= 3); b) close-up view of a cemented deformation band in the lower part of the

succession; c) close-up view of two deformation bands with stereographic projection of the orientation of the deformation bands in the lower part of the succession (n=2 and n=3); d) close-up view of a 0.5-cm-thick deformation band with the related stereographic projection of the band orientation (n=5); e) close-up view of deformation bands in the upper part of the succession; f) stereographic projection showing the orientation of all deformation bands (n=13).83

Fig. 34: Schematic model of a pull-apart basin.84

Fig. 35: Steinhuder Meer Fault. Shear-deformation bands with normal displacement in pit 89 near Altenhagen with stereographic projection of the deformation band orientation (fault traces after Baldschuhn and Kockel, 1987).87

Fig. 36: Sand pit near Altenhagen with stereographic projections of the deformation band and fault orientation. The dotted line shows the orientation of the Steinhuder Meer Fault.88

Fig. 37: Growth strata. a) Schematic model of growth strata (modified according to Williams et al. 1989); b) growth strata in the Altenhagen pit. Growth strata are sediment packages with thickness-variations caused by fault movement.89

Fig. 38: Major basement faults revealing neotectonic activity. The major basement faults analyzed are shown in red. (Faults are based on Kley and Voigt 2008).93

Fig. 39: Tectonic activity in northern Germany. The cross-section shows Lateglacial neotectonic activity, historic earthquake activity and recent (instrumental) earthquake activity at several fault systems in northern Germany (based on Brandes et al. 2019; Leydecker 2011; Müller et al. *in press a*). Unlike the other faults, the Elbe Lineament and the Thor Suture are terrane boundaries. The dashed line represents the uncertain location of the Thor Suture. Cross-section modified according to Kley et al. (2008), (Müller et al., *in press b*).....95

Fig 40: Schematic model of the formation and distribution of deformation bands in the process zone of a reverse fault (modified according to Ballas et al., 2015)..... 101

Fig. 41: Tectonic activity along seven major basement faults in northern Germany analyzed in this study. The figure shows neotectonic activity, historic earthquakes and recent earthquakes (modified according to Brandes et al., 2015, Müller et al., *in press b*). The red arrows show the recent stress field in northern Germany. The numbers represent the year of each earthquake listed in Table 15. The faults analyzed in this study are shown in bold; the Elbe Lineament is shown as dashed line because it represents a terrane boundary; LGM: Last Glacial Maximum; the shaded area represents the ice sheet expansion during the Weichselian LGM..... 106

List of tables

Table 1: SAR protocol used for equivalent dose determination of feldspar and quartz samples taken at the Harz Boundary Fault. (a) 100 ms on and 400 ms off.	60
Table 2: SAR protocol used for equivalent dose determination of feldspar samples taken at the Steinhuder Meer Fault. (a) 100 ms on and 400 ms off.	61
Table 3: Sand and gravel pits with deformation structures and the uncertainty of the interpretation at the Harz Boundary Fault.* Note that the ages of outcrop 5 show luminescence ages of the latest fault movement.	66
Table 4: Dosimetry results and dose rates for the samples from Benzingerode (outcrop 5). An a-value of 0.09 ± 0.02 was used for the feldspar samples and an a-value of 0.04 ± 0.01 for the quartz samples.	72
Table 5: Quartz and feldspar luminescence ages from Benzingerode (outcrop 5). ...	73
Table 6: Sand pits with deformation structures and the uncertainty of the interpretation at the Osning Thrust. Luminescence ages are derived from Roskosch et al. (2012). (X) means that the observation cannot unambiguously be defined as a cryoturbation feature. Note that the ages are the ages of the faulted deposits and thus imply the time of fault movement.	74
Table 7: Sand and gravel pits with deformation structures and the uncertainty of the interpretation at the Halle Fault system.	77
Table 8: Sand pits with deformation structures and the uncertainty of the interpretation at the Aller Valley Fault.	81
Table 9: Sand pits with deformation structures and the uncertainty of the interpretation at the Gardelegen Fault.	85
Table 10: Sand pits with deformation structures and the uncertainty of the interpretation at the Steinhuder Meer Fault.* Note that the ages of pit 89 show luminescence ages at the time of fault movement.	86
Table 11: Dosimetry results and dose rates for the samples from Altenhagen (pit 89). An a-value of 0.09 ± 0.02 was used for the feldspar samples.	90
Table 12: Feldspar luminescence ages from Altenhagen (pit 89).	91
Table 13: Sand pits with deformation structures and the uncertainty of the interpretation at the Elbe Lineament.	91
Table 14: Major basement faults in northern Germany where this study found evidence of neotectonic movements. The numbers represent the pit numbers shown in Fig. 24.	94
Table 15: Tectonic activity along seven major basements faults in northern Germany analyzed in this study. Neotectonic activity, paleo-earthquakes, historic earthquakes and recent earthquakes with the timing of each tectonic event are listed. The selected historic earthquakes are located up to 20 km away from the fault. The Wittenburg and Soltau events are more than 20 km away from a fault but are listed because of their high magnitude and the resulting importance for the hazard assessment. The Rotenburg 2004 event has yet to be unequivocally classified as natural or triggered. The numbers (X*) are related to the study of Brandes et al. (2019) and have been adopted for a better assignment. However, the 2014 and 2018 earthquakes near	

Walsrode and Rethem were most likely too deep to be related to the Aller Valley Fault. Some of the historic earthquakes are assigned to different major faults because the accuracy of the epicenter is low. * M_w was calculated using the equation $M_w = 0.682 \log_{10} + 0.16$ according to Grünthal et al. (2009). 107

Table A1: All sand and gravel pits and sinkholes along the Harz Boundary Fault in the Subhercynian Basin. 112

Table A2: All sand pits along the Osning Thrust. 113

Table A3: All sand and gravel pits along the Halle Fault system..... 114

Table A4: All sand pits along the Aller Valley Fault..... 115

Table A5: All sand and gravel pits along the Gardelegen Fault. 118

Table A6: All sand pits along the Elbe Lineament..... 119

Table A7: All sand and gravel pits along the Steinhuder Meer Fault. 120

Table A8: PalSeisDB. Fault in a sinkhole near Benzingerode (outcrop 5) (Harz Boundary Fault)..... 121

Table A9: PalSeisDB. Deformation bands near Könnern (pit 25) (Halle Fault system). 122

Table A10: PalSeisDB. Deformation bands near Eitze (pit 42) (Aller Valley Fault). 123

Table A11: PalSeisDB. Deformation bands near Altenhagen (pit 89) (Steinhuder Meer Fault)..... 124

This project includes the following scientific contributions:

Publications:

Müller, K., Polom, U., Winsemann, J., Steffen, H., Tsukamoto, S., Günther, T., Igel, J., Spies, T., Lege, T., Frechen, M., Franzke, H.-J., Brandes, C. (in press a). Structural style and neotectonic activity along the Harz Boundary Fault, northern Germany: A multimethod approach integrating geophysics, outcrop data and numerical simulations. *International Journal of Earth Sciences*.

Müller, K., Winsemann, J., Pisarska-Jamroży, M., Lege, T., Spies T., Brandes, C. (in press b). The challenge to distinguish soft-sediment deformation structures (SSDS) formed by glaciotectonic, periglacial and seismic processes in a formerly glaciated area: a review and synthesis. *In: Steffen, H., Olesen, O., Sutinen, R. (Eds.), Glacially-Triggered Faulting. Cambridge University Press.*

Müller, K., Winsemann, J., Tanner, D.C., Lege, T., Spies T., Brandes, C. (in press c). Glacially-Induced Faults in Germany. *In: Steffen, H., Olesen, O., Sutinen, R. (Eds.), Glacially-Triggered Faulting. Cambridge University Press.*

Conference abstracts:

Müller, K., Brandes, C., Polom, U., Tsukamoto, S., Spies, T., Lege, T., Frechen, M., Winsemann, J. (2017). Paleoseismological analysis of the Harz Boundary Fault, northern Germany. *5th International Colloquium Historic Earthquakes, Paleoseismology, Neotectonics and Seismic Hazard, Hanover, Germany.*

Müller, K., Brandes, C., Polom, U., Tsukamoto, S., Spies, T., Lege, T., Frechen, M., Winsemann, J. (2018). Neotectonic analysis of the Harz Boundary Fault (northern Germany). *EGU General Assembly, Vienna, Austria.*

Müller, K., Polom, U., Winsemann, J., Tsukamoto, S., Steffen, H., Spies, T., Lege, T., Frechen, M., Franzke, H.-J., Brandes, C. (2018). Active faults and paleoseismicity in northern Germany induced by glacial isostatic adjustment: An example from the Harz Boundary Fault zone. *Symposium on Postglacial faults, Kautokeino, Norway.*

Müller, K., Winsemann, J., Polom, U., Igel, J., Tsukamoto, S., Steffen, H., Spies, T., Lege, T., Frechen, M., Brandes, C. (2019). Paleoseismological investigation of northern Germany. *EGU General Assembly, Vienna, Austria.*

Müller, K., Winsemann, J., Polom, U., Frechen, M., Tsukamoto, S., Igel, J., Spies, T., Lege, T., Steffen, H., Brandes, C. (2019). Lateglacial reactivation of the Harz Boundary Fault (northern Germany) caused by glacial isostatic adjustment. *INQUA, Dublin, Ireland.*

Müller, K., Winsemann, J., Polom, U., Steffen, H., Tsukamoto, S., Günther, T., Igel, J., Spies, T., Frechen, M., Brandes, C. (2019). Neotectonics and paleoseismicity - The reactivation potential of faults in northern Germany due to glacial isostatic adjustment. *BGE - Tage der Standortauswahl, Braunschweig, Germany.*

Abstract

Northern Germany is an intraplate region and has long been regarded as a low seismicity area. However, historic sources show that several significant natural earthquakes have occurred in northern Germany since the 10th century. In recent years natural earthquakes and earthquakes in the vicinity of active gas fields likely to have been associated with the recovery of hydrocarbons have been repeatedly instrumentally recorded in northern Germany. The assessment of the hazardous seismic activity in northern Germany is highly relevant to finding a location for the storage of nuclear waste, future hydrocarbon production and geothermal projects. Paleoseismic investigation, which provides knowledge of seismic events further into the past, is therefore necessary in order to better estimate the return period of earthquakes and their hazard.

Seven WNW-ESE trending major basement faults with a high potential for reactivation due to glacial-isostatic adjustment were analyzed with regard to paleo-fault activity. Deformation bands and seismites in Pleistocene sand and gravel pits are indicators for paleo-fault activity.

Northern Germany was repeatedly affected by glaciations and periglacial processes during the Pleistocene. The main difficulty is to distinguish the vast glaciotectionic deformation structures that are present in northern Germany from neotectonic features. Processes like cryoturbation, depositional loading in water saturated sediments and rapid rates of deposition can generate soft-sediment deformation structures (SSDS) that may also be mistaken for earthquake-induced structures. The analysis of neotectonic activity in northern Germany is challenging because recently observed vertical crustal movements along NW-SE-striking faults do not often correspond to visible morphological features and fault scarps are rapidly destroyed by climatic conditions.

Evidence for neotectonic movements, indicated by the occurrence of shear-deformation bands in Middle to Late Pleistocene sediments, was identified along five of the seven major basement faults that were analyzed in northern Germany during this study. There is evidence for neotectonic fault activity that took place between the Middle Pleistocene Saalian and the beginning of historic times. Evidence was found at the Aller Valley Fault, the Halle Fault system, the Harz Boundary Fault, the Steinhuder

Meer Fault and the Osning Thrust. Brandes and Winsemann, (2013) already identified deformation structures at the Osning Thrust that could be ascribed to a paleo-earthquake. Luminescence dating of mixed alluvial-aeolian sediments at the Osning Thrust (15.9 ± 1.6 ka to 13.1 ± 1.5 ka) revealed the fault activity took place in the Lateglacial between 16-13 ka as suggested by Brandes et al. (2012). It was possible to estimate the timing of the neotectonic activity of the faulted Pleistocene sediments by means of luminescence dating at two basement faults (Harz Boundary Fault, Steinhuder Meer Fault). The estimated ages of faulted debris-flow deposits at the Harz Boundary Fault (14.2 ± 0.8 ka and 15.2 ± 0.8 ka) point to fault movements after ~15 ka corresponding to the reactivation of the Osning Thrust. The estimated age of growth strata at the Steinhuder Meer Fault (158 ± 4 ka and 189 ± 5 ka) indicate fault movements in Middle Pleistocene Saalian times. The results of this two-year project do not exclude neotectonic movements and paleo-earthquakes at faults where no geological evidence like SSDS or deformation bands was found in the sand and gravel pits studied.

Zusammenfassung

Norddeutschland ist eine Intra-Plattenregion und galt lange Zeit als Gebiet mit geringer Seismizität. Historische Quellen zeigen, dass in Norddeutschland seit dem 10. Jahrhundert mehrere bedeutende natürliche Erdbeben stattgefunden haben. Auch instrumentell wurden in Norddeutschland in den letzten Jahrzehnten Erdbeben registriert. Zudem treten Erdbeben in der Nähe von Erdgasfeldern auf, die mit der Gewinnung von Kohlenwasserstoffen in Verbindung gebracht werden. Die Ermittlung der seismischen Gefährdung Norddeutschlands ist relevant für die Suche nach Standorten für die Entsorgung radioaktiver Abfälle. Außerdem ist sie relevant für andere Nutzungen des tieferen Untergrundes, wie Förderung von Erdgas und Erdöl sowie tiefe Geothermie. Daher sind paläoseismische Untersuchungen notwendig, um das Wissen über seismische Ereignisse weiter in die Vergangenheit auszudehnen und so die Wiederholungsrate von Erdbeben und damit die seismische Gefährdung besser abschätzen zu können.

Sieben WNW-ESE orientierte Hauptstörungszonen, die aufgrund der isostatischen Ausgleichsbewegung Skandinaviens ein hohes Reaktivierungspotenzial aufweisen, wurden auf neotektonische Störungsaktivität untersucht. Indikatoren für neotektonische Aktivität sind Deformationsbänder und Seismite in pleistozänen Sedimenten, die in Sand- und Kiesgruben aufgeschlossen sind.

Während des Pleistozäns war Norddeutschland von Vergletscherungen und periglazialen Bedingungen betroffen. Die Hauptschwierigkeit besteht darin, die in Norddeutschland vorhandenen glazitektonischen Verformungsstrukturen von neotektonischen Strukturen zu unterscheiden. Darüber hinaus können Prozesse wie Kryoturbation und Auflast wassergesättigter Sedimente Deformationsstrukturen in unverfestigten Sedimenten (SSDS) erzeugen, die mit Strukturen verwechselt werden können, die durch seismische Wellen entstehen. Zudem ist die Analyse neotektonischer Aktivität in Norddeutschland schwierig, da die beobachteten vertikalen Krustalbewegungen entlang der NW-SE verlaufenden Störungen meist nicht sichtbare morphologische Merkmale zeigen und Bruchstufen aufgrund der klimatischen Bedingungen schnell zerstört werden.

In diesem Projekt konnten Hinweise auf neotektonische Bewegungen in mittel- bis spätpleistozänen Sedimenten identifiziert werden, die entlang von fünf, der

untersuchten sieben Hauptstörungszonen in Norddeutschland aufgeschlossen waren. Diese Deformationsstrukturen wurden in Sandgruben entlang der Allertal-Störung, des Halle-Störungssystems, der Harznordrand-Störung, der Steinhuder Meer-Störung und der Osning-Störung gefunden. Neotektonische Störungsaktivität lässt sich seit dem Mittelpleistozän (saalezeitlich) nachweisen und fand bis in historische Zeiten statt. An der Osning-Störung konnten die in einer Studie von Brandes und Winsemann, (2013) bereits identifizierte Strukturen mit einem Paläo-Erdbeben verknüpft werden. Durch Lumineszenzdatierung von gemischten alluvial-äolischen Sedimenten an der Osning-Störung ($15,9 \pm 1,6$ ka bis $13,1 \pm 1,5$ ka) konnte die Störungsaktivität auf 16 - 13 ka datiert werden. Bei zwei weiteren großen Störungssystemen (Harznordrand-Störung, Steinhuder Meer-Störung) konnte der Zeitraum der neotektonischen Bewegungen mittels Lumineszenzdatierung ermittelt werden. Das ermittelte Alter von versetzten Schuttstromablagerungen an der Harznordrand-Störung ($14,2 \pm 0,8$ ka und $15,2 \pm 0,8$ ka) zeigt Störungsbewegungen nach ~ 15 ka an und stimmt damit zeitlich mit dem Alter der Reaktivierung der Osning-Störung überein. Das ermittelte Alter von syntektonisch abgelagerten Sedimenten an der Steinhuder Meer-Störung (158 ± 4 ka und 189 ± 5 ka) deutet auf eine pleistozäne saalezeitliche Störungsaktivität hin. Die Ergebnisse dieses zweijährigen Projekts schließen neotektonische Störungsaktivität und Paläo-Erdbeben an Störungen nicht aus, an denen in den untersuchten Sand und Kiesgruben keine geologischen Hinweise, wie zum Beispiel SSDS oder Deformationsbänder gefunden wurden.

1. Introduction

1.1. Background

Northern Germany is commonly regarded as a low seismicity area far from active plate boundaries (e.g. Leydecker and Kopera, 1999). But a number of historic earthquakes with intensities of up to VII have occurred in this region during the last 1200 years (Leydecker, 2011). Continuing seismic activity has also been instrumentally detected over the last 50 years. Many of the epicentres of the recent earthquakes are clustered around the vicinity of active gas fields and have been interpreted as a consequence of hydrocarbon recovery (Dahm et al., 2007, 2015). Earthquakes without an anthropogenic trigger have also been recorded, such as the more recent Wittenburg event in 2000 with a magnitude of M_L 3.2, the Rostock earthquake of 2001 with a magnitude of M_L 3.4 and two earthquakes in the Halle/Leipzig area in 2015 and 2017 with magnitudes of M_w 3.2 and M_w 2.8 respectively (Leydecker, 2011; Dahm et al., 2018). Between 2000 and 2018 seven deep earthquakes with hypocentre depths of 17.0 – 31.4 km were registered in northern Germany with magnitudes of M_L 1.7 – 3.1 (Brandes et al., 2019). Stress build up in northern Germany is driven by collisional forces from the Alpine orogeny and the Atlantic ridge push (Marotta et al., 2004; Kaiser et al., 2005). Possible trigger mechanisms for the natural earthquakes are lithospheric stress changes due to glacial-isostatic adjustment (Brandes et al., 2015).

Recent work has shown that northern Germany is a seismically active intraplate region. Long intervals and spatial and temporal distribution between individual earthquakes are typical for earthquakes in intraplate areas (Gangopadhyay and Talwani, 2003). Seismic activity concentrates at one fault for a certain time and then shifts to the next fault (McKenna et al., 2007). Intraplate earthquakes can be characterized as episodic, clustered and migrating.

1.2. Paleoseismic studies in northern Germany

A number of paleoseismic studies have been carried out in northern Germany. However, these studies have frequently focused on a single fault or been restricted to a certain region. Evidence for paleo-earthquakes is provided in Brandes et al. (2012)

and Brandes and Winsemann (2013) for the Osning Thrust. Soft-sediment deformation structures and deformation bands in mixed alluvial-aeolian Late Pleistocene sediments indicate young tectonic activity in this location. Ludwig (2011), Hoffmann and Reicherter (2012) and Pisarska-Jamroży et al. (2018) found evidence for seismic activity in Middle to Late Pleistocene sediments along the southwestern coast of the Baltic Sea. Further studies of Hübscher et al. (2004), Brandes and Tanner (2012), Brandes et al. (2011, 2013), Brandes et al. (2018a) and Grube (2019a, b) also indicate higher neotectonic activity in northern Germany than previously thought. There is consequently a demand for a systematic study of paleoseismic activity in northern Germany.

1.3. Aim of the paleoseismic project in northern Germany

The aim of *Project 201-10079313 "Paläoseismische Untersuchung Norddeutschlands"* is to analyze the main fault zones in northern Germany in order to find indications of paleo-earthquakes or at least neotectonic fault activity and thus to extend the historic earthquake catalogue into the geological past. The results are important for the assessment of the seismic hazards in northern Germany and are relevant for finding a suitable repository for deep nuclear waste, future hydrocarbon recovery and geothermal projects. They are also transferable to geologically similar, seismically active intraplate regions worldwide, e.g. in North America, Scandinavia and Russia.

The results of this study have been presented at several scientific conferences (5th International Colloquium Historic Earthquakes, Paleoseismology, Neotectonics and Seismic Hazard; 2017 in Germany, PGF Symposium, 2018 in Norway, the EGU General Assembly 2018, 2019 in Vienna, the INQUA 2019 in Ireland and at the BGE – Tage der Standortauswahl in Germany) and will be published in relevant scientific journals.

1.4. Project approach

The first project phase analyzed outcrops in unconsolidated Middle to Late Pleistocene sediments along seven major fault zones (Elbe Lineament, Aller Valley Fault, Osning

Thrust, Steinhuder Meer Fault, Harz Boundary Fault, Halle Fault system and Gardelegen Fault). These fault zones were chosen for several reasons:

- 1) Brandes et al. (2012) have already identified evidence for paleoseismic activity at the eastern section of the Osning Thrust.
- 2) A paleoseismic study relies on soft-sediment deformation structures produced by the passage of seismic waves. In general, such structures are produced by earthquakes with magnitudes greater than 5 (e.g. Atkinson et al., 1984; Rodríguez-Pascua et al., 2000). Only large faults with a rupture length of 10 km can produce earthquakes of magnitude 6 (cf. Wells and Coppersmith, 1994). In northern Germany, potential faults of this size are the Harz Boundary Fault, the Aller Valley Fault and the Elbe Lineament. The Gardelegen Fault was chosen because several historic earthquakes occurred in this area. The Steinhuder Meer Fault was analyzed, because near-surface faults in young sediments have been described at a location close by (personal com. H. J. Brink, 2013). The sediments exposed in the area of the Steinhuder Meer Fault date from the Middle Pleistocene Saalian (Jordan et al., 1979; Voss et al., 1979; Jordan et al., 1980; Voss et al., 1982).

Natural outcrops of Pleistocene and Holocene sediments are rare in northern Germany. A systematic problem in northern Germany is that young (Holocene) sediments are difficult to access. Commonly they are economically unimportant and not exploited. We therefore analyzed Pleistocene sediments in sand and gravel pits located in the vicinity of the major basement faults. This is more efficient than trenching (the standard way to carry out paleoseismic studies), and the high density of pits in northern Germany offers reasonable coverage of the major fault zones. The present report can therefore be viewed as a reconnaissance study, the results of which may provide the basis for future detailed trench studies and geophysical investigations.

The current stress field in northern Germany is roughly N-S oriented and the seven faults are favourably oriented to be reactivated by it. Sand and gravel pits along the faults were firstly identified using geological maps and aerial photos (GoogleEarth). Sedimentological and structural analyses of the exposed sediments were carried out and documented. Samples were taken in the outcrops to determine the age (luminescence dating) of the faulted sediments. The data obtained in the field were analyzed in the second phase of the project. Photo panels and sedimentological

profiles made during the fieldwork allow the depositional environment to be reconstructed, which is necessary in order to interpret the deformation structures. The orientations of the tectonic structural elements, exposed in the sand and gravel pits, are shown as stereographic projections. The analysis of the deformation mechanism and the classification of the stress regime were carried out based on these structural data sets. The sediment and deformation history was then determined and indications of paleo-earthquakes and neotectonic movements were derived based on the sedimentological and tectonic structures. The age of the samples was estimated with luminescence dating to determine the age of the tectonic deformation during this phase. The results were finally interpreted taking into account that northern Germany was repeatedly affected by glaciations and related periglacial processes during the Middle and Late Pleistocene.

This final report comprises a description of the geological background of the study area including the structural style and geological history of the seven major fault zones in northern Germany. A detailed chapter covering the scientific background on deformation structures (glaciotectonic deformation structures, neotectonic deformation structures, earthquake-induced structures and cryoturbation features) is followed by a chapter describing the workflow and the methods. The results for each of the major fault zones are summarised focusing on the deformation structures that were found in the sand and gravel pits. All these results have previously been presented in six interim project reports (Müller et al, 2016, 2017a, b; 2018a, b, c). The limitations of the methods available for identifying paleo-earthquakes and possible indicators for neotectonic movements and paleo-earthquakes are discussed. Evidence for paleoseismicity has been included in data sheets of the paleoseismic database of Germany (PalSeisDB v.1.0) based on Hürtgen (2017). The neotectonic deformation structures observed during this study have been combined with tectonic maps and the historic earthquake catalogue (Leydecker, 2011).

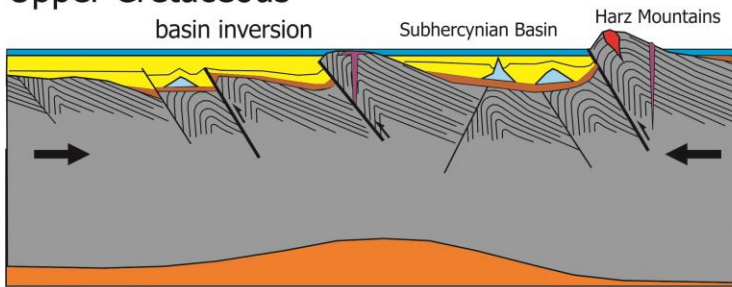
2. Geological setting

2.1. Geological evolution of the study area

Northern Germany forms part of the Central European Basin System (CEBS). The geological evolution of northern Germany is briefly visualized in Fig. 1. After the Rhenohercynian Ocean was closed and the Variscan orogeny formed, the CEBS (Fig. 2a) evolved out of a carboniferous Variscan foreland basin (Betz et al., 1987). During the Permian, after the peripheral foreland basin had filled, a rift system developed in northern Germany (e.g. Gast and Gundlach, 2006). Major structural elements included north-south trending normal faults. Subsidence in this area during the Mesozoic (e.g. Van Wees et al., 2000) was followed by a distinct tectonic inversion phase in the Late Cretaceous to Early Paleocene (e.g. Mazur et al., 2005). This inversion phase has been discussed in detail in Baldschuhn et al. (1991) and Kley and Voigt (2008). Many extensional structures, such as normal fault arrays and graben systems, were transformed into compressional features during this phase (Kockel, 2003).

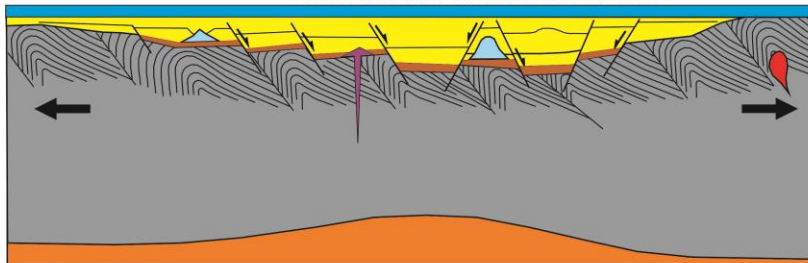
Today, the Central European Basin System consists of several subbasins, such as the Lower Saxony Basin, the Subhercynian Basin and the Northeast German Basin (Fig. 2a). As a consequence of different tectonic phases, northern Germany is characterized by a dense fault array with several major faults (oriented NW-SE) and fault zones with minor faults oriented NE-SW or NNE-SSW (Reicherter et al., 2005; Fig. 2b, c).

Upper Cretaceous



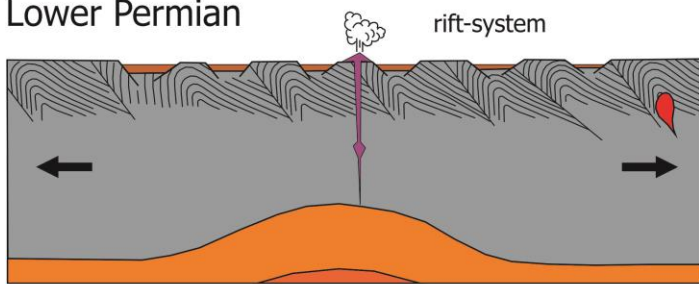
During the Late Cretaceous, a tectonic inversion phase cause the uplift of the Harz Mountains and the deformation of parts of the basin-fill. Pre-existing faults were reactivated and several new faults formed.

Upper Permian-Triassic-Jurassic-Lower Cretaceous



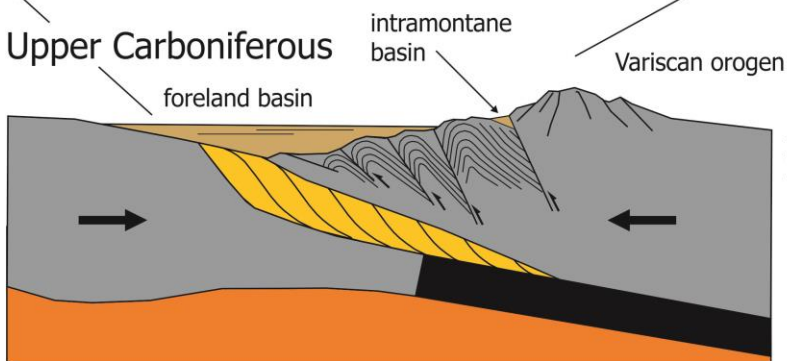
During the Late Permian to Early Cretaceous the basin was under subsidence (repeated pulses of extension and thermal subsidence).

Lower Permian



The Variscan orogen was eroded, subsequently lithosphere extension caused the formation of a new sedimentary basin (Southern Permian Basin). This extension was accompanied by volcanic processes. Important faults were created.

Upper Carboniferous



After the Rhenohercynian Ocean was subducted, the Saxothuringian terrane collided and the Variscan orogen formed.

Lower Carboniferous

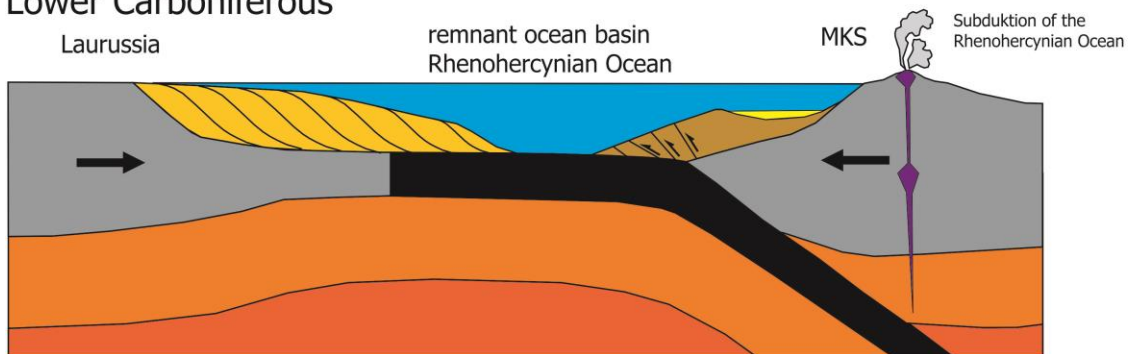


Fig. 1: Geological evolution of northern Germany. (Drawing by C. Brandes according to Gast and Gundlach 2006; Kley and Voigt 2008; von Raumer et al. 2013).

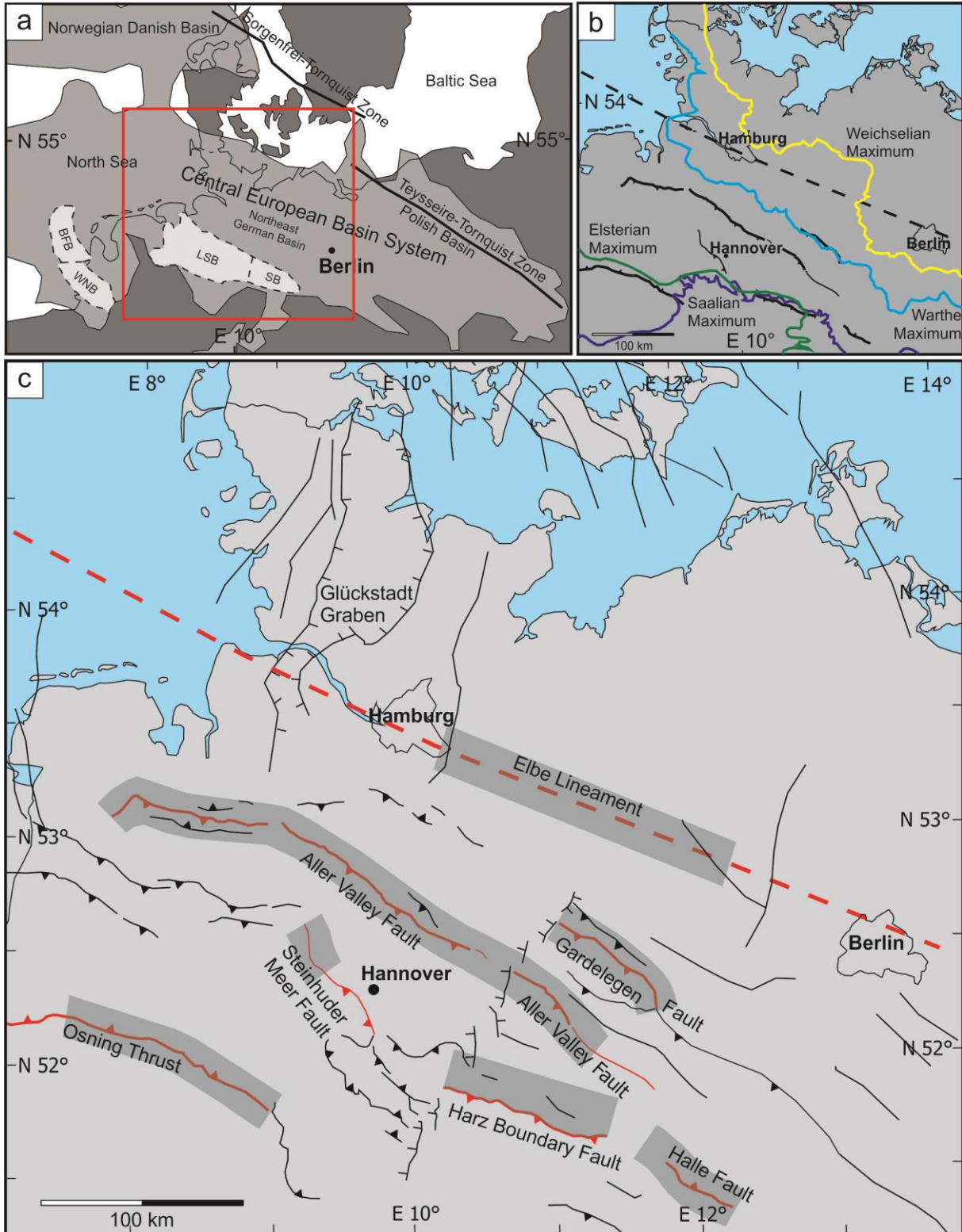


Fig. 2: Geological setting. a) Overview of the sedimentary basins in the study area; BFB: Broad Fourteens Basin; LSB: Lower Saxony Basin; SB: Subercynian Basin; WNB: West Netherlands Basin, (modified according to Scheck-Wenderoth and Lamarch, 2005); b) northern Germany with the maximum extent of the Elsterian (green), Saalian (dark and light blue) and Weichselian (yellow) ice sheets (modified according to Ehlers et al., 2011); c) fault map of northern Germany, the faults analysed are shown in red (based on Kley and Voigt, 2008). The grey strip marks the area in which sand and gravel pits were investigated.

During the Pleistocene, the study area was influenced by three major glaciations referred to as the Elsterian, Saalian and Weichselian glaciations (Ehlers et al., 2011; Fig. 2b) and therefore affected by glacial loading and unloading stresses. Repeated ice advances led to the deformation of near-surface sediments and sedimentary rocks in many areas of northern and central Europe (Aber and Ber, 2007). Three ice advances during the Elsterian glaciation have been recorded in the study area (Knoth, 1995; Eissmann, 2002; Ehlers et al., 2011). These ice sheets advanced from northerly and northeasterly directions (Eissmann, 2002) and can probably be correlated with marine isotope stages MIS 12 and MIS 10 (Fig. 3; Lang et al., 2012; Roskosch et al., 2015).

MIS stages represent oscillating warm and cold periods in the Earth's paleoclimate, which are based on marine oxygen isotope data reflecting temperature changes in the ocean (e.g. Wright, 2001). The data are often derived from the $\delta^{18}\text{O}/^{16}\text{O}$ ratio of ice cores and benthic foraminifera. Even numbers represent high ^{18}O values and are typical for cold climates and odd numbers represent low ^{18}O values and are typical for warm periods (e.g. Wright, 2001).

Marine isotopic stages	Northwest Europe (Cohen & Gibbard, 2016; Huijzer & Vandenberghe, 1998)		Northern Germany Böse et al., 2012; Roskosch et al., 2015; Lang et al., 2018;		Litt et al., 2007
	MIS 1	Holocene		Holocene	Holocene
MIS 2	Late Pleistocene	Lateglacial			
MIS 3		Pleni-glacial	Weichselian	Weichselian	Weichselian
MIS 4			Weichselian	Weichselian	Weichselian
MIS 5d-a		Early Glacial			
MIS 5e		Eemian	Eemian	Eemian	
MIS 6	Middle Pleistocene	Saalian	Saalian	Saalian	Warthe Drenthe
MIS 7			Saalian	Saalian	Dömnitz
MIS 8			Saalian	Saalian	Fuhne
MIS 9			Holsteinian	Holsteinian	
MIS 10			Elsterian	Elsterian	
MIS 11			Holsteinian		Ruhme
MIS 12			Elsterian	Elsterian	Cromerian

Fig. 3: Chronostratigraphy of the Pleistocene in northern Central Europe. The blue arrows represent ice advances. Two different stratigraphic charts exist for NW Europe and Central Europe.

Three major ice advances with several sub-phases occurred during the Saalian glaciation (Eissmann, 2002; Litt et al., 2007; Ehlers et al., 2011; Lang et al., 2018). These repeated ice advances are commonly correlated with MIS 6 and are referred to as the Drenthe and Warthe ice advances (Fig. 3; Litt et al., 2007; Ehlers et al., 2011; Lang et al., 2018). However, there is increasing evidence for an ice advance during MIS 8 (see discussion in Roskosch et al., 2015). These Saalian ice sheets advanced from northerly, northeasterly and easterly directions (Meinsen et al., 2011; Winsemann et al., 2011; Lang et al., 2018). The younger Saalian Warthe ice advances did not reach as far as the older Saalian and Elsterian ice sheets (Fig. 2b). The Late Pleistocene Weichselian ice sheets did not cross the Elbe River and periglacial conditions prevailed in the study area (Eissmann, 2002; Reinecke, 2006; Litt et al., 2007; Meinsen et al., 2014). Three main ice-marginal positions are known in northeastern Germany from the Weichselian glaciation. The peak of the Eurasian ice sheet in global ice volume, often referred to as the LGM, occurred at around 21-20 ka (Hughes et al., 2016), although it does not correspond with the maximum ice extent in northeastern Germany. The maximum extent of the Weichselian ice sheet in northeastern Germany was reached at around 30 ka (Hardt et al., 2016), while further west in Mecklenburg and Schleswig-Holstein the maximum ice extent was reached at around 24 ka (Böse et al., 2012). The ice margin position was located northeast of the Elbe Lineament (Fig. 2b), whereby the Elbe Valley acted as a major channel for meltwater flows (Ehlers et al., 2011; Lang et al., 2019). The ice subsequently melted back rapidly and a stillstand phase during the downwasting period occurred, which was later followed by a third minor re-advance (Lüthgens and Böse, 2011; Hardt et al., 2016; Hardt and Böse, 2018).

2.2. Recent stress field and glacial-isostatic adjustment (GIA)

The present-day stress field in the CEBS is characterized by NW-SE compression and NE-SW extension (Reinecker et al., 2004; Heidbach et al., 2016). As mentioned above, there are three individual tectonic processes at work in northern Germany. The major control on the stress field that effects the faults in the CEBS is a force with an E-W or NW-SE direction induced by the North Atlantic ridge push, and an N-S-directed force caused by Alpine collision see Fig. 4 (Marotta et al., 2004; Kaiser et al., 2005).

A key tectonic phase in northern Germany was the Late Cretaceous/Paleogene inversion phase when major basement faults were reactivated (Lohr et al., 2007; Kley and Voigt, 2008). After this inversion phase, the stress field in northern Germany was N-S to NE-SW and rotated counterclockwise from NE-SW to NW-SE in the

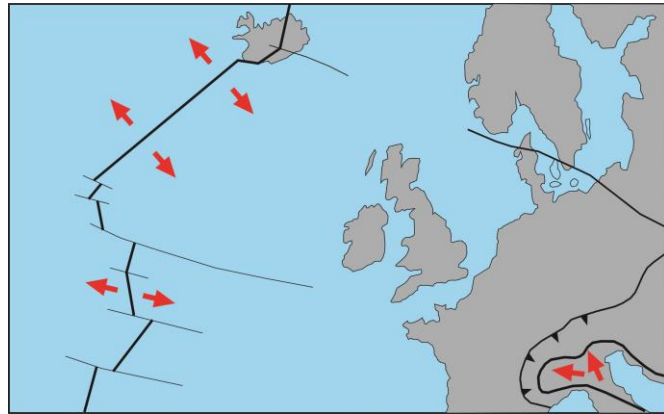


Fig. 4: Schematic sketch of the north Atlantic ridge push and the N-S-directed force caused by Alpine collision (modified according to Grünthal and Stromeyer, 1992).

Neogene (Kley and Voigt, 2008). From the Pleistocene onward to the present day, the main factor influencing the stress field is the post glacial rebound of Fennoscandia (Kaiser et al., 2005). This rebound also affects the area outside the former glaciated area. Ice loading and unloading during the Middle and Late Pleistocene in northern Central Europe led to lagged crustal movement because the elastic response is instantaneous and the viscoelastic response of the mantle is slower (Stewart et al., 2000). Due to elastic crustal flexure, a bowl-shaped depression occurred below the centre of the ice sheet as a result of the crustal loading and the outward flow of the deep mantle material away from the maximal ice load (Stewart et al., 2000).

When ice retreats, crustal unloading is faster than the crustal loading during the ice advance (Stewart et al., 2000) because the ice melts much faster than it develops. The rapid release of vertical stress leads to a fast crustal rebound during deglaciation and the resulting stress changes can trigger earthquakes in intraplate settings (e.g. Grollimund and Zoback, 2001).

A glacial forebulge develops in front of the ice sheet due to the flexure of the lithosphere. The forebulge area is characterized by uplift and extension (Fig. 5; Stewart et al., 2000).

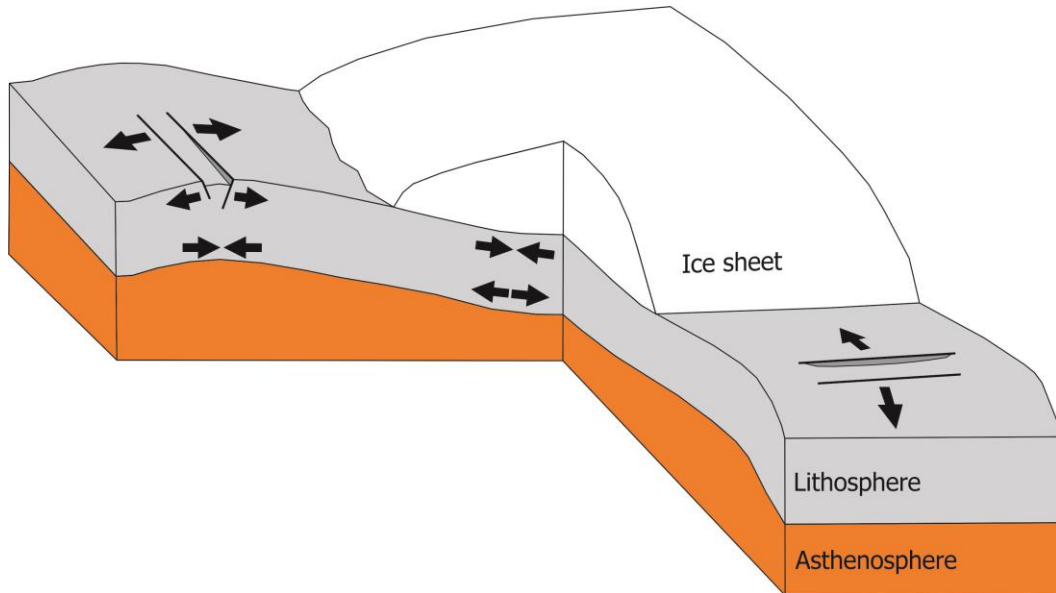


Fig. 5: Conceptual model for stresses during a glaciation. Lithosphere deflection causes bending stress in the lithosphere. A glacial forebulge develops in front of the ice sheet due to the flexure of the lithosphere. The forebulge area is characterized by uplift and extension. The faults parallel to the ice margin have a high reactivation potential (modified according to Stewart et al., 2000).

The collapse of the Late Pleistocene forebulge in northern Germany is ongoing. The recent maximum subsidence rate is 1.0 - 1.5 mm/a at latitudes of between 50.5 - 53°N (Frischbutter, 2001; Nocquet et al., 2005; Kierulf et al., 2014) and can be interpreted as a result of forebulge collapse. The Late Pleistocene Weichselian forebulge was probably located several hundreds of kilometers in front of the ice sheet (Kiden et al., 2002; Nocquet et al., 2005; Busschers et al., 2008; Sirocko et al., 2008; Winsemann et al., 2015) including the study area (Fig. 6).

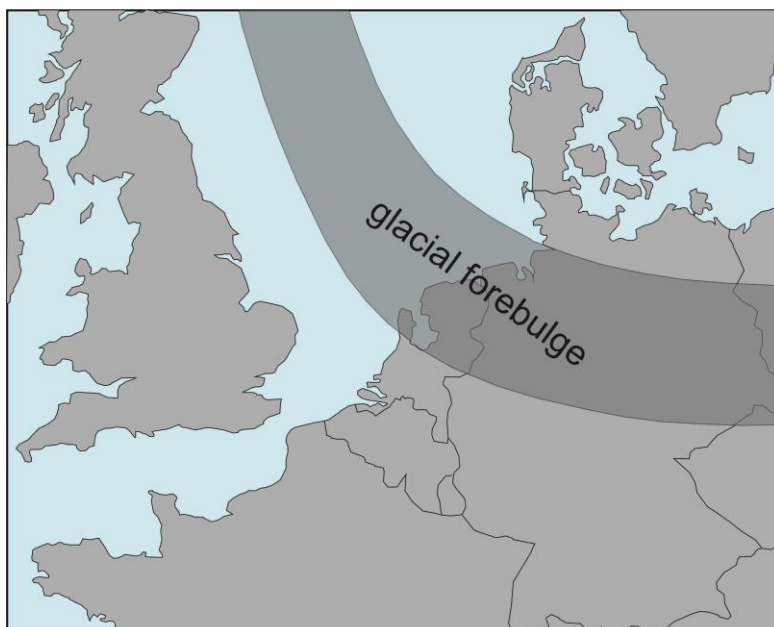


Fig. 6: The position of the Late Pleistocene glacial forebulge (shaded area) (according to Kiden et al., 2002).

The stress field induced by the Scandinavian ice sheets matches the orientation of the paleo-stress field in northern Germany. These varying NNE-SSW-oriented stress conditions lead to the reactivation of pre-existing

Mesozoic faults. The reactivation potential of faults running parallel to the former ice margins is the greatest (Fig. 5). The WNW-ESE trending major basement faults analyzed in this study therefore have a high potential for neotectonic reactivation (Brandes et al., 2015).

2.3. Harz Boundary Fault

The Harz Boundary Fault is a major structural element of the Central European Basin System (CEBS) and a key element of intraplate deformation during the Late Cretaceous inversion phase. The Harz Boundary Fault separates the Palaeozoic rocks of the Harz Mountains from the Mesozoic sedimentary rocks of the Subhercynian Basin (von Eynatten et al., 2008; Voigt et al., 2008). The sand and gravel pits analyzed here are located in the Subhercynian Basin, a WNW-ESE-striking basin with a Mesozoic sedimentary fill, unconformably overlain by thick Quaternary glacial and fluvial deposits (Bode et al., 1926; Weissermel et al., 1926; Schröder et al., 1929a; Schröder et al., 1929b; Schröder et al., 1931; Feldmann, 2002; Weymann, 2004; Reinecke, 2006; Lang et al., 2018).

The southwestern margin of the Subhercynian Basin is characterized by the NW–SE-trending Harz Boundary Fault (Fig. 2c), which is approximately 100 km long. The fault evolved in the Late Cretaceous during the tectonic inversion phase of the CEBS. A large fault-propagation fold developed above the tip of the Harz Boundary Fault that reached the seafloor not before the Late Coniacian (Voigt et al., 2006). In the Early Campanian, rock fragments composed of Paleozoic rocks were shed from the Harz Mountains (von Eynatten et al., 2008), implying ongoing unroofing of the fault-propagation fold. These observations indicate a major phase of tectonic activity along the Harz Boundary Fault between the Coniacian and the Campanian, which is also supported by apatite fission track ages from the Harz Mountains (Kley and Voigt, 2008).

A kinematic analysis of the Harz Boundary Fault was provided by Franzke and Schmidt (1993), but there is an ongoing debate about the general nature of the Harz Boundary Fault. It is interpreted either as wrench fault system (Wrede, 1988, 2008) or a dip-slip thrust (Voigt et al., 2006). Depending on the kinematics of the Harz Boundary Fault,

the Subhercynian Basin is regarded as a wrench fault basin (Wrede, 1988) or as a piggy-back basin on the top of a basement thrust system (Voigt et al., 2006).

2.4. Osning Thrust

The Osning Thrust is a NW-SE-trending thrust system located at the southern margin of the Lower Saxony Basin (Fig. 2c). This fault zone is referred to as the “Osning Thrust”, “Osning Zone” or “Osning Lineament” (Drozdowski, 1988; Baldschuhn and Kockel, 1999) and has a length of approximately 115 km. During the last century, the Osning Thrust was the focus of many studies (Stille, 1924; Lotze, 1929; Stille, 1953; Keller, 1974; Rosenfeld, 1983). The nature of the thrust has been discussed in detail over the last two decades. Drozdowski (1988) interpreted it as a strike-slip fault. However, Baldschuhn and Kockel (1999), who have presented the most comprehensive analysis of the fault kinematics to date, could not find any evidence for significant strike-slip movement. According to their dataset, the first movements along the Osning Fault probably took place in the Late Triassic. At that time the Osning Fault was a NNE-dipping normal fault (Baldschuhn and Kockel, 1999). The southward Münsterland Block acted as the footwall. In the Coniacian, inversion of the Lower Saxony Basin began (Kockel, 2003). During this inversion, the fill of the basin was overthrust southwards along the Osning Thrust onto the Münsterland Block (Baldschuhn and Kockel, 1999), i.e. the former normal fault was transformed into a thrust. The present-day structure in the study area is characterized by low-angle thrust faults (Keller, 1974). Lateglacial (Brandes et al., 2012; Brandes and Winsemann, 2013) and historic seismicity (Vogt and Grünthal, 1994; Leydecker, 2011) indicate ongoing activity along the Osning Thrust.

2.5. Halle Fault system

The Halle Fault belongs to the NE-SW-trending intramontane Saale Basin, a local basin related to the Variscan orogen (Rappsilber, 2003). It is interpreted as a transtensional strike-slip basin that developed in the Late Carboniferous to Early Permian and is filled with material derived from the Variscan orogen (Rappsilber, 2003).

The Halle Fault plays a significant structural role because it separates two tectonic units: the Merseburg-Scholle and the Halle-Wittenberg-Scholle (Schwab et al., 2006). The fault is approximately 40 km long and trends NW-SE to E-W (Fig. 2c). It underwent multiphase tectonic evolution and is interpreted as an Early Permian strike-slip fault (Rappsilber, 2003) that was reactivated as reverse fault in Late Cretaceous times (Rappsilber, 2003; Schwab et al., 2006; Kley and Voigt, 2008). The area surrounding the Halle Fault is characterized by a NW-SE and NE-SW-oriented fault pattern that formed during the compressive tectonic phase in the Late Cretaceous and Early Paleogene (Knoth et al., 1998; Rappsilber and Schwab, 2006). Historic and recent seismicity in the Halle area (Leydecker, 2011) may indicate young tectonic movements along the Halle Fault system.

2.6. Aller Valley Fault

The Aller Fault zone trends NW-SE and extends from the Magdeburg area across Lower Saxony into the area of Oldenburg over a distance of 250 km (Fig. 2c). The southeastern part of the Aller Fault zone reaches the surface and is exposed along the northeastern margin of the Subhercynian Basin. Early studies consequently focused on this area (Woltstedt, 1924; Brinckmeier, 1925). The central and northwestern segments of the Aller Fault zone are not exposed and have therefore mainly been studied with seismic sections (Mazur et al., 2005; Lohr et al., 2007). From a tectonic point of view, the Aller Fault zone is a complex inversion structure (Jubitz et al., 1991; Kockel, 2003) that underwent multiphase tectonic evolution with extension in the Triassic and Jurassic followed by contraction and inversion in the Cretaceous (Best, 1996; Lohr et al., 2007). Initial normal fault movements along the southeastern part of the Aller Fault during the Late Triassic are indicated by the development of thick growth-strata packages, e.g. as shown on geological cross-sections in Baldschuhn et al. (1996). Normal faulting prevailed throughout the Mesozoic and ended in the Early Cretaceous (Albian) (Best and Zirngast, 2002). Contraction and inversion followed (Best and Zirngast, 2002). Comparable observations were also made for the central part of the Aller Fault by Lohr et al. (2007). These authors provided a detailed kinematic analysis based on seismic reflection data. Initial extension in the Late Triassic was directed NNE-SSW and created normal faults. This phase was followed by an E-W

extension in the Middle Jurassic that led to transtensional movements along the central part of the Aller Fault. In the Cretaceous, E-W contraction occurred during the Santonian to Campanian, and an N-S contraction occurred during the Coniacian to Maastrichtian. This contraction partially prevailed into the Paleocene (Lohr et al., 2007).

2.7. Gardelegen Fault

The Gardelegen Fault is an approximately 70-km-long Permo-Carboniferous structure reactivated during the Late Cretaceous inversion of the NE German Basin (Fig. 2c; Kossow and Krawczyk, 2002). The Gardelegen reverse fault trends NW-SE (Kossow and Krawczyk, 2002; Kley and Voigt, 2008), has pronounced listric geometry, a vertical offset of 5-6 km (Otto, 2003) and soles out into a subhorizontal detachment at a depth of 25 km (DEKORP Basin Research Group, 1999; Kley, 2013). A cluster of historic earthquakes in the Altmark area (Leydecker, 2011) probably indicates young seismic activity at the Gardelegen Fault.

2.8. Steinhuder Meer Fault

The Steinhuder Meer Fault is located west of Hannover (Fig. 2c). It is 50 – 70 km long, but the exact length of the fault trace is difficult to define due to the close connection to the Bokeloh salt structure. The Steinhuder Meer Fault passes into the Stemmer Berg thrust in the south (BGR, 2012). The Stemmer Berg thrust is interpreted as a slight listric fault that reaches a depth of approximately 15 km (Müller et al., 2016).

The tectonic history of the Steinhuder Meer Fault is poorly documented. Cross-sections shown in Kley et al. (2008) and Müller et al. (2016) relate the Steinhuder Meer Fault to deep-seated faults in the pre-Permian basement. The thickness distribution of potential growth strata along the fault shown in Baldschuhn et al. (1996) implies potential normal fault movements in the Middle Jurassic followed by reverse movements in Late Cretaceous times. Reverse faulting led to the formation of a tight fault propagation fold in the area of the Stemmer Berg as indicated on a cross-section shown in Baldschuhn et al. (1996).

2.9. Elbe Lineament

The Elbe Lineament is a major crustal structure in northern Germany. It is also referred to as the Elbe Line (Scheck et al., 2002). According to Franke and Hoffmann (1999a), the Elbe Lineament is a NW-SE-oriented zone of faults. It represents two different NW-SE fault zones in Central Europe, the northern Elbe Line and the southern Elbe Line (Franke and Hoffmann, 1999a). The northern part of the Elbe Lineament extends from the southern North Sea (Lower Elbe Line) (Franke and Hoffmann 1999a; Abramovitz and Thybo, 2000; Tesauro et al., 2007), across northern Germany (Rabbel et al., 1995) and into Poland where it includes the Cracow-Lubliniec Zone (Franke and Hoffmann, 1999a). The southern Elbe Lineament trends from Hamburg towards Dresden into the Czech Republic and comprises the Wittenberg, Haldensleben and Gardelegen faults (Franke and Hoffmann, 1999a). This fault zone is named Elbe Fault System in Scheck et al. (2002). Each of these segments represents different kinds of terrane boundaries of varying ages (Franke and Hoffmann, 1999a).

The Elbe Lineament is interpreted as a deep crustal structure characterized by a drop in the p-wave velocity (e.g. Franke and Hoffmann, 1999a; Scheck et al., 2002). Strong changes in the crustal thickness and composition have been observed (Tesauro et al., 2007). The Elbe Lineament has been interpreted either as a major strike-slip fault that defines the NE extent of eastern Avalonia and the southwestern margin of the Baltic Shield (Tanner and Meissner, 1996) or an intra-Avalonian subterranean boundary (Krawczyk et al., 2008). It separates the Holstein Block in the north from the Pompeckj and Niedersachsen Block in the south (Rabbel et al., 1995). Deep seismic surveys indicate frequently occurring listric faults, which may be the result of recent tectonic movements (Franke and Hoffmann, 1999b).

The Lower Elbe Line has been analyzed and is referred to as the Elbe Lineament in this project. This segment of the Elbe Lineament strikes NW-SE parallel to the Teisseyre-Tornquist Zone (Fig. 2c) and represents an important geological boundary (Rabbel et al., 1995; Tesauro et al., 2007). The Elbe Lineament only appears subordinated in geophysical analyses within the Mesozoic and Cenozoic rocks (Franke and Hoffmann, 1999a).

3. Deformation structures

Different deformation structures have developed in the sand and gravel pits. Common structures are shear-deformation bands, folds, various soft-sediment deformation structures (SSDS) and cryoturbation features. These deformation structures were formed by different processes.

3.1. Deformation processes

Deformation processes include neotectonic deformation processes, glaciotectonic deformation processes and cryoturbation processes. The different processes and the resulting soft-sediment deformation structures are explained below.

3.1.1. Neotectonic deformation processes

First it is necessary to explain the term “neotectonics” as several definitions exist. Three definitions are given below:

“Any earth movements or deformations of the geodetic reference level, their mechanisms, their geological origin, and their implications for various practical purposes and their future extrapolations” (Mörner, 1978).

“The study of young tectonic events (deformation of upper crust), which have occurred or are still occurring in a given region after its final orogeny (at least for recent orogenies) or more precisely after its last significant reorganisation” (Pavrides, 1989).

“The study of the post-Miocene structures and structural history of the Earth’s crust” (AGI, 2009).

It is clear from these three different definitions that neotectonics describes young tectonic activity. How young this activity can be, however, remains open. In this study we use the terms “neotectonic deformation” or “neotectonic processes” for evidence of young fault movements and young tectonic deformation structures during the Pleistocene and Holocene. In terms of hazard assessment, it is important to know whether the neotectonic deformation observed is being produced by seismogenic or non-seismogenic processes. Faults can rupture and emit seismic waves or they can

creep without emitting seismic waves. However, not all neotectonic deformation is associated with earthquakes (McCalpin, 2003).

In this report “neotectonic deformation” is used to mean post-Miocene tectonic seismogenic or non-seismogenic movements along major basement faults.

3.1.2. Glaciotectonic deformation processes

Glaciotectonic deformation structures were induced by the Middle and Late Pleistocene advances of the Scandinavian ice sheets. These structures and the deformation mechanisms are described in Chapter 3.3.3.

3.1.3. Cryoturbation deformation processes

The periglacial environment is the marginal zone of an ice sheet that is not directly influenced by the glacier but is affected by permafrost (French, 2017). Large parts of the study area were affected by periglacial conditions. Cryoturbation is a widely used term for different deformation structures that develop in unconsolidated sediments under periglacial climate conditions (Edelman et al., 1936) and refers to freeze and thaw processes (Bryan, 1946; Tarnocai and Zoltai, 1978; Washburn, 1980; French, 2017). These structures and the deformation mechanisms are described in Chapter 3.3.4.

3.2. Deformation mechanisms

The pits analyzed frequently contain different styles of soft-sediment deformation structures (SSDS). Important factors that control the formation of SSDS are the hydraulic gradient and permeability, tensile strength and flexural resistance of the deposits (e.g. Mörz et al., 2007; Obermeier, 2009; Rodrigues et al., 2009; Brandes and Winsemann, 2013; Pisarska-Jamroży and Woźniak, 2019).

Lowe (1975) identified three main fluid escape processes in soft-sediments referred to as seepage, liquefaction and fluidization. The main characteristics of these processes are briefly summarised below.

3.2.1. Seepage

Seepage is the slow upward movement of pore water in response to a pressure gradient. During seepage, the grain-to-grain stress increases and a slow transformation of an unstable grain framework into one of greater stability occurs. The resulting fluid drag on the grains is generally negligible and the grain fabric is not disturbed (e.g. Lowe, 1975; Cobbold and Rodrigues, 2007; Rodrigues et al., 2009).

3.2.2. Liquefaction

Liquefaction is the loss of grain-to-grain contact resulting from increased pore pressure of a static fluid (Frey et al., 2009). During liquefaction, a rapid temporary increase in the pore-fluid pressure occur leading to a sudden loss of shearing resistance associated with grain framework collapse and the mobilization and deformation of the liquefied layer. As fluid flow rapidly dissipates upwards, a grain-supported framework is re-established (e.g. Lowe, 1975; Rodrigues et al., 2009; Ross et al., 2011). Reversed density gradients in the liquefied sediments lead to the formation of SSDS (Anketell et al., 1970).

Characteristic SSDS caused by liquefaction are convolute bedding, ball-and-pillow structures, flame structures and slumps (Fig. 7). Several processes can cause liquefaction. These include depositional loading and high pore water pressure (e.g. during advancing and/or overriding glaciers) storm waves, groundwater circulation, seismic events as well as freeze and thaw cycles in periglacial environments (e.g. Boulton et al., 1993; Boulton and Caban, 1995; Alfaro et al., 2002; Collinson et al., 2006; Brandes and Winsemann, 2013; Van Loon et al., 2016; Bertan et al., 2019a).

3.2.3. Fluidization

Fluidization is a process that requires pore fluid to move upwards with sufficient velocity to suspend or carry individual grains with it. The increased pore pressure leads to the expansion of the pore spaces until grain interaction is negligible and particles are free to move with the fluid (e.g. Lowe, 1975; Nichols et al., 1994; Frey et al., 2009). The fluid tends to follow preferred escape paths (e.g. faults, heterogeneities in material properties and layer thicknesses) while the surrounding sediment remains largely unfluidized (Mörz et al., 2007; Frey et al., 2009; Ross et al., 2011). The primary lamination is disturbed in fluidized zones, and fluid-escape structures develop that crosscut the primary bedding, accompanied by the injection of sand or mud into overlying layers (Lowe and LoPiccolo, 1974; Lowe, 1975; Hurst and Cartwright, 2007; Frey et al., 2009; Hurst et al., 2011).

Characteristic SSDS are sand or mud volcanoes, clastic dykes, sills, irregular sand intrusions, dish-and-pillar structures (Fig. 7; Collinson et al., 2006). Fluidization can be caused by different mechanisms such as depositional loading, seismic events and freeze and thaw cycles in periglacial environments (Collinson et al., 2006; Brandes and Winsemann, 2013; Bertran et al., 2019a).

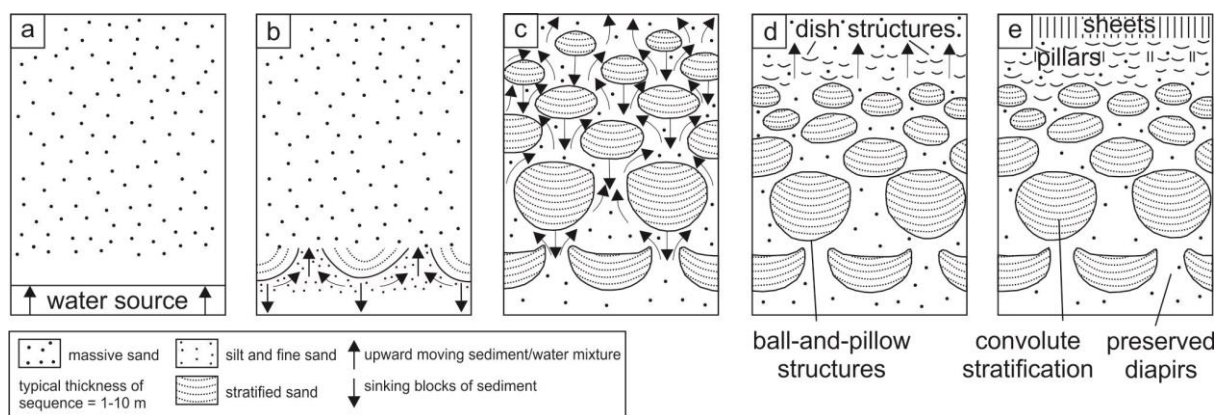


Fig. 7: A model for the gradual development of convolute bedding, ball-and-pillow structures, dish structures, pillar structures and sheet dewatering. Excess pore fluid pressure drives the escape of sediment and water upwards. Gravity assists the downward movement of larger intact blocks (modified according to Cheel and Rust, 1986; Collinson et al., 2006).

3.3. Driving mechanisms for soft-sediment deformation structures

3.3.1. Depositional loading

The simplest way to form soft-sediment deformation structures is depositional loading in water-saturated sediments (e.g. Sullwood, 1959; Lowe, 1975; Moretti et al., 2001; Oliveira et al., 2009). These structures may include all styles of liquefaction and fluidization if the overburden is high enough. Hydraulic fractures can form when the fluid overpressure reaches values approximately equal to the weight of overburden plus the tensile strength of the material (Owen, 2003; Rodríguez et al., 2009; Brandes and Winsemann, 2013).

3.3.2. Neotectonic activity

Neotectonic activity in northern Germany can be seen as a consequence of collisional forces from the Alpine orogeny and the Atlantic ridge push (Marotta et al., 2004; Kaiser et al., 2005). Neotectonic activity can lead to seismogenic and non-seismogenic neotectonic deformation (McCalpin, 2003). A trigger mechanism for neotectonic movements can be postglacial isostatic crustal rebound (e.g. Lehné and Sirocko, 2007; Lehné and Sirocko, 2010; Brandes et al., 2015). Lehné and Sirocko (2007) and Lehné and Sirocko (2010) show subsidence rates in the Glückstadt Graben in the North German Basin of 0.42 mm/a on a regional scale, which is related to ongoing isostatic adjustment. The subsidence rates on a local scale may partly be significantly higher. Some active faults were detected in the Glückstadt Graben via aerial photography and satellite images of lineaments and outcropping surface faults (Lehné and Sirocko, 2010). The highest recent activity was documented at the fault zone Segeberg/Plön on the eastern margin of the Glückstadt Graben although it cannot be linked to earthquakes.

3.3.2.1 Earthquakes

Seismic events can lead to liquefaction and fluidization of sediments depending on the earthquake magnitude and strength of the substrate (Rodríguez-Pascua et al., 2000). However, no unambiguous geological indicator for past earthquake activity exists. The

frequency of earthquakes in northern Germany an intensity larger than 5 is low (Leydecker and Kopera, 1999). The earthquake activity is difficult to analyze because there are few prominent earthquake indicators such as fault scarps (Kaiser, 2005).

The repeated growth and decay of ice sheets during the Middle and Late Pleistocene can induce lithospheric stress changes that may foster neotectonic movement which can initiate earthquakes (Reicherter et al., 2005).

Many studies rely on fluidization and liquefaction features as an indicator of neotectonic and paleoseismic events (Hoffmann and Reicherter, 2012; Brandes and Winsemann, 2013; Van Loon and Pisarska-Jamroży, 2014). Hoffmann and Reicherter (2012) analyzed soft-sediment deformation structures in Late Pleistocene sediments that are interpreted to have been induced by earthquakes at the SW Baltic Sea Coast in NW Germany. Brandes et al. (2012) and Brandes and Winsemann (2013) found evidence of paleo-earthquakes in Lateglacial deposits near the Osning Thrust where a large variety of soft-sediment deformation structures have developed in mixed alluvial-aeolian sediments. Van Loon and Pisarska-Jamroży (2014) found indications of paleo-earthquakes in Poland that can be related to glacial-isostatic rebound near the Polish/German border. Soft-sediment deformation structures have occurred in the vicinity of the Lower Odra Fault Zone in this low-seismicity region (Van Loon and Pisarska-Jamroży, 2014).

3.3.2.1.1. Seismites

Layers or a set of layers of seismically induced SSDS are named seismites (Moretti et al., 2016). Seismites related to earthquakes at the end of the Late Pleistocene Weichselian glaciation are well documented known in Germany, Denmark, Sweden, Poland and Latvia (e.g. Schwan et al., 1980; Mörner 2003; Hoffmann and Reicherter, 2012; Brandes and Winsemann, 2013; Van Loon and Pisarska-Jamroży, 2014; Van Loon et al., 2016; Grube, 2019a, 2019b; Pisarska-Jamroży et al., 2018; Pisarska-Jamroży and Woźniak, 2019).

The term "seismites" was first used by Sailacher (1969) and only referred to sediment beds that had been deformed by shaking. Deformed beds occur as layers sandwiched between undeformed beds (Van Loon et al., 2016). Seismites are deformation

structures resulting from seismic waves (Vittori et al., 1991; Rodríguez-Pascua et al., 2000) that cause liquefaction and fluidization of sediment if the magnitude of earthquakes is high enough ($M \geq 5.0$) (e.g. Atkinson et al., 1984; Rodríguez-Pascua et al., 2000). An earthquake with the intensity of 5 to 6 can cause fluidization and liquefaction of sediments that occur at a distance of up to 40 km from the epicenter, depending on the nature of the sediments (Galli, 2000).

The most common SSDS originating from seismic waves are load casts, pseudonodules and flame structures, which are mainly related to liquefaction (Van Loon, 2009; Van Loon and Pisarska-Jamroży, 2014). Brittle deformation and water-escape structures (e.g. sand volcanoes and hydrofractures) related to fluidization can also occur due to seismic waves (Brandes and Winsemann, 2013).

3.3.2.1.2. Deformation bands

The term “deformation band” in connection with sandstones was first applied by Aydin (1978) and Ayden and Johnson (1978). Deformation bands are tabular zones of local deformation that can occur in unconsolidated porous, sandy sediments and porous sedimentary rocks (Fossen et al., 2007). The bands define a millimetre- to centimetre-thick zone of deformation with small offsets (Fossen et al., 2007). Faults form in non-porous material. In contrast to deformation bands, faults with small offsets are distinct features and the deformation concentrates on the fault surface. The various types of tabular deformation zones that occur are governed by factors such as porosity, mineralogy, grain size and grain shape, lithification, state of stress and burial depth (Fossen et al., 2007).

Two different classifications exist for deformation bands. They can be classified kinematically as dilation bands, shear bands, compaction bands and a hybrid of these types (Fig. 8; e.g. Aydin et al., 2006).

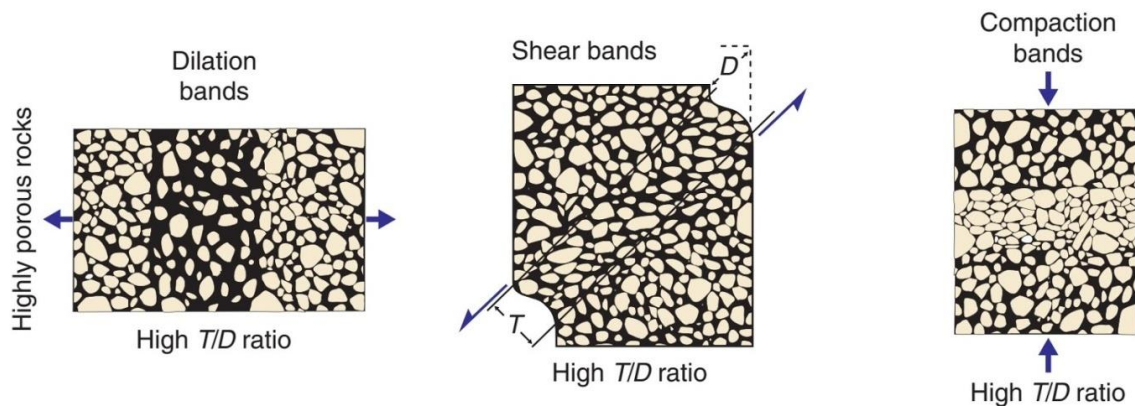


Fig. 8: Kinematic classification of deformation bands. T, thickness; D, displacement (from Fossen, 2010a)

The majority of deformation bands are shear bands, which can be affected by compaction (compaction shear-bands; Fossen et al., 2007). Deformation bands can also be classified according to their characteristic deformation mechanism (Fig. 9).

The most important mechanisms are granular flow, catalysis, phyllosilicate smearing, dissolution and cementation (Fossen, 2010b). Depending on the deformation mechanisms, the principal types of deformation bands are disaggregation bands, phyllosilicate bands, cataclastic bands and solution and cementation bands (Fossen et al., 2007). Fossen et al. (2010a) showed differences in disaggregation bands that formed syndepositionally in soft sediments and due to tectonic activity in sandstones. Synsedimentary bands are associated with soft-sediment deformation structures, whereas tectonic bands are typically clustered in the vicinity of faults. Tectonic bands are often affected by cataclasis, have a consistent orientation and commonly form conjugate sets. Recent studies show that near-surface deformation bands that formed in unconsolidated sediments can develop due to earthquakes along active basement faults

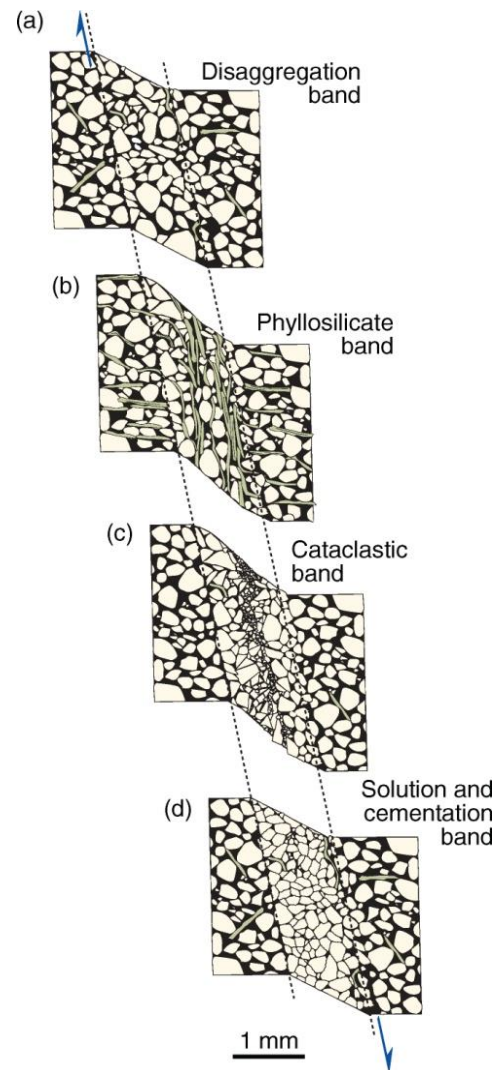


Fig. 9: The principal types of deformation bands according to the deformation mechanism (from Fossen, 2010a).

(Cashman et al., 2007; Brandes et al., 2018a, b). Deformation bands are a relevant tool in paleoseismology and neotectonic deformation processes because they are a strong indicator for active faults. Unlike glaciotectonically induced shear-deformation bands that form in near-surface sediments, deformation bands caused by neotectonics often affect the whole sedimentary succession and show the same orientation as the nearby basement faults (Brandes et al., 2018a). Deformation bands might be also formed by cryoturbation processes. In this case they reflect the local near-surface extension and contraction of the sediments related to freeze and thaw processes (Bertran et al., 2019a).

3.3.3. Ice loading and unloading

Several different deformation structures can develop due to glaciotectonic deformation. The processes and products of glaciotectonic deformation have been studied in great detail during the last few decades (e.g. Dredge and Grant, 1987; Eybergen, 1987; Meyer, 1987; Feeser, 1988; Ingólfsson, 1988; Van der Wateren et al., 2000; Knight, 2002; Phillips et al., 2002; McCarrol and Rijdsdijk, 2003; Bennett et al., 2004; Thomas and Chiverrell, 2007; Benediktsson et al., 2008; Phillips et al., 2008; Phillips and Merritt, 2008; Roberts et al., 2008; Burke et al., 2009; Gehrmann and Harding, 2018). Deformation styles include proglacial compressional structures that form at the margin of an ice sheet and subglacial extensional deformation beneath the ice sheet (Hart and Boulton, 1991). Different deformation structures commonly develop due to stress field variations caused by the advancing ice sheet (Fig. 10 and 11).

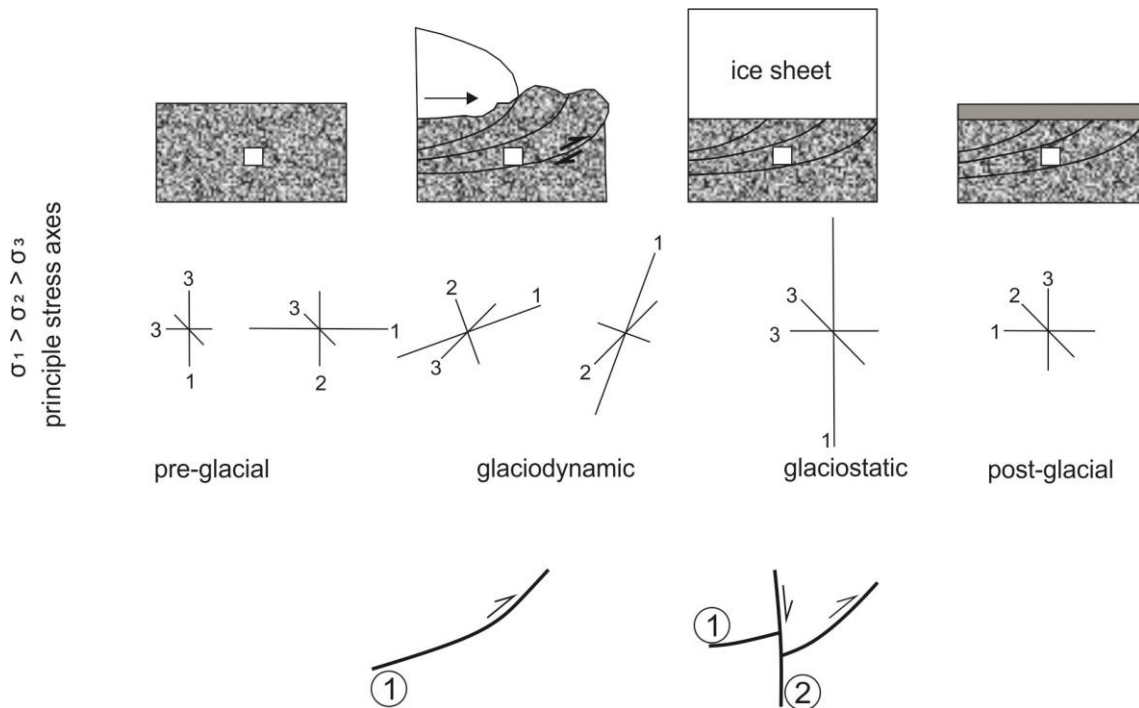


Fig. 10: Classification of glacial deformation mechanisms due to ice sheet-related stress field variations (modified according to Feeser, 1988).

3.3.3.1. Proglacial deformation

Proglacial deformation leads to the formation of large-scale contractional structures such as folds, reverse and thrust faults (Van Gijssel, 1987; Croot, 1988; Fernlund, 1988; Houmark-Nielsen, 1988; Bennett, 2001; Aber and Ber, 2007; Phillips et al., 2008; Gehrmann and Hardinger, 2018). The island of Rügen is an example of large-scale glaciotectonic folding and thrusting with three deformation phases caused by different ice advances (Kenzler et al., 2010; Gehrmann et al., 2017; Gehrmann et al., 2018). Depending on the rheology and the competence of the deposits and the behaviour of the ice sheet, folding (ductile deformation) or faulting (brittle deformation) may occur (Hart and Boulton, 1991). A so-called glaciotectonic complex (composite ridges) can form at the front of the ice sheet, which is characterized internally by contractional deformation structures. Glaciotectonic complexes have a restricted distribution at glacial margins and provide information on the extent of the Pleistocene ice sheets and related fast-moving ice streams (Bennett, 2001; Lang et al., 2018). Many of these proglacial structures were overridden later by the advancing ice sheet (Fig. 11; Hart and Boulton, 1991).

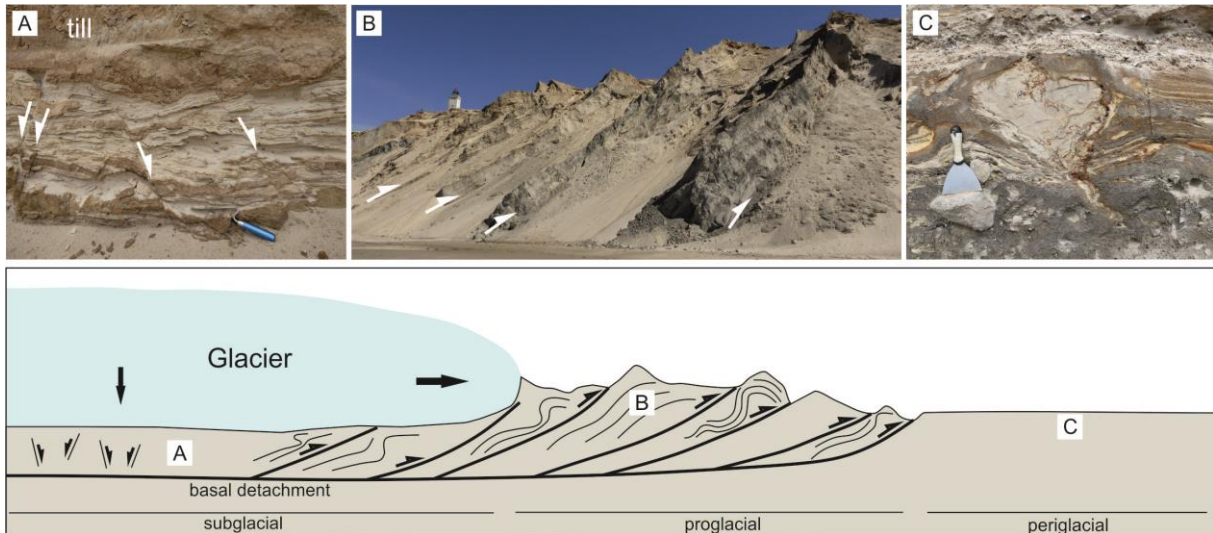


Fig. 11: Glaciotectonic complex. Subglacial deformation is highly variable in style and intensity and can result in normal faulting and the formation of horst and graben structures as well as heterogeneous folds, soft-sediment deformation structures and ductile shearing. Proglacial deformation leads to the formation of large-scale contractional structures such as folds, reverse and thrust faults. Cryoturbation features can occur in the periglacial environment (based on Aber and Ber, 2007; Müller et al., *in press* c).

3.3.3.2. Subglacial deformation

Subglacial deformation is highly variable in style and intensity and can result in normal faulting and the formation of horst and graben structures as well as heterogeneous folds, soft-sediment deformation structures and ductile shearing, which is associated with the formation of a subglacial shear zone (Fig. 12; e.g. Rappol and Stoltenburg, 1985; Amark, 1986; Fitzsimons et al., 2000; Menzies, 2000; Van der Wateren et al., 2000; Piotrowski et al., 2004; Lee and Phillips, 2008; Phillips and Merritt, 2008). The initial water content of the deformed sediments governs the pattern of deformation within the shear zone (Phillips et al., 2008). Dredge and Grant (1987) show that subglacial deformation can also affect the bedrock, as on Rügen, where Cretaceous limestone and Pleistocene sediments were deformed by the advancing ice sheets (Katzung et al., 2004; Kenzler et al., 2010; Gehrmann and Harding, 2018).

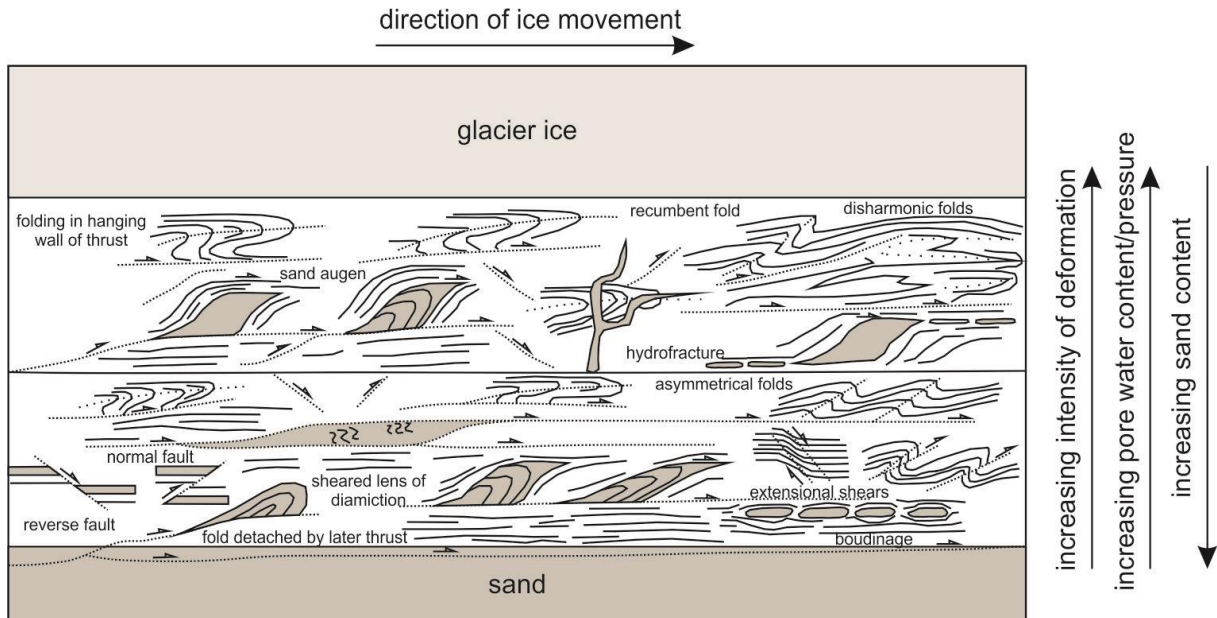


Fig. 12: Deformation model showing the development of different deformation structures in a subglacial shear zone (modified according to Lee and Phillips, 2008).

Proglacial and subglacial deformation can take place in unfrozen conditions (Van der Wateren, 1981). Examples are shown in Fig. 13. Unfrozen subglacial deformation commonly occurs beneath the centre of large ice sheets (Hart and Boulton, 1991), whereas frozen conditions prevail at the ice margins (Benn and Evans, 2013). Soft-sediment deformation structures can develop at the margin of large ice sheets due to high pore water pressure in front or at the toe of the glacier (Boulton et al., 1993; Boulton and Caban, 1995).

Dead ice collapse and basal crevasse infills can also lead to sediment deformation (Hart and Boulton, 1991).

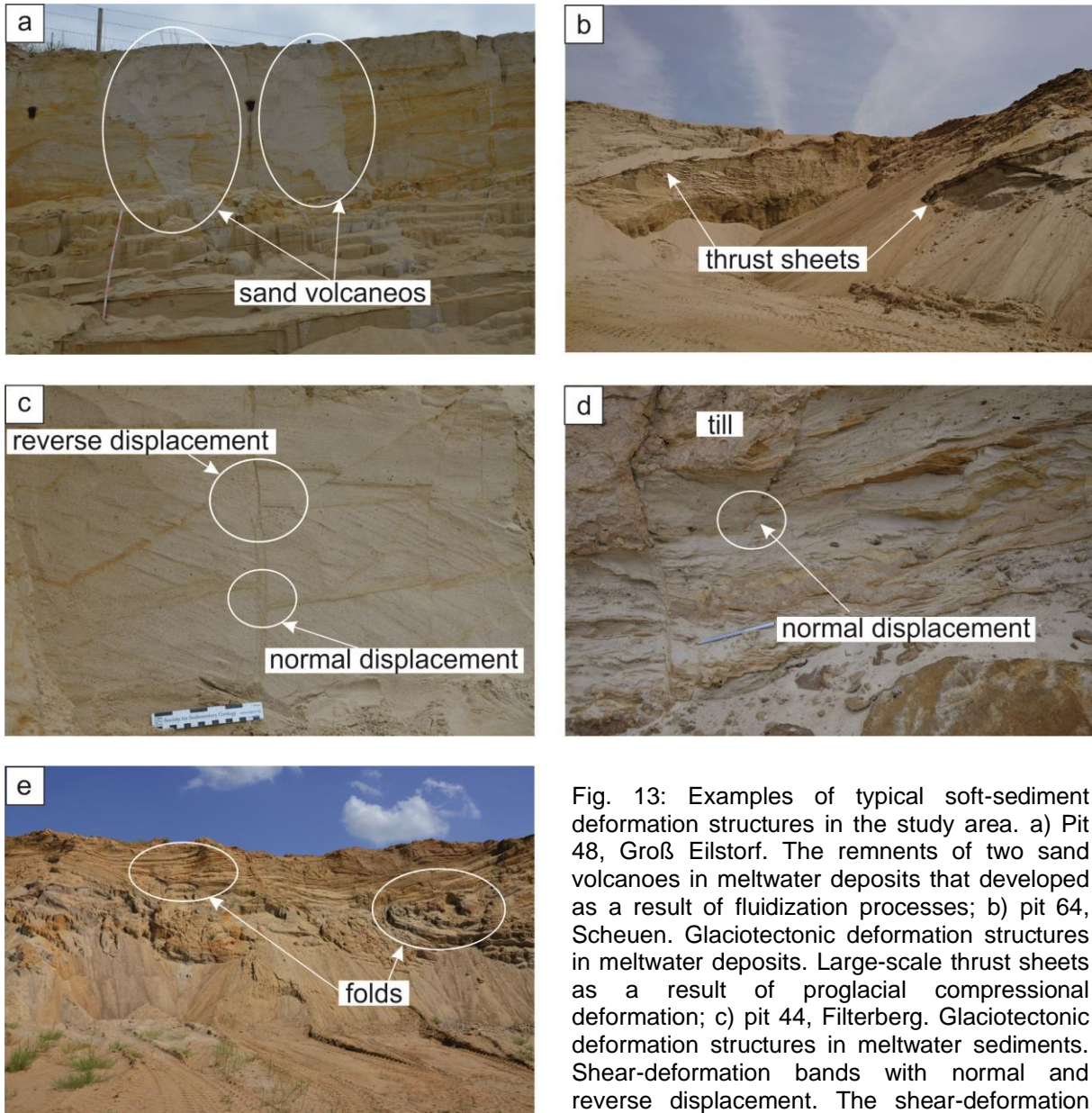


Fig. 13: Examples of typical soft-sediment deformation structures in the study area. a) Pit 48, Groß Eilstorf. The remnants of two sand volcanoes in meltwater deposits that developed as a result of fluidization processes; b) pit 64, Scheuen. Glaciotectonic deformation structures in meltwater deposits. Large-scale thrust sheets as a result of proglacial compressional deformation; c) pit 44, Filterberg. Glaciotectonic deformation structures in meltwater sediments. Shear-deformation bands with normal and reverse displacement. The shear-deformation band with normal displacement is offset by a younger shear-deformation band with reverse displacement; d) pit 72, Dolle. Glaciotectonic deformation structures in meltwater deposits. Shear-deformation band with normal displacement overlain by a till bed. The shear-deformation band developed subglacially due to ice loading; e) pit 80, Ferbitz. Glaciotectonic deformation structures in meltwater deposits. Overview image with large scale folds.

3.3.4. Freeze and thaw cycles

These processes mainly occur in the so-called active layer, which thaws and freezes seasonally (Fig. 14; e.g. Dobinski, 2011).

Cryostatic pressure and gravity are processes that produce cryoturbation structures and cause soil movements (Bockheim and Tarnocai, 1998), differential frost heave and

loading (Ogino and Matsuoka, 2007). Periglacial involutions often have swirl-like or teardrop patterns (Fig. 15; type 2, 3; Bockheim and Tarnocai, 1998).

Vandenberghe (1988, 2013) published a classification of cryoturbation structures. He distinguished six morphological types (see Fig. 15) according to their diagnostic sedimentary architecture comprising the symmetry, the amplitude and the wavelength ratio of the folds as well as the pattern and frequency of occurrence (Fig. 15; Vandenberghe, 2013). The amplitude of cryoturbation structures generally occurs within a range of 0.60 - 1.90 m (e.g. Vandenberghe, 1988). Recent studies have shown that large cryoturbation structures (4.0 - 4.5 m amplitude) are unusual but can occur if massive ice layers exist within the permafrost body. These large cryoturbation structures form during the degradation of the permafrost due to depositional loading and high pore pressure (Vandenberghe et al., 2016).

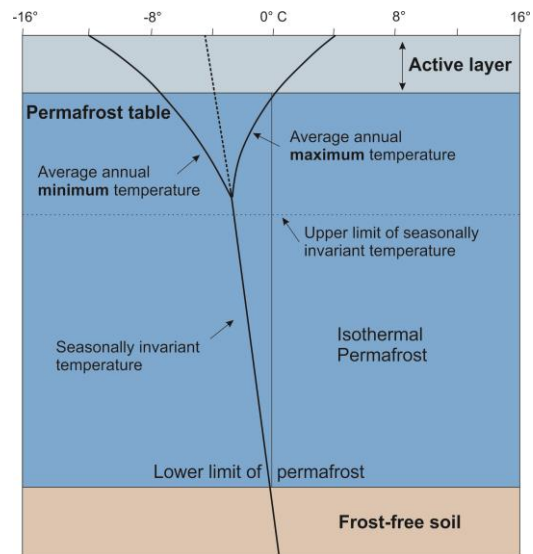


Fig. 14: Model of permafrost in a periglacial climate environment (modified according to Dobinski, 2011).

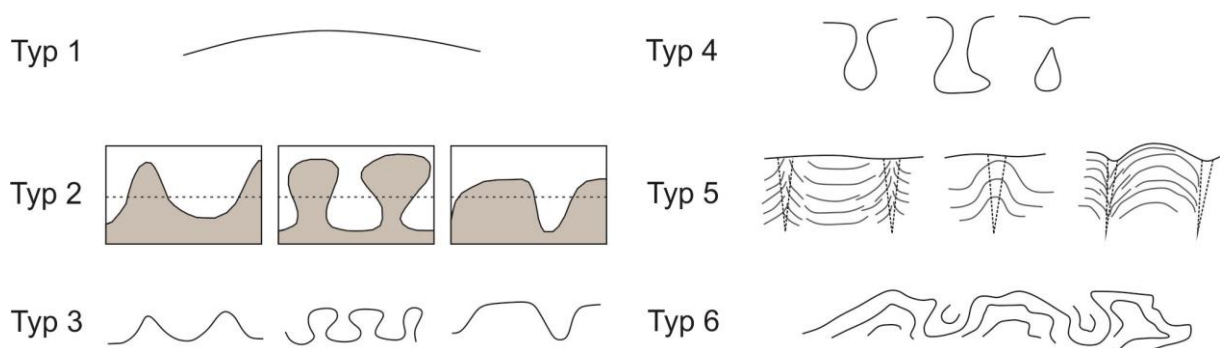


Fig. 15: Different cryoturbation structures (modified according to Vandenberghe, 2013). Type 1 cryoturbation features are undulations or small folds with low amplitude (dm) and large wavelength (m). Type 2 cryoturbations include a series of closely spaced symmetrical (amplitude 0.5 and 2 m) intensively folded forms. The lower parts are sometimes flat. The size varies with the lithology and the thickness of the sediment. Type 3 is very similar to type 2 but smaller in size (cm - dm). Type 4 cryoturbation structures have symmetrical geometries (very similar to types 2 and 3) but with individual geometries and different amplitudes. Type 5 looks similar to type 2 but, unlike type 3, the lower sediment has risen along platy dykes. The upper sediment of type 5 has subsided sack-wise. Type 6 is classified as having structures of irregular shape and all dimensions.

3.3.4.1. Ice wedges and ice wedge casts

Ice wedges are massive, generally wedge-shaped bodies with a downward-pointing apex (Fig. 16). They are composed of foliated or vertically banded ice (Harry, 1988). Ice wedges occur in thermal contraction cracks in which hoar frost forms. Water from melting snow then penetrates these cracks. The formation of an ice wedge takes many years and is caused by thermal cracking of the ground during rapid cooling events (Weise, 1983). Thermal cracking occurs when the temperature below 0°C drops by 15°C within 12 hours (Van Vliet-Lanoë et al., 2004). Repeated cracking due to annual contraction of the ice in the wedge followed by water refreezing in the crack leads to a gradual increase of the width and depth of the wedge and the vertical banding of the ice mass (Harry, 1988; Collinson et al., 2006).

The size of ice wedges varies from less than 10 cm to more than 3 m in width at the top. Some ice wedges may extend downward up to 25 m and can also have non-wedge-like shapes (Harry, 1988).

There are two types of ice wedges: epigenetic and syngenetic ice wedges (e.g. Washburn, 1980; Harry, 1988; French, 2013). Epigenetic ice wedges grow in the pre-existing substrate, are characteristically wedge-shaped and extend downwards to the isothermal permafrost (see Fig. 14). Syngenetic ice wedges are typically irregular in shape, extend deeper down than epigenetic ice wedges and form during continued sedimentation (Weise, 1983). Ice wedges that grow as a result of repeated winter cracking are called active ice wedges. They occur primarily in areas of continuous permafrost by mean annual temperatures of -6°C to -8°C (Weise, 1983). Inactive ice wedges can be stable and remain for many centuries without changing (Harry, 1988).

Ice wedge casts are remaining structures that indicate permafrost in the Pleistocene sediments. An ice wedge cast fills the space formerly occupied by ice. Ice wedge casts are recognised as the most precise and widespread indicators of past periglacial conditions and permafrost (Péwé, 1973). Examples are shown in Figure 17a, b.

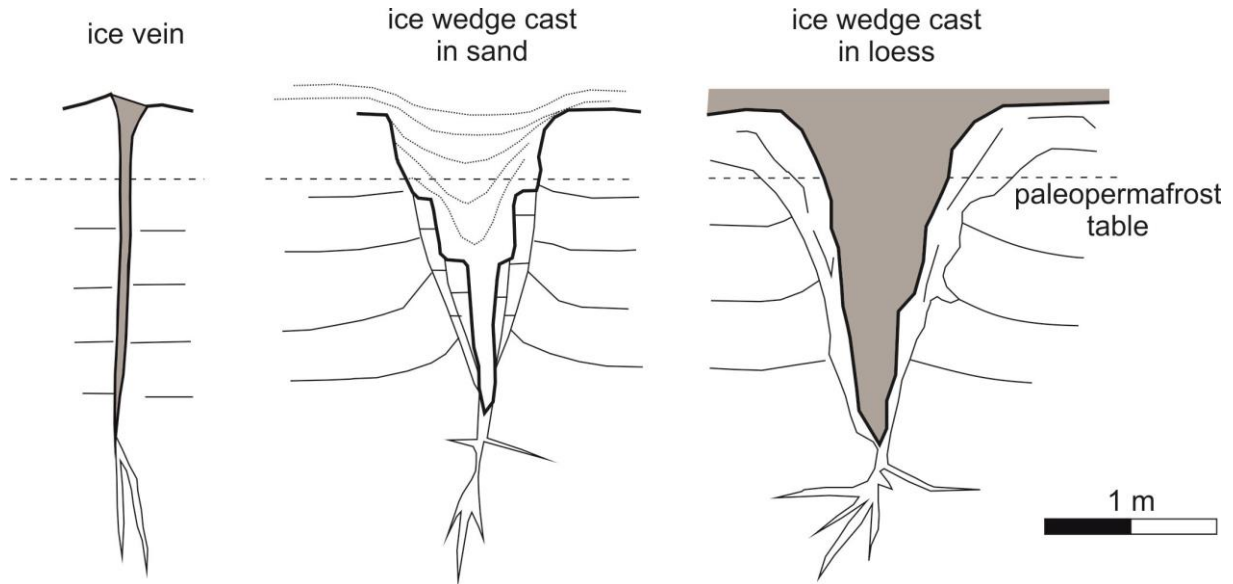


Fig. 16: Periglacial ice wedges and ice wedge casts in different sediments (modified according to Van Vliet-Lanoë et al., 2004).

3.3.4.2. Periglacial involutions

Another frequent indicator of cryoturbation are so-called involutions (Fig. 15). Involution and convolute bedding describe comparable structures that originate from liquefaction (Vandenberghe, 2013). Evidence of involutions has been widely reported from past or present periglacial environments with permafrost or deep seasonal frost (Ogino and Matsuoka, 2007; Vandenberghe, 2013). Involutions in regions with seasonal frost have smaller vertical amplitudes (0.6 m) than involutions that have developed in permafrost region, which can reach amplitudes of up to 2 m (Murton and French, 1993, cf. Vandenberghe, 2013). However, the size of involutions can also differ with the lithology and forming process (Ogino and Matsuoka, 2007). Examples of periglacial involution are shown in Fig. 17c.

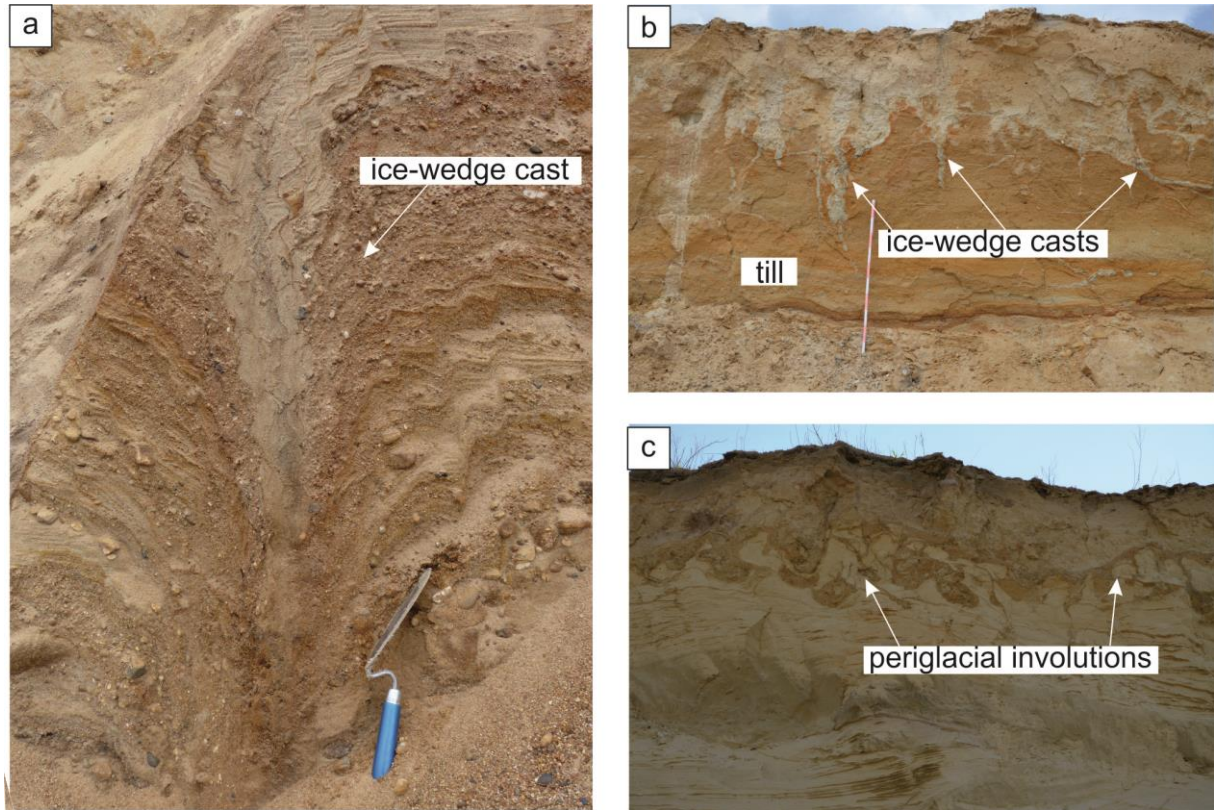


Fig. 17: Examples of typical cryoturbation structures. a) Pit 90, Bolsehle. Ice wedge cast in glaciolacustrine deposits; b) pit 45, Garßen. Ice wedge casts in the upper part of a 3.5-m-thick till bed; c) pit 54, Hülseberg. Periglacial involutions in meltwater sand and silt.

3.4. Summary

Various soft-sediment deformation structures can result from neotectonic and glaciotectonic deformation and cryoturbation processes. Because many different processes can produce comparable soft-sediment deformation structures, it is difficult to derive the driver for these structures. Figure 18 presents a summary of soft-sediment structures with the related deformation mechanism and the possible driver.

Drivers are flood events, seismic events, depositional loading, glacial loading proglacial and subglacial compression, periglacial freeze and thaw processes that trigger deformation.

Liquefaction can cause load structures, flame structures, pseudonodules, ball-and-pillow structures, convolute bedding and involutions, whereas fluidization causes intrusions, dish-structures, dish-and-pillar structures, clastic and irregular branched and stepped dykes and sand volcanoes.

Proglacial and subglacial glaciotectonic stress can lead to the formation of thrust sheets, folds and deformation bands with normal and reverse displacement as well as liquefaction and fluidization structures. However, deformation bands can be produced by additional drivers such as seismic events and freeze and thaw processes. Thermal cracking can lead to the formation of ice wedges. There are no unambiguous structures that indicate earthquakes.

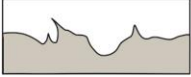





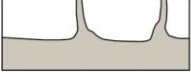
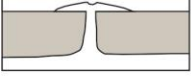
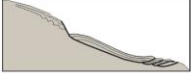



Sedimentary structures	Deformation mechanism	Possible driver
 load casts flame structures	liquefaction	depositional loading (Owen 2003); storm wave loading (Molina et al. 1998); glacial loading (Rijsdijk 2001); freezing and thawing (Bertran et al. 2019a); seismic event (Suter 2011)
 ball-and-pillow structures (pseudonodules)	liquefaction	depositional loading (Owen 2003; Owen & Moretti 2008); storm wave loading (Molina et al. 1998; Chen & Lee 2013); glacial loading (Rijsdijk 2001); freezing and thawing (Weise 1983; Bertran et al. 2019a); seismic event (Brandes & Winsemann 2013)
 convolute bedding (involutions)	liquefaction	depositional loading (Collinson et al. 2006); freezing and thawing (Weise 1983); seismic event (Chamley 1990)
 intrusions diapirs	liquefaction fluidization	depositional loading (Owen 2003; Suter et al. 2011); seismic event (Brandes & Winsemann 2013)
 dish-and-pillar structures	fluidization	depositional loading (Suter et al. 2011); seismic event (Suter et al. 2011)
 irregular branched and stepped dykes	fluidization	depositional loading (Alfaro et al. 2002); seismic event (Brandes & Winsemann 2013)
 clastic dykes	fluidization	depositional loading (Alfaro et al. 2002); glacial loading (Boulton & Caban 1995); freezing and thawing (Weise 1983; Bertran et al. 2019a); seismic event (Rodríguez-Pascua et al. 2000; Suter 2011; Brandes & Winsemann 2013)
 mud and sand volcanoes (sand blows, sand boils)	fluidization	depositional loading (Alfaro et al. 2002; Pisarska-Jamroży & Weckwerth 2013); storm wave loading (Chen & Lee 2013); flood events (Li et al. 1996); glacial loading (Benn & Evans 2013); freezing and thawing (Bertran et al. 2019a); seismic event (Brandes & Winsemann 2013)
 folds and thrusts	slumping, creeping	gravity-induced sediment failure (Collinson et al. 2006; Pisarska-Jamroży 2013); freezing and thawing (Bertran 1993); seismic event (Perucca et al. 2014)
 folds, thrusts and thrust-sheets	glacial stress	proglacial compression (Phillips et al. 2008; Brandes & Le Heron 2010; Pedersen 2014)
 ice-wedge casts	thermal cracking	freezing and thawing (Weise 1983)
 deformation bands	tectonic or gravitational stress	glacial loading (Phillips et al. 2008); proglacial compression (Phillips et al. 2008); freezing and thawing (Bertran et al. 2019a); fault movements (Brandes et al. 2018a); salt tectonics (Fossen 2010)

Fig. 18: Formation of soft-sediment deformation structures by different mechanisms and drivers (modified according to Müller et al., *in press c*).

4. Methods

4.1. Selection of outcrops and fault systems

The traces of the seven major fault zones (Aller Valley Fault, Halle Fault system, Harz Boundary Fault, Gardelegen Fault, Osning Thrust, Steinhuder Meer Fault and Elbe Lineament) were transferred to satellite images taken from GoogleEarth. The fault traces were taken from publications (e.g. Baldschuhn and Kockel, 1999; Lohr et al., 2007; Kley and Voigt, 2008) and geological maps (e.g.

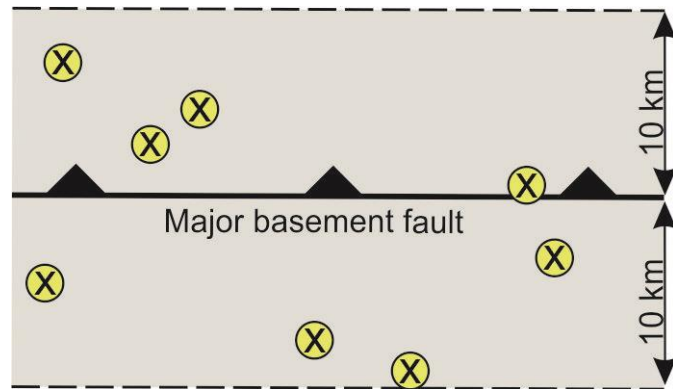


Fig. 19: Schematic representation of the 20-km-wide study area along a major basement fault. The yellow dots represent sand and gravel pits (X marks the number of the pit) within this strip that are feasible for further analyses. Increasing distance from the major basement fault decreases the likelihood of earthquake indicators expected in this intraplate setting.

Baldschuhn and Kockel, 1987; Martiklos et al., 2001). All sand and gravel pits in the vicinity of the fault traces were mapped from GoogleEarth images. Pits located within a 10 - 20 km wide strip along the individual fault zones were taken into account (Fig. 19). All pits up to 10 km away from the major basement fault were selected for the analysis (see Fig. 19) resulting in a 20-km-wide study area around the fault trace. At the Harz Boundary Fault only the sand and gravel pits north of the fault were investigated within a 20-km-wide area.

Natural outcrops of Pleistocene sediments are almost absent and trench studies of all major basement faults is very time consuming and expensive. Sand and gravel pits in Middle to Late Pleistocene deposits were therefore selected as the best compromise for the analysis of deformation structures in the vicinity of the major faults. Geological maps (scale 1:25 000 and 1:50 000) and reports and borehole logs from LBEG NiBis mapserver were used to estimate the depositional ages of the exposed sediments. The results of this outcrop selection process are summarised in Interim Report 1 (Müller et al., 2016). 97 sand and gravel pits were identified for a further analysis in total. All pits selected as part of this project are listed in the Appendix in Table A5 – A11. The different working steps are summarized in a flow chart (Fig. 20).

4.2. Fieldwork

The fieldwork investigated the depositional environment and the deformation structures. We used a handheld GPS (Garmin 60CSx) to derive the exact location of the outcrops. Geological maps were used for an initial stratigraphic overview. A geological compass (Clar method) was used to measure the orientation and dip of sedimentary and deformation structures. Cameras and field books were used for documentation. Material for luminescence dating (metal tubes, sample bags and tape) was used in some locations.

The orientation of tectonic fabrics and sedimentary structures was measured with a standard Freiberg compass (GeKom model from Breithaupt, Kassel). All measurements were executed using the Clar method, which allows the orientation and dip of a plane to be deduced in one single process. This is especially useful for measuring fabrics in unconsolidated sediments where the structures might otherwise be destroyed. The Clar method has a clear advantage over the strike and dip method, which is two-step procedure and often unsuited to structures in unconsolidated sediments. The Clar method measures the dip-direction of a plane as an azimuth. The results are expressed in the format XXX/YY, where XXX is the dip-direction (0 – 360°) and YY is the dip angle (0 – 90°). This value represents the orientation of a tectonic fabric (e.g. a fault plane) and can be easily visualized in stereographic projections.

4.2.1. Sedimentological analysis

A sedimentological analysis of the exposed sediments based on sedimentary facies and facies associations was carried out to reconstruct the depositional environment.

Outcrops were first documented using photographs and sketches. Bedform geometries and the lateral and vertical stacking patterns of sedimentary facies were then mapped from the outcrops to determine the depositional environment. The main paleo-flow direction was determined based on the dip direction of e.g. foreset beds of dunes and ripples using a geological compass.

The exposed sediments comprise aeolian, alluvial, fluvial, glaciofluvial and glaciolacustrine Middle to Late Pleistocene deposits.

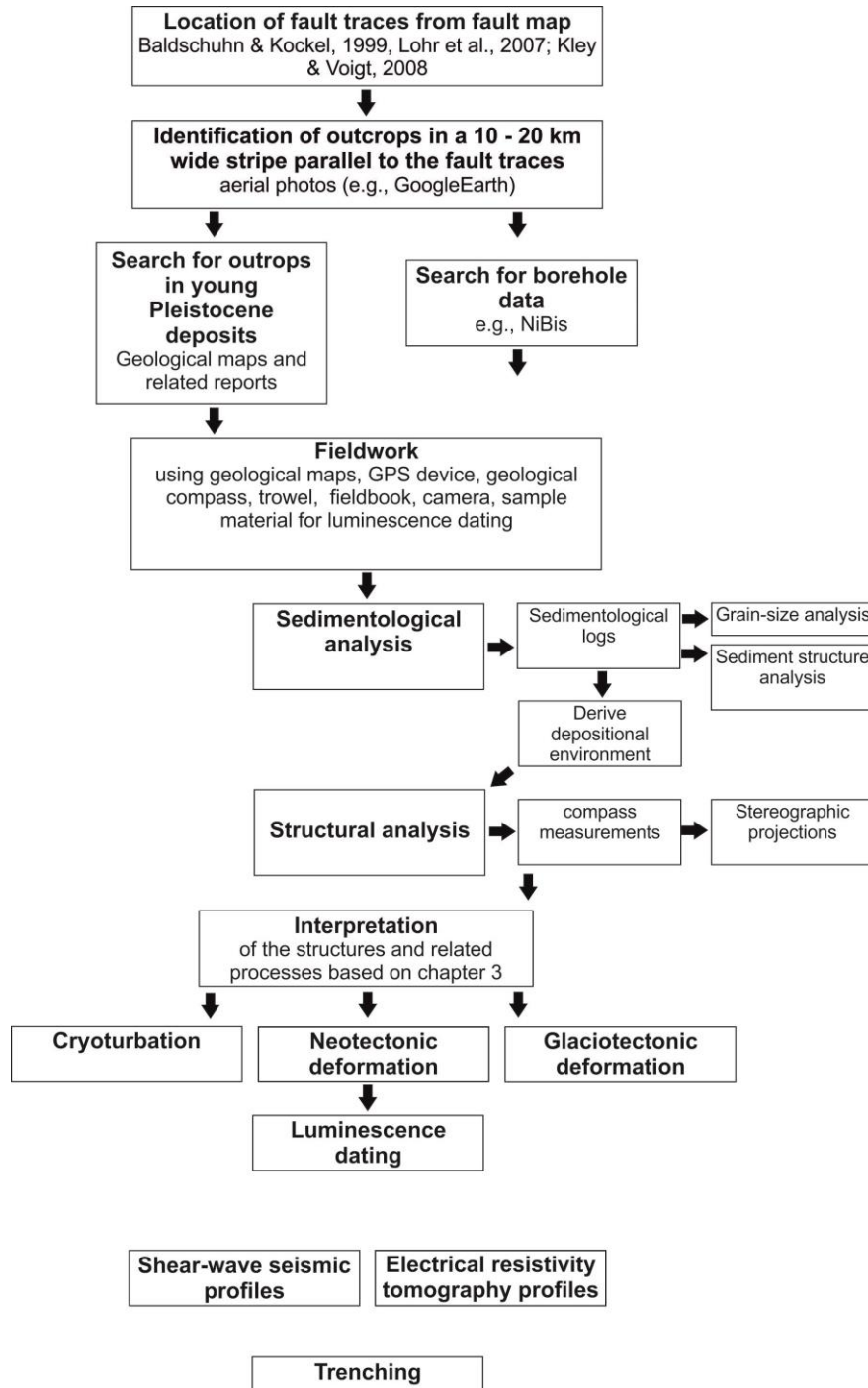


Fig. 20: Flow chart of the different working steps for finding evidence of neotectonic movements, especially paleo-earthquakes along major basement faults. The steps not connected with arrows (shear wave seismic profiles, electrical resistivity tomography profiles and trenching) were not part of the project, but constitute key methods for further analysis.

4.2.2. Structural analysis

It is important to analyze the entire outcrop to provide a robust interpretation of the deformation structures. The identification and classification of the different deformation structures is the basis for correctly identifying driving processes. Knowledge about the

depositional environment is important for the interpretation of the deformation structures. If an outcrop is revealed to have a till bed, it is evident that the area was overridden by a glacier and potential structural elements are most likely the product of glaciotectonic processes rather than neotectonic features caused by basement fault activity. The next step is to analyze the exposed deformation. The interpretation of the deformation structures is based on the latest methods described in Chapter 3. The type (fold, fault, shear-deformation band with normal or reverse displacement) of structure and the stratigraphic unit in which they have developed is important. Knowledge of the orientation of these structures is required for a correct interpretation and a subsequent paleo-stress field analysis.

The orientation of the soft-sediment deformation structures analyzed was then compared with the direction of ice sheet advances and the orientation of the major basement faults. The orientation of tectonic fabrics and sedimentary structures analyzed are displayed as stereographic projections. These projections are commonly used in geoscience and represent the lower hemisphere of a sphere (Fig. 21) as well as the orientation of planar and linear tectonic fabrics like fault planes and striations in 2D. The line of intersection of a plane and the sphere surface generates a so-called great circle that visualizes the dip angle and dip direction of the plane (e.g. Reuther, 2012).

Linear tectonic fabrics such as striations are projected as points. Striations on a fault plane appear as points on the great circle, where the points represent the direction of movement and the great circle represents the orientation of the fault plane.

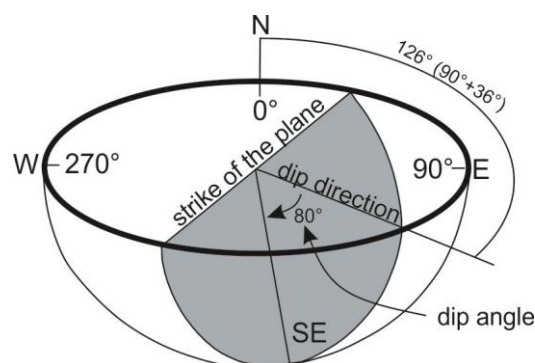


Fig. 21: Example of a stereographic projection of a plane that dips 80° SE (modified according to Möbus, 1989).

4.3. Luminescence dating

Luminescence dating was used to derive the age of the fault movement in places where growth strata had developed.

Luminescence dating has great potential in paleoseismic studies for younger Holocene and Late Pleistocene sediments and for a better understanding of neotectonic processes (Rittenour, 2008; Rhodes, 2011). Direct sampling of target features and deposits is possible. Samples are taken from tectonically disturbed and overlying undisturbed sediments to estimate the time of deformation. However, the dating of glacial sediments is challenging because the deposits may have been poorly bleached. In addition, the uncertainty of individual luminescence ages typically ranges between 5 - 10% (Duller, 2008), which limits the age estimate for Middle Pleistocene fault movements.

Luminescence dating gives absolute ages that indicate the last time when sediments were exposed to the sunlight. In most cases, this represents the depositional age of sediments (Aitken, 1998).

The basic concept behind the luminescence method is the increase of radiation damage in the crystal lattice of nonconductive minerals, e.g. quartz and feldspar (Fuchs and Owen, 2008). Energy is trapped and released in the crystals over a period of time (Aitken, 1985). Due to natural radiation in the sediment, energy is added to electrons in the crystal, which move from a lower to a higher energy level. Some of these electrons can be trapped in a metastable state in crystal defects between these two energy levels. By adding energy in the form of light or temperature these electrons drop back to a lower energy level by emitting photons. This light emission is named luminescence. Luminescence dating measures the intensity of the light emitted, which is proportional to accumulated dose and time since deposition (Fig. 22; Duller, 2008). More details are given in Aitken (1998).

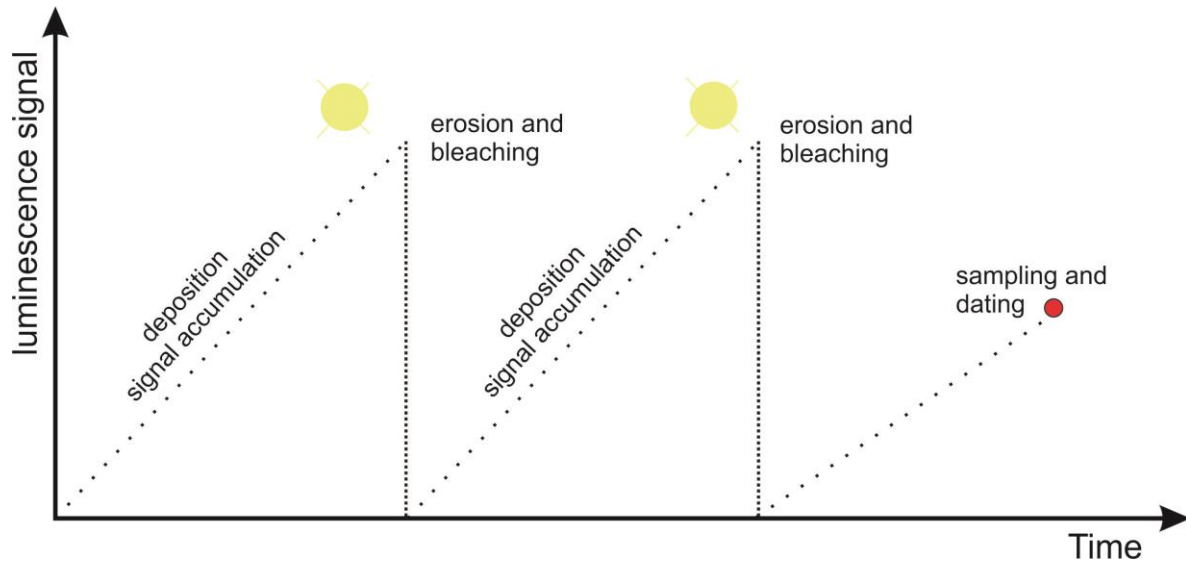


Fig. 22: Accumulation of the luminescence signal through time (modified according to Aitken, 1998).

4.3.1. Sample collection and preparation

Samples for luminescence dating were taken from outcrops near the Harz Boundary Fault (Benzingerode outcrop 5) and the Steinhuder Meer Fault (Altenhagen pit 89) for this study.

Opaque metal tubes were hammered into the freshly cleaned sediment surface and covered with aluminum foil to avoid light exposure during the sample collection. Additionally, samples (700 g) were taken from the surrounding sediment at each sample position to determine the dose rate.

The outer ends (2 cm) of the undisturbed material in cylinders were removed to exclude the sediment that had been exposed to light. 50 - 100 g of the sample material was dried at $\leq 50^{\circ}\text{C}$ to measure the luminescence signal.

There are two different ways to prepare samples for luminescence dating. A distinction must be made between a) coarse-grained samples; here we used the fraction 150 - 200 μm and b) fine-grained samples; here we used the fraction 4 - 11 μm . The preparation of the samples for the luminescence measurements was carried out under subdued red light in the luminescence laboratory at the Leibniz Institute for Applied Geophysics (LIAG), Hannover.

The samples were chemically treated with 10% hydrochloride acid (HCl) until the reaction stopped. 200 ml disodium oxalate ($\text{Na}_2\text{C}_2\text{O}_4$) was then added for 2 hours and 30% hydrogen peroxide (H_2O_2) was added for 12 hours to dissolve carbonates, break up aggregates and to eliminate the organic matter. Different steps followed A) and B) depending on the grain size.

A) Fine-grained samples

The grain fraction of 4 - 11 μm was separated to measure the luminescence signal of quartz and polymineral fine grains. For the quartz aliquots, a part of the sample was treated with 40% hexafluorosilicic acid (H_2SiF_6) to remove minerals other than quartz (Prasad, 2000; Fuchs et al., 2005). Finally, the polymineralic and quartz aliquots were mounted on aluminium discs to measure the luminescence signal.

B) Coarse-grained samples

Coarse-grained samples were sieved before they were chemically treated to obtain the fractions: $>250 \mu\text{m}$, 200 - 250 μm , 150 - 200 μm , 100 - 150 μm , $<100 \mu\text{m}$. We chose the fraction 150 - 200 μm for further analysis.

A separation of feldspar and quartz minerals was implemented by using sodium polytungstate (2.62 g/cm^3). This procedure was implemented twice more with densities of 2.58 g/cm^3 and 2.70 g/cm^3 . Sodium polytungstate with a density of 2.58 g/cm^3 was used for the separation of potassium feldspar and plagioclase and a density of 2.70 g/cm^3 was used for the separation of quartz and heavy minerals. For the quartz aliquots, a part of the sample was treated with 40% hexafluorosilicic acid (H_2SiF_6) to remove the outer layers of the minerals affected by α -radiation. Finally, the feldspar aliquots were mounted on stainless steel discs using silicone to measure the luminescence signal.

4.3.2. Dose rate determination

The radionuclide concentrations of uranium (U), thorium (Th), and potassium (K) were measured using high-resolution gamma spectrometry. 700 g of the sediment surrounding each sample was dried ($130 \text{ }^\circ\text{C}$) homogenized and packed into Marinelli beakers. The samples were stored for at least six weeks before measuring in order to achieve an equilibrium between radon and its daughter nuclides. The radiation dose

rates were calculated using the conversion factors of Guérin et al. (2011) and the beta attenuation factors of Mejdahl (1979). An a -value of 0.04 ± 0.01 for quartz and an a -value of 0.09 ± 0.02 for feldspar was used (Rees-Jones, 1995). The in-situ water content of all samples was measured and used for the correction of the α -, β - and γ -dose rates. The cosmic dose rate was calculated depending on altitude, geomagnetic latitude and sediment thickness according to Prescott and Hutton (1994).

4.3.3. Luminescence dating

Feldspar and quartz luminescence signals were measured with two automated Risø TL/OSL readers (DA-20) with calibrated $^{90}\text{Sr}/^{90}\text{Y}$ beta sources (1.48 GBq = 40 mCi and 2.96 GBq = 80 mCi). Polyminerals were used for infrared stimulated luminescence (IRSL) dating, in which only the feldspar is stimulated by pulsed IR light-emitting diodes (LED) with wavelengths of 870 nm. In order to detect a stable IRSL signal with reduced anomalous fading, the feldspar signal was detected in the off-periods of each pulsed cycle with a Schott BG39/Corning 7-59 filter combination (Tsukamoto et al., 2006). The quartz signal was stimulated by blue LED diodes, emitting at 470 nm and detected through a Hoya U-340 filter. A single aliquot regenerative dose (SAR) protocol (Murray and Wintle, 2000) was applied for equivalent dose (D_e) determination.

Polymineral fine grain (feldspar)

Only sample Ben-2 (DF-1) was dated using polymineral fine grain because the other samples did not yield a measurable feldspar signal. A total of 8 aliquots were measured for the D_e determination. For the measurement, a preheat temperature of 250°C for 60 s and a pulsed IRSL signal was used (Table 1). The pulsed IR stimulation was performed at 50°C (IR_{50}) (see Table 1). To reduce anomalous fading of the feldspar, the signal was only detected in the off-period of the light source, 21.5 μs after the LED pulses are switched off (Tsukamoto et al., 2006, 2017; Jain et al., 2015).

A dose recovery test was carried out using 4 aliquots to check whether the protocol was suitable. The aliquots were bleached for 4 hours in the solar simulator for the dose recovery ratio. A dose close to the expected natural one was given and the same SAR protocol was applied to check whether the given dose could be accurately recovered.

The protocol is considered suitable, if the dose recovery ratio is within the range of 0.9-1.1 (Wintle and Murray, 2006).

Quartz fine grain

A total of 8 quartz aliquots per samples were measured at Benzingerode. The preheat temperature, which should be selected for accurate equivalent dose determination (D_e), was determined by applying the preheat plateau test at six different preheat temperatures (160 - 260°C) with a fixed low cutheat temperature of 160°C. This low cutheat temperature is suggested for dating young samples (Madsen and Murray, 2009). A dose recovery test was also performed. Details about this procedure are shown in Wintle and Murray (2006). According to the results, we selected a preheat temperature of 240°C for the quartz D_e measurement of samples Ben-2 to Ben-7 using the SAR protocol shown in Table 1. Only sample Ben-2 yielded a reliable quartz luminescence age. The other samples (Ben-3 to -7) were in saturation.

Table 1: SAR protocol used for equivalent dose determination of feldspar and quartz samples taken at the Harz Boundary Fault. (a) 100 ms on and 400 ms off.

Step	Treatment Feldspar IRSL (polym mineral)	Quartz OSL	Observed
1	Give dose	Give dose	
2	Preheat, 250°C, 60 s	Preheat, 240°C, 10 s	
3	Pulsed IRSL, 50°C, 500 s _a	OSL, 125°C, 40 s	Lx
4	Test dose	Give test dose	
5	Preheat, 250°C, 60 s	Heat to 160°C	
6	Pulsed IRSL, 50°C, 500 s _a	OSL, 125°C, 40 s	Tx
7	Return to step 1	Return to step 1	

Feldspar coarse grain

12 aliquots per sample were used for feldspar D_e determination of Alt-1 and Alt-2. A pulsed infrared stimulated luminescence (IRSL) single aliquot regenerative (SAR) dose protocol (Table 2) was used for the measurement. The pulsed IRSL signal was measured at 50°C (IR₅₀) and used to reduce anomalous fading from feldspar.

At least 12 aliquots per sample were measured and only aliquots passing the following criteria were used: recycling ratio limit within 10% of unity, maximal test dose error

10%, and signal intensity larger than 3 sigma above the background. Dose response curves were fitted with a saturating exponential function to calculate D_e values.

Table 2: SAR protocol used for equivalent dose determination of feldspar samples taken at the Steinhuder Meer Fault. (a) 100 ms on and 400 ms off.

Step	Treatment	Observed
	Feldspar IRSL (polym mineral)	
1	Give dose	
2	Preheat, 250°C, 60 s	
3	Pulsed IRSL, 50°C, 500 s ^a	Lx
4	Test dose	
5	Preheat, 250°C, 60 s	
6	Pulsed IRSL, 50°C, 500 s ^a	Tx
7	Return to step 1	

Fading tests

Fading tests are necessary because feldspar minerals are affected by a phenomenon called anomalous fading, in which a loss of trapped electrons induced by tunnelling has occurred (Wintle, 1973; Spooner, 1994). This phenomenon can lead to an underestimation of the age (Wintle, 1973; Jain et al., 2015). A fading correction was therefore performed for feldspar aliquots by determining the anomalous fading rate under laboratory conditions (Huntley and Lamothe, 2001; Kars et al., 2008). For young samples (up to 50 ka) age correction models relating to the “linear part” of the dose response curve are used (Huntley and Lamothe, 2001). Fading rates (g-values) were determined by using 8 aliquots per sample using the log-decay model (Huntley and Lamothe, 2001).

Age calculation

The fading uncorrected pulsed IR₅₀ feldspar and quartz ages were calculated using the mean D_e value of all accepted aliquots. The fading corrected age of feldspar sample Ben-2, Alt-1 and Alt-2 was calculated using R-software (R version 3.3.2). This is based on Huntley and Lamothe (2001). The IRSL and OSL ages were calculated by dividing the D_e by the total dose rate.

4.4. Further analyses

Further analyses should be conducted to verify structures that indicate potential neotectonic movements or paleo-earthquakes (e.g. deformation bands and/or seismites, see Fig. 20). Shear wave seismics and electrical resistivity tomography are well-suited methods for providing insight into the structure of the near-subsurface. Following successful geophysical analyses, the next step would be the trenching of the fault zone. These further analyses were not part of the present project.

5. Seismic database and Environmental Seismic Intensity scale (ESI)

5.1. Important catalogue of historic earthquakes

The catalogue important for this study is Leydecker (2011) *Erdbebenkatalog für Deutschland mit Randgebieten für die Jahre 800 - 2008*.

5.2. The ESI scale

The ESI scale (Environmental Seismic Intensity scale, ESI 2007) is a 12-degree macroseismic intensity scale based on the effects triggered by an earthquake in the natural environment (Fig. 23; Michetti et al., 2007). In contrast to other scales, which are based on impacts on buildings and humans, the ESI 2007 relies on earthquake-related effects observed in the natural environment. Indicators are surface faulting and tectonic uplift or subsidence (so-called primary effects), landslides, ground cracks, liquefaction, displaced boulders, tsunamis and hydrological anomalies (so-called secondary effects) (Michetti et al., 2007). The ESI 2007 scale follows the same basic structure as e.g. the Mercalli Intensity Scale (MCS), the Modified Mercalli Intensity Scale (MMIS), the Medvedev-Sponheuer-Karnik Scale (MSK) and the European Macroseismic Scale (EMS) (Michetti et al., 2007).

5.3. The paleoseismic database of Germany and adjacent regions (PalSeisDB)

Tectonically active faults and paleoseismic features have been differently and inconsistently studied and documented in Germany and adjacent regions. The aim of the paleoseismic database of Germany (PalSeisDB) is to provide a harmonized, extended paleoseismic database (Hürtgen, 2017) that contains a large number of key publications. PalSeisDB contains the basic idea of the ESI scale that includes all environmental effects caused by earthquakes. It provides information on seismic hazard analyses. The time window covered by the database is limited to a period between the Eemian (MIS 5e, ca. 125 ka; Cohen and Gibbard, 2016) and prehistoric times (approx. 1000 BP).

The structure of PalSeisDB v.1.0 is based on paleoseismic features: the paleoseismic source, paleoseismic event and paleoseismic evidence (Hürtgen, 2017). A paleoseismic source is a fault, the event is an earthquake and evidence are e.g. SSDS in trenches, mass movements or other evidence (Hürtgen, 2017). The PalSeisDB is based on the Environmental Seismic Intensity scale, ESI 2007 according to Michetti et al. (2007).

Fig. 23: The Environmental Seismic Intensity scale (ESI 2007) is a seismic scale used for measuring the intensity of earthquakes on the basis of their effects on the natural environment (from Michetti et al., 2007).

ESI-2007		PRIMARY EFFECTS		SECONDARY EFFECTS WITH GEOLOGICAL AND GEOMORPHOLOGICAL RECORD				OTHER SECONDARY EFFECTS		AFFECTED AREA AND TYPE OF RECORD	
		SURFACE RUPTURES	TECTONIC UPLIFT/SUBSID	GROUND CRACKS	SLOPE MOVEMENTS	LIQUEFACTION PROCESSES	ANOMALOUS WAVES AND TSUNAMIS	HYDROGEOLOGICAL ANOMALIES	TREE SHAKING	Affected Area	Type of Record
		Offset	Length	Width	Length	ENVIRONMENTAL EFFECTS ARE VERY RARE AND CANNOT BE USED AS DIAGNOSTIC					
OBSERVED DAMAGING DESTRUCTIVE VERY DESTRUCTIVE DEVASTATING	I-III										
	IV	ABSENT	ABSENT	Rare and local	Rare and local	Only dewatered levels (seismites)	cm Temporary sea-level changes	Temporary level changes Temp. turbidity changes Temporary F+Q changes		Rare and local	Geological frequent and exceptionally geomorphological
	VII	Rare and local	Permanent ground dislocations (< 10 cm)	mm	mm	1 cm 3 cm 50 cm	dm Waves < 1 m			Local within epicentral zone	
	VIII	cm	< 1 m	cm	cm	1 m	1-2 m	Temp. temperature changes		100 km ²	Geological and geomorphological characteristic
	X	dm	< 10 m	m	m	0.5 m	3-5 m	Temp. spring drying		1,000 km ²	
	XI	metric	> 10 m	> 1 m	m	> 5 m	> 10 m	Permanent river changes		5,000 km ²	
	XII	> 100 km	> 100 km	> 5 m	m	> 5 m	Tsunamis Giant waves			10,000 km ²	
		Dip and strike-slip offset of coseismic ruptures	Permanent ground dislocation	Width and length of cracks and fractures in soils and rocks	Bulk volume of mobilised material	Dimension of liquified levels and sand boils	Transitory sea-level changes, standing waves and Tsunamis	Base-level changes in springs, rivers, aquifers	Tree branches and tree-trunk falling, rupture, etc...	50,000 km ²	

6. Results

The main results of the outcrop analysis located in the vicinity of the major basement faults are described in this chapter (Fig. 24). A detailed analysis of the different pits was presented in the Interim Reports 1 to 6 (Müller et al., 2016; 2017a, b; 2018a, b, c).

Deformation structures have been found in 47 of the 97 pits analyzed. The results of this final report only deal with the sand and gravel pits in which deformation structures were found. Fig. 24 only shows the sand and gravel pits with deformation structures for a better overview. All pits were listed in the Appendix in Tables A1 – A7. All pits analyzed were described in detail in the Interim Reports 1-6 (Müller et al., 2016; 2017a, b; 2018a, b, c). The deformation structures have been caused by glaciotectonic, neotectonic and cryoturbation processes. In a few cases, it was not possible to determine the deformation process because the structures were inaccessible and prevented further analysis.

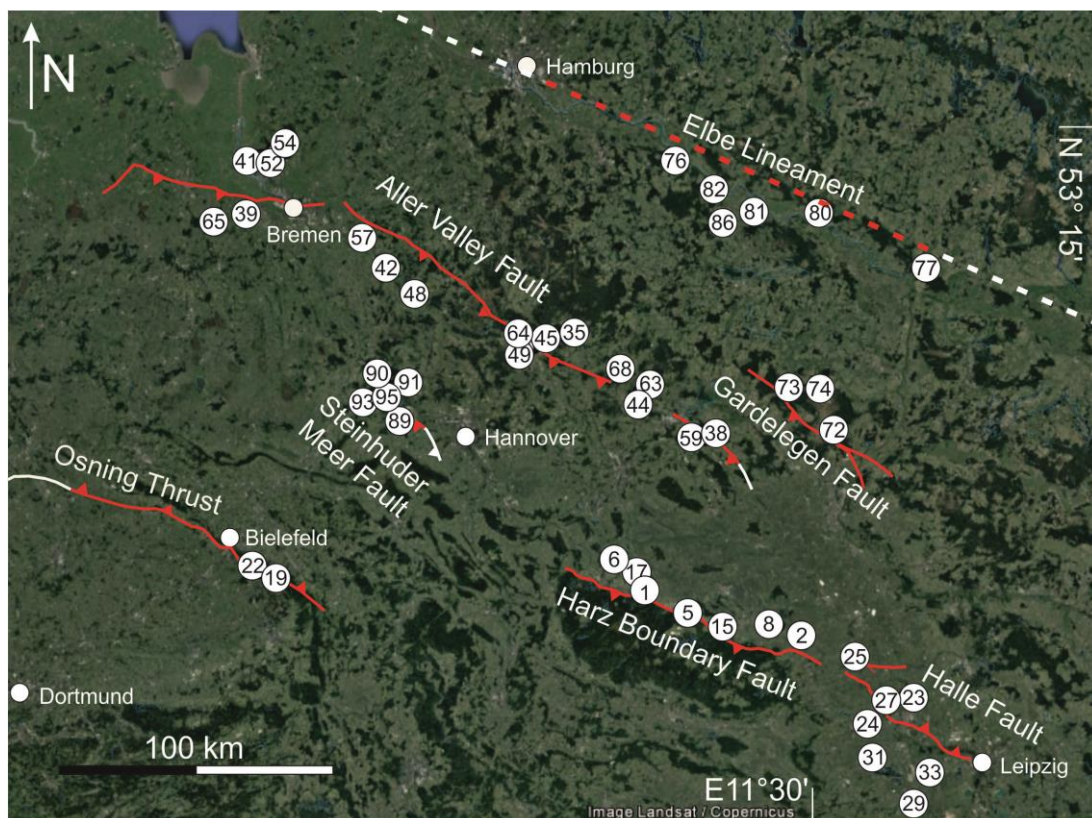


Fig. 24: Map of the seven major fault zones in northern Germany with the location of sand and gravel pits analyzed. Only the sand and gravel pits are shown in which deformation structures are exposed in this figure. Fault traces are taken from Baldschuhn and Kockel (1987, 1996), Martiklos et al. (2001), Lohr et al. (2007), Kley and Voigt (2008). Red marks the section of the fault analyzed (see also Fig. 2c)

The deformation structures are summarized in seven tables, one for each fault system. The deformation structures are interpreted based on Chapter 3. The uncertainty of the interpretation is then estimated. Low uncertainty means that the interpretation is reliable because various indicators allow the deformation process to be classified (see Tables 3, 6, 7, 8, 9, 10, 13). Medium uncertainty means that there were clear indicators that allow the deformation process to be classified, but the number of the deformation structures was low. High uncertainty means that the deformation structures could not be unambiguously interpreted because the structures were inaccessible due to high outcrop walls thus preventing further analysis. The age estimates of Pleistocene deposits are based on geological maps and luminescence dating. Note that these ages may not represent the age of the deformation unless mentioned. X marks the interpreted deformation process (based on Chapter 3) responsible for the deformation structure.

6.1. Harz Boundary Fault

17 sand and gravel pits and sinkholes were identified using geological maps and GoogleEarth images at the Harz Boundary Fault. Five of these pits were abandoned and refilled. No deformation structures occur in four pits and deformation structures are exposed in eight outcrops (see Table 3 and Fig. 24, 25). A detailed analysis of all outcrops is given in Interim Report 2 (Müller et al., 2017a).

Table 3: Sand and gravel pits with deformation structures and the uncertainty of the interpretation at the Harz Boundary Fault.* Note that the ages of outcrop 5 show luminescence ages of the latest fault movement.

Pit Nr.	Location	Glaciotec. features	Neotec. features	Cryo. features	Uncertainties	Age of deposits
1	Abbenrode	X			Low	Eocene
2	Aschersleben 1			X	Low	Middle Pleistocene
5	Benzingerode		X		Low	*Late Pleistocene *OSL15.2 ± 0.8 ka *IRSL14.2 ± 0.8 ka
6	Beuchte			X	Low	Middle Pleistocene
8	Hoym	X			Low	Middle Pleistocene

11	Quedlinburg		X	Low	Middle Pleistocene
15	Warnstedt	X	X	Low	Pleistocene
17	Wiedelah		X	Low	Pleistocene

The sand and gravel pits analyzed in the vicinity of the Harz Boundary Fault expose Pleistocene meltwater and fluvial deposits partly covered by loess. In addition, young faulted debris-flow deposits exposed in two sinkholes were analyzed. Some small-scale extensional and contractional deformation structures as well as cryoturbation features occur in the sand and gravel pits analyzed. Extensional structures include shear-deformation bands with normal displacement. Contractional features include folds. Cryoturbation features comprise ice wedge casts and large-scale involutions. The orientation and the temporal framework of the extensional and contractional structures imply that these structures evolved as near-surface glaciotectonic features during the Middle Pleistocene glaciations. Cryoturbation features are indicators for later periglacial conditions.

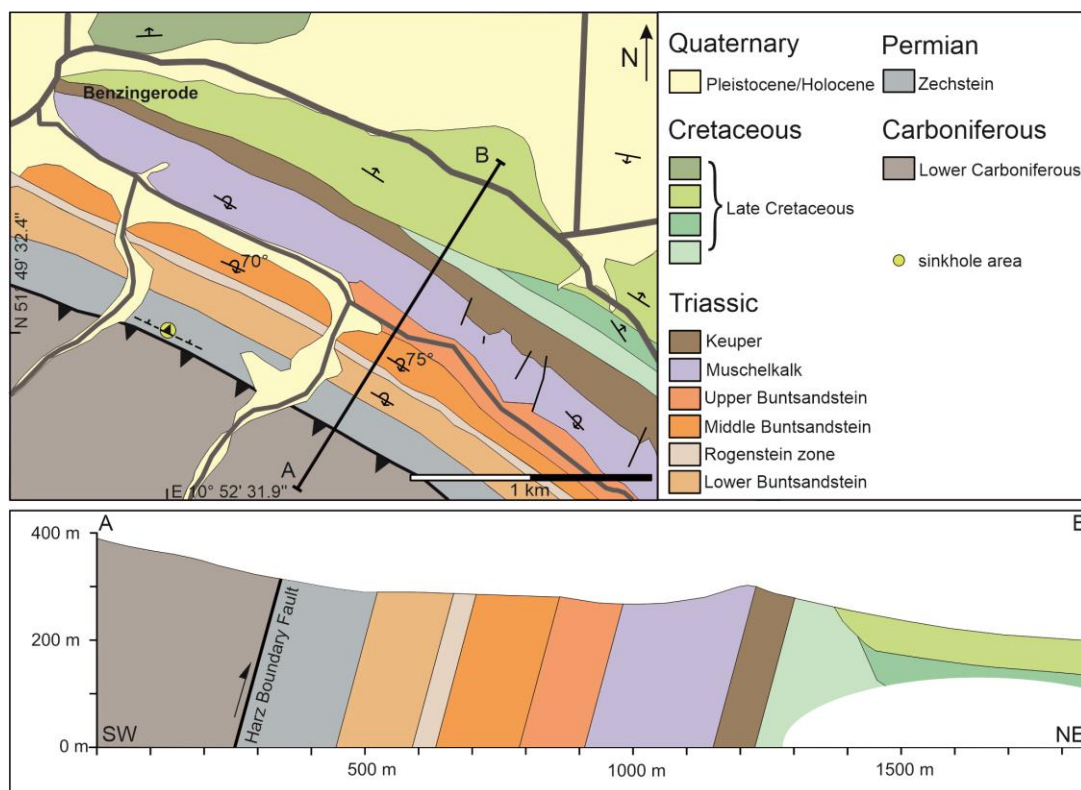


Fig. 25: Geological map of the study area with geological cross-section (modified according to Schröder et al. 1927; from Müller et al., *in press a*).

In one of the sinkholes near Benzingerode (Fig. 25, 27), which is located directly at the Harz Boundary Fault, a fault is exposed that cuts through unconsolidated debris-flow deposits. The sinkhole formed in the overturned Zechstein Werra-sulfate that belongs to the Zechstein Z1 sequence (Schröder et al., 1927; Franzke et al., 2015), approximately 30 m north (Fig. 26 and 27) of the Harz Boundary Fault. The sinkhole has a depth of 2 m and a diameter of 3 m and exposes three different debris-flow deposits (Fig. 27a) that differ in colour, matrix and clast composition.

The basal debris-flow deposit (DF-1) has a reddish silty matrix and contains 60 - 70% angular greywacke clasts. This reddish debris-flow deposit is overlain by a whitish debris-flow deposit (DF-2) that contains 80% angular Zechstein clasts embedded in a silty carbonaceous matrix. These two debris-flow deposits are displaced by the fault and are overlain by a yellowish debris-flow deposit (DF-3) that is ~30 cm thick and seals the fault. This uppermost debris-flow deposit has a silty to fine-grained sandy carbonaceous matrix and contains 20% angular Zechstein clasts.

In the lower two debris-flow deposits (DF-1 and DF-2), an NNE-ward dipping and WNW-ESE striking planar fault has developed (Fig. 27). The limited outcrop situation in the sinkhole hinders the exact offset along the fault from being derived. The normal offset of the reddish debris-flow (DF-1) must have been at least 150 cm because the northern part of the debris-flow is not exposed in the sinkhole. This normal fault offset was not fully compensated by the later reverse offset of the fault.

The fault is characterized by two small bends that separate the fault plane into three segments. The lower segment has an average dip of 76° and the middle segment has an average dip of 60°. In contrast, the upper segment has a much steeper dip angle of 80° (Fig. 27b). Two sets of striations have developed on the fault plane (Fig. 27c). These striations indicate initial normal fault movements and a later reactivation of the fault as an oblique reverse fault (Fig. 27c). Similar fault kinematics of this fault were described by Franzke et al. (2015). The tip of the fault is sealed by the third yellowish debris-flow deposit (DF-3). The outcrop reveals that the fault has a complex structure, with a 7 - 9 cm thick core that contains several thin slip planes characterized by polished and striated surfaces and similar to fault cores shown in e.g. Faulkner et al. (2011) or Shipton and Cowie (2003). In addition, the fault core is partly flanked by an alteration halo. This alteration halo can be interpreted as part of the fault damage zone

that contains near-field, fault-related deformation (Vermilye and Scholz, 1998; Shipton and Cowie, 2003). The damage zone is likely to be the product of rupture processes (cf. Kim et al., 2004).

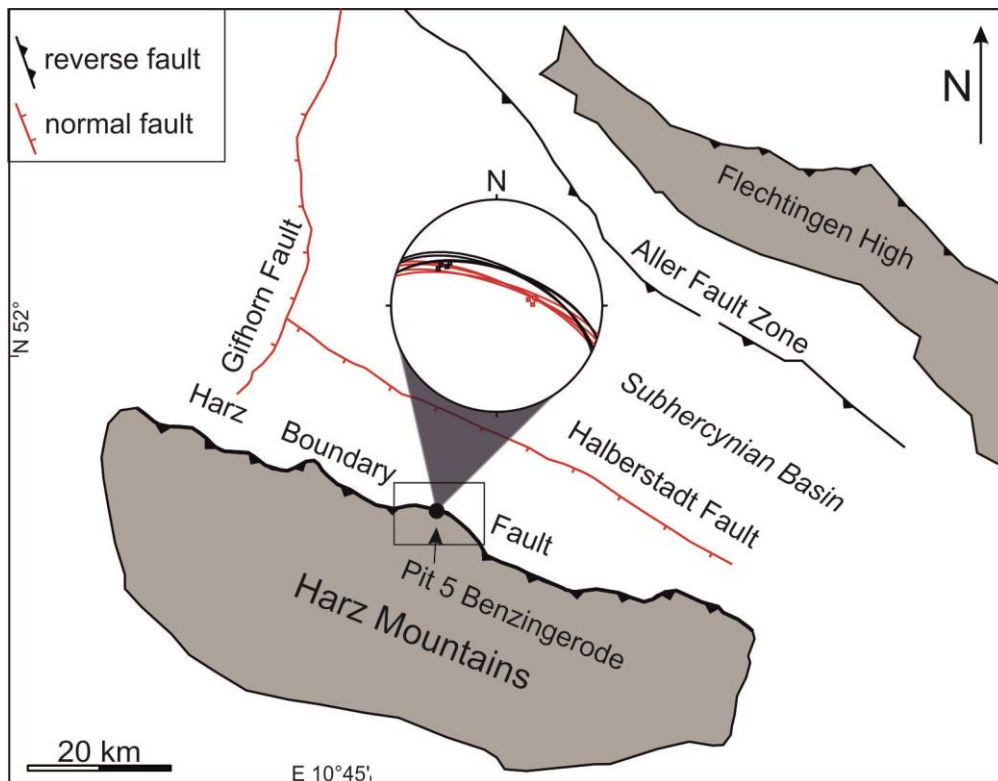


Fig. 26: Fault zone exposed in a sinkhole near Benzingerode (outcrop 5) showing a two-fault evolution with normal and reverse components. The fault follows the trend of the Harz Boundary Fault. This indicates a close relation between the Harz Boundary Fault and the fault in the sinkhole. The stereonet shows the data from the outcrop in the sinkhole (fault traces according to Martiklos et al. 2001).

We conducted luminescence dating of the faulted debris-flow deposits to estimate the time of fault movement (Fig. 27a). Seven samples were taken from the faulted sediments exposed in the sinkhole (N51°49'32.4" E10°52'31.9") close to the Harz Boundary Fault. In general, debris-flow deposits are difficult to date (e.g. Döhler et al., 2018), especially carbonate-rich debris-flows that are poor in quartz and feldspar minerals. Therefore, as many samples as necessary were taken to obtain a good coverage of the luminescence ages of the debris-flow deposits.

One sample (Ben-2) was taken from the basal reddish debris-flow (DF-1) in the footwall south of the exposed fault trace. Three more samples (Ben-1, Ben-3, Ben-4) were derived from the hanging wall block north of the fault plane (lower whitish debris-flow deposit; DF-2). Three further samples (Ben-5, Ben-6, Ben-7) were taken from the

yellowish debris-flow (DF-3) that seals the fault tip (Fig. 27a). The sample material of Ben-1 was too poor for luminescence dating because not enough material of the required grain-size was obtained during sample preparation.

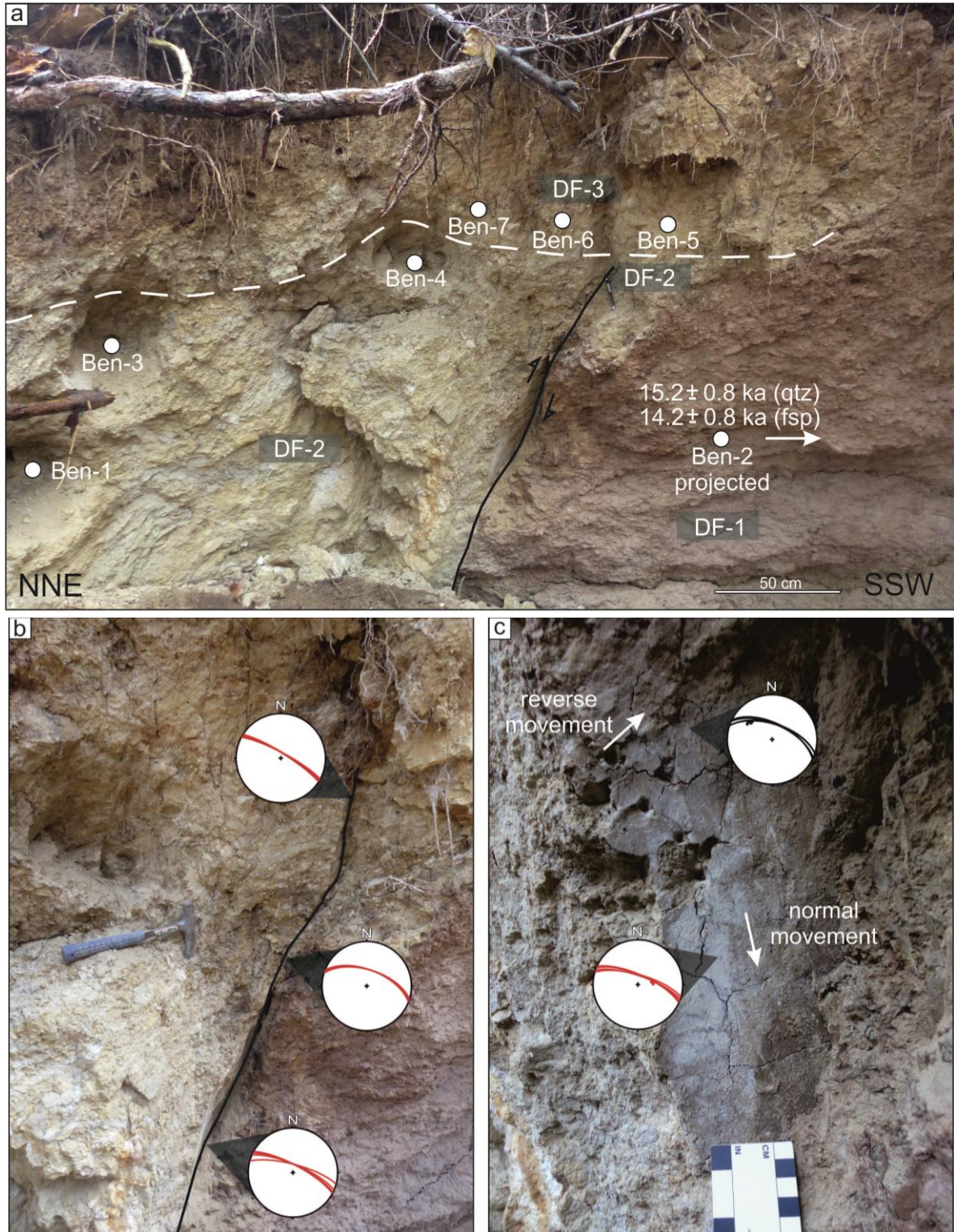


Fig. 27: Faulted debris-flow deposits exposed in a sinkhole near Benzingerode. a) Fault plane in Lateglacial debris-flow deposits and location of OSL and IRSL samples; b) stereographic projections of the normal fault component; c) stereographic projections showing normal and reverse fault kinematic components (modified according to Müller et al., *in press* a).

Results of luminescence dating

Basal reddish debris-flow (DF-1)

Sample (Ben-2) provided reliable luminescence ages. The dose recovery ratios 0.93 ± 0.01 for the pulsed IR₅₀ signal and 1.08 ± 0.01 for quartz OSL signal that were close to unity (0.9 - 1.1; Wintle and Murray, 2006) show that the applied SAR protocols were suitable for the D_e measurements.

The pulsed IR₅₀ signal of the fine grain fraction yielded a recycling ratio of 1.04 ± 0.03 and the quartz OSL recycling ratio was 1.02 ± 0.05 . The values are within 10% of unity (cf. Wintle and Murray, 2006) and show that the SAR protocol corrected sensitivity changes successfully during the measurements.

The fading test gave a mean g-value of $1.4 \pm 0.2\%$. The pulsed IR₅₀ age (12.8 ± 0.7 ka) was fading corrected using the R-software (R version 3.3.2.) based on Huntley and Lamothe (2001). The fading corrected polymineral fine grain age (feldspar) is 14.2 ± 0.8 ka.

The estimated dosimetry results and dose rates from samples from Benzingerode (outcrop 5) are listed in Table 4.

The estimated luminescence ages from the reddish debris-flow deposits (Ben-2) range in age from 14.2 ± 0.8 ka (polymineral, feldspar) to 15.2 ± 0.8 ka (quartz).

Whitish (DF-2) and yellowish debris-flow deposits (DF-3)

No IRSL signal could be detected by measurements of the polymineral fine grain fraction of samples Ben-3 to 7. The quartz minerals (Ben-3, 4, 5, 6, 7) were regarded as in saturation. Chapot et al. (2012) showed that, although the laboratory OSL dose response curve continued to grow, the natural OSL signal saturated at ~150 Gy. Therefore, all quartz D_e values > 150 Gy were considered in saturation. Consequently, the calculated ages of samples Ben-3 to 7 are minimum ages of the deposits before transport (Table 5).

The quartz and fading corrected feldspar ages are listed in Table 5.

Table 4: Dosimetry results and dose rates for the samples from Benzingerode (outcrop 5). An a-value of 0.09 ± 0.02 was used for the feldspar samples and an a-value of 0.04 ± 0.01 for the quartz samples.

Sample	Water content (%)	Depth (m)	Radionuclide concentrations			Dose rate				Total dose rate	
			Potassium (%)	Thorium (ppm)	Uranium (ppm)	D_{α} (mGy a^{-1})	D_{β} (mGy a^{-1})	D_{γ} (mGy a^{-1})	D_{cosmic} (mGy a^{-1})	Feldspar (mGy a^{-1})	Quartz (mGy a^{-1})
Ben-2	10±5	1.8	2.24±0.12	12.00±0.64	3.27±0.18	1.21±0.2	2.53±0.09	1.43±0.08	0.22±0.2	4.81±0.24	-
						0.56±0.3	2.53±0.14	1.43±0.09	0.22±0.2	-	4.24±0.21
Ben-3	7±4	0.84	1.11±0.7	4.97±0.29	4.88±0.6	0.51±0.3	1.64±0.12	0.95±0.09	0.22±0.2	-	3.06±0.20
Ben-4	7±4	1.03	0.65±0.4	2.52±0.17	4.45±0.4	0.42±0.2	1.15±0.11	0.68±0.08	0.22±0.2	-	2.28±0.19
Ben-5	4±2	0.93	0.53±0.4	2.32±0.16	2.79±0.6	0.28±0.0	0.84±0.09	0.49±0.08	0.22±0.2	-	1.75±0.17
Ben-6	7±4	0.94	0.78±0.5	2.90±0.19	3.40±0.9	0.34±0.1	1.13±0.10	0.64±0.08	0.22±0.2	-	2.17±0.18
Ben-7	8±4	0.83	0.94±0.6	3.74±0.23	4.35±0.3	0.44±0.2	1.40±0.11	0.80±0.08	0.22±0.2	-	2.61±0.19

Table 5: Quartz and feldspar luminescence ages from Benzingerode (outcrop 5).

Sample	Debris-flow deposit	Quartz		Feldspar		uncorr.	corr.
		D _e (Gy)	Age (ka)	D _e (Gy)	Age (ka)	Age (ka)	Age (ka) corr.
Ben-2	DF-1	64.3±0.7	15.2±0.8	60.5±0.5	12.6±0.6	14.2±0.8	
Ben-3	DF-2	>378±12	>123±9	-	-	-	-
Ben-4	DF-2	>273±13	>119±11	-	-	-	-
Ben-5	DF-3	>217±7	>124±13	-	-	-	-
Ben-6	DF-3	>356±11	>164±14	-	-	-	-
Ben-7	DF-3	>285±5	>109±8	-	-	-	-

The ages of the faulted debris-flow deposits indicate fault movements after ~15 ka see Table 5.

Further analyses were performed outside of this project including shear wave seismic and ERT surveys. Shear wave seismic profiles revealed a fault system with splay faults and back thrusts close to the Harz Boundary Fault that cuts through Late Pleistocene sediments. The ERT profiles traced the lateral extent of the NNE-ward dipping fault, outcropping in the sinkhole, for at least 50 m parallel to the Harz Boundary Fault. Numerical simulation of Coulomb failure stress variations was used to support the age of fault movements estimated using luminescence dating. These initial results are presented in et al. (*in press a*), and imply that the fault is most likely to be related to neotectonic movements along the Harz Boundary Fault in the Lateglacial. Furthermore, a recent earthquake occurred in the year 1908 near Quedlinburg with an intensity of 3.0. This may support the hypothesis of neotectonic activity along the Harz Boundary Fault, although it is not clear if the Harz Boundary Fault is the source of this earthquake.

6.2. Osning Thrust

Five sand pits were identified at the Osning Thrust using geological maps and GoogleEarth images. Three of these pits were abandoned and refilled. Deformation structures (see Table 6 and Fig. 24, 28) are exposed in two pits. A detailed analysis of all outcrops is given in Interim Report 6 (Müller et al., 2018c).

Table 6: Sand pits with deformation structures and the uncertainty of the interpretation at the Osning Thrust. Luminescence ages are derived from Roskosch et al. (2012). (X) means that the observation cannot unambiguously be defined as a cryoturbation feature. Note that the ages are the ages of the faulted deposits and thus imply the time of fault movement.

Pit Nr.	Location	Glaciotec. features	Neotec. features	Cryo. features	Uncertainties	Age of faulted deposits
19	Augustdorf 1		X	(X)	Low	Late Pleistocene Late Pleniglacial to Lateglacial
22	Oerlinghausen		X	(X)	Low	OSL 15.9 ± 1.6 ka to 13.1 ± 1.5 ka

The sand pits analyzed in the vicinity of the Osning Thrust expose alluvial and mixed alluvial-aeolian deposits (Meinsen et al., 2014). A few small-scale extensional and a few contractional deformation structures are exposed within these sediments. Extensional structures include shear-deformation bands with normal displacement; contractional features include low-angle deformation bands with reverse displacement and anticlines in the hanging-wall and inversion structures. Soft-sediment deformation structures (flame structures, ball-and-pillow structures, sharp-sided dykes, irregular branched and stepped dykes, intrusive sediment bodies and sand volcanoes) also occur. The current outcrop is rather limited and many of the previously exposed structures have been destroyed or covered. The previous results of Brandes et al. (2012) and Brandes and Winsemann (2013) have therefore been included in study.

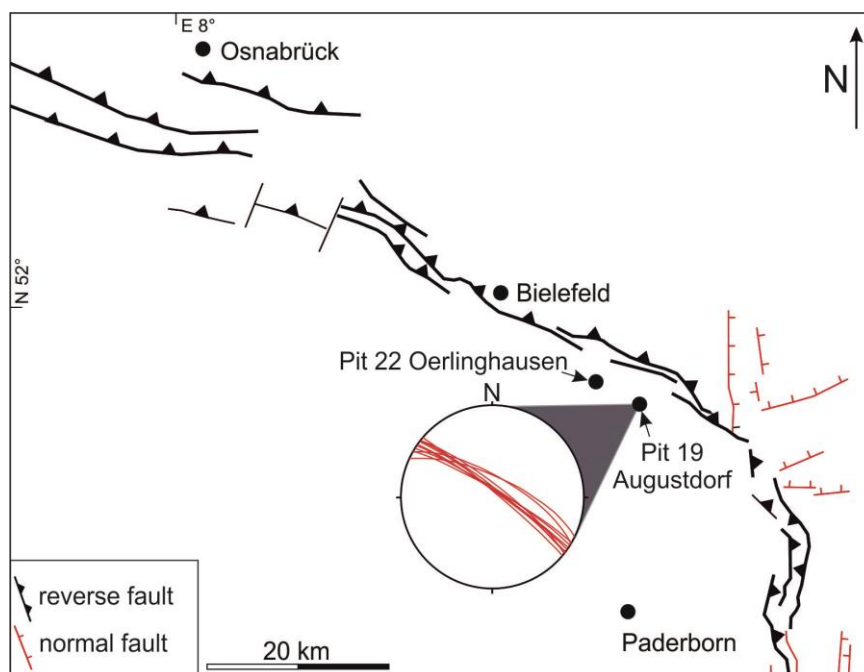


Fig. 28: Osning Thrust. Shear-deformation bands with normal displacement in pit 19 near Augustdorf with stereographic projection of the deformation band orientation (fault traces according to Baldschuhn and Kockel 1999).

The orientation of the extensional structures (shear-deformation bands) observed in pit 19 near Augustdorf have an NW-SE strike and follow the orientation of the Osning Thrust (Fig. 28). A few soft-sediment deformation structures reveal the earliest stage of fluidization and may have been triggered by seismic waves. Alternatively, they may have formed as a consequence of cryoturbation processes.

In the alluvial-plain deposits in the lower part of pit 22 near Oerlinghausen, soft-sediment deformation structures such as flame structures and ball-and-pillow structures have developed. The SSDS are the product of liquefaction and fluidization processes caused by a seismic event, rapid depositional loading and cryoturbation (Brandes and Winsemann, 2013). The soft-sediment deformation structures in the mixed alluvial-aeolian deposits were most likely seismically driven. An explanation for the development of these soft-sediment deformation structures is strong hydraulic forces that are not expected in alluvial-aeolian environments where the groundwater table is low (Brandes and Winsemann, 2013). However, Bertran et al. (2019a) showed in experimental studies that similar soft-sediment deformation structures may be caused by the formation of ground ice and related pore water overpressure in the underlying sediment if water is available. This means that not all soft-sediment deformation structures are an unambiguous indicator for seismic waves in this case. This does not change the interpretation for paleo-earthquakes at the Osning Thrust.

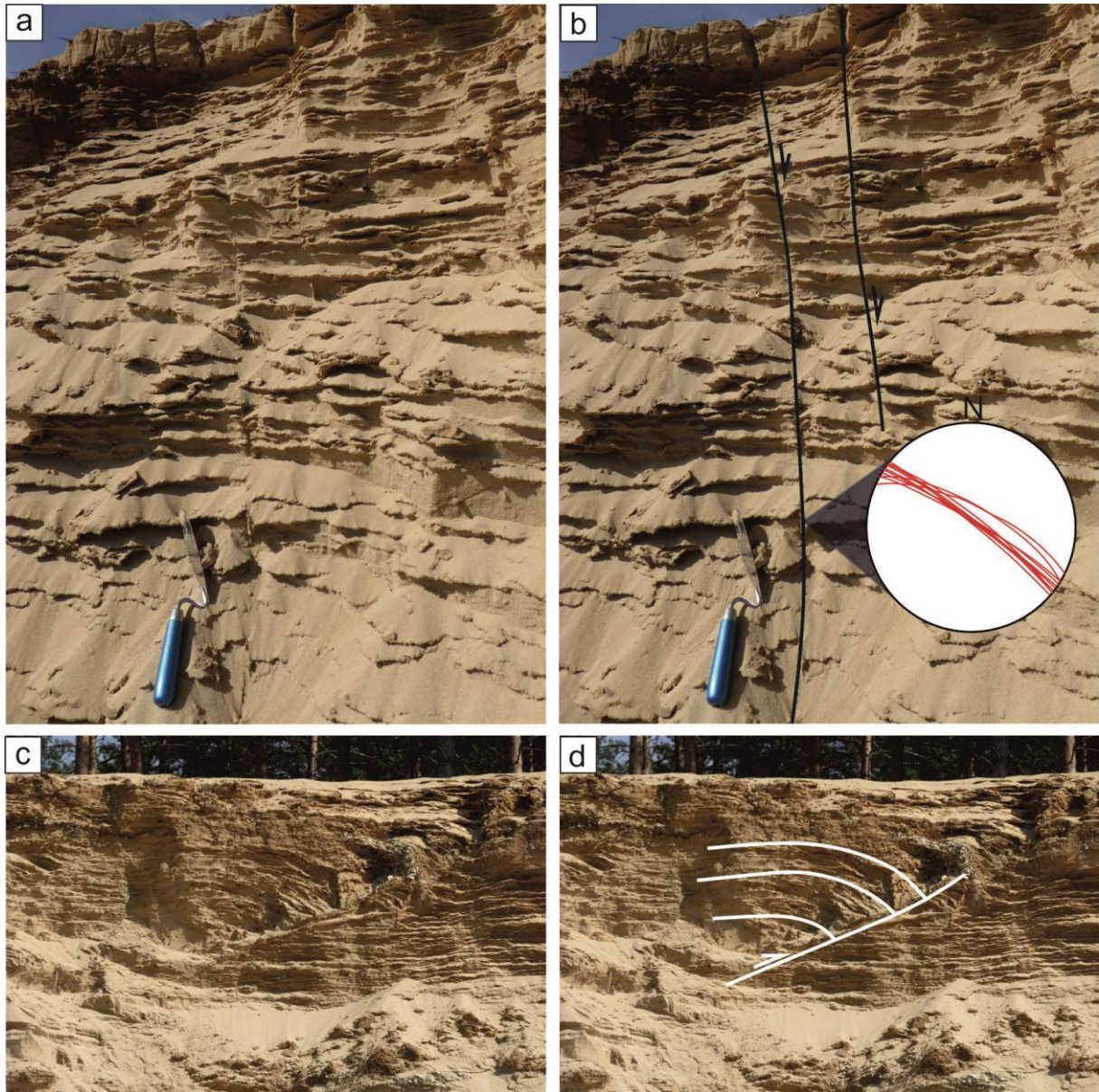


Fig. 29: Osning Thrust. a) Pit 19, Augustdorf. Shear-deformation bands in alluvial-fan and aeolian deposits; b) interpretation of image a) and related stereographic projection of the band orientation, trowel for scale; c) pit 22, Oerlinghausen. Low-angle deformation band with reverse displacement and anticline in the hanging wall developed in mixed alluvial-aeolian deposits; d) interpretation of image c).

However, the inversion structures and deformation bands observed in the pits near Oerlinghausen (pit 22) and Augustdorf (pit 19) are clear indicators of tectonic activity along the Osning Thrust during the Late Pleniglacial or early Lateglacial (Fig. 29; Brandes et al., 2012; Brandes and Winsemann, 2013). The kinematic behaviour is interpreted as a consequence of deformation in the area of the Late Pleistocene Weichselian glacial forebulge. The forebulge formed during ice advance and extensional stresses have led to normal fault formation (cf. Stewart et al., 2000). During the decay of the Late Pleistocene Weichselian Scandinavian ice sheet, the forebulge

collapsed and this caused a reactivation of the Osning Thrust with fault propagation into near-surface sediments that led to the formation of the structures observed in the Oerlinghausen pit 19. Historic earthquakes in the vicinity of Bielefeld in the year 1612, near Oerlinghausen in 1767 and a recent earthquake in the NE of Paderborn (Leydecker, 2011, BGR, 2019) underpin the conclusion of neotectonic activity along the Osning Thrust (see Table 15; Brandes and Winsemann, 2013).

6.3. Halle Fault system

12 sand and gravel pits were identified at the Halle Fault system using geological maps and GoogleEarth images. Four of these pits were abandoned and refilled. The sediments are undeformed in one pit. Deformation structures in seven pits (see Table 7 and Fig. 24, 30) are exposed. A detailed analysis of all outcrops is given in Interim Report 3 (Müller et al., 2017b).

Table 7: Sand and gravel pits with deformation structures and the uncertainty of the interpretation at the Halle Fault system.

Pit Nr.	Location	Glaciotec. features	Neotec. features	Cryo. features	Uncertainties	Age of deposits
23	Gutenberg	X			Low	Middle Pleistocene Saalian
24	Köchstedt			X	Low	Middle Pleistocene Saalian
25	Könnern		X		Low	Middle Pleistocene Saalian
27	Morl		X		Medium	Paleogene
29	Nellschütz			X	Low	Middle Pleistocene Saalian
31	Niederwünsch	X			Low	Middle Pleistocene Saalian
33	Schladenbach 1			X	High	Middle Pleistocene Saalian

The sand and gravel pits analyzed in the vicinity of the Halle Fault expose Middle Pleistocene Saalian fluvial and meltwater deposits. Paleogene kaolin sand is exposed in one pit (27 Morl). Small-scale extensional and contractional deformation structures occur in these sediments. Extensional structures include shear-deformation bands with normal displacement. Contractional structures include large thrust sheets, folds and deformation bands with reverse displacement and hanging wall anticlines. Cryoturbation features are represented by ice wedge casts and involutions at the top

of the pits. The orientation of the deformation bands and the spatial and temporal framework imply that some of these structures evolved as near-surface glaciotectonic features during the Middle Pleistocene glaciations.

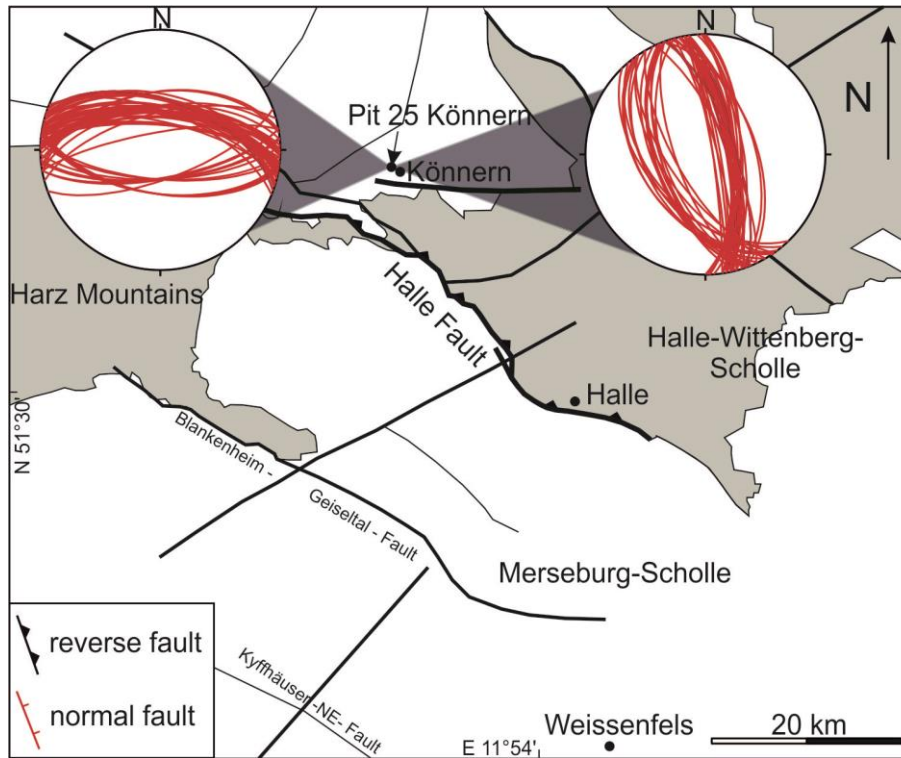
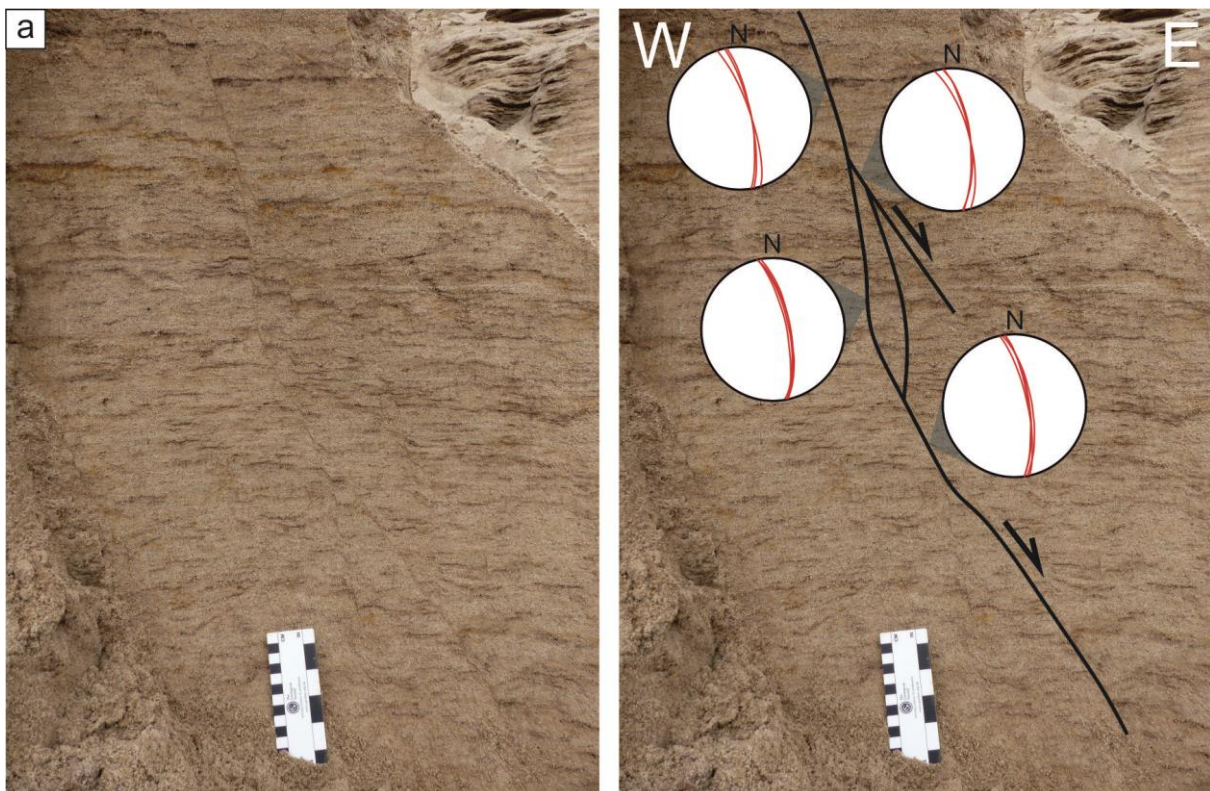


Fig. 30: Halle Fault system. Shear-deformation bands with normal displacement in meltwater sand in pit 25 near Könnern with stereographic projections of the deformation band orientation. The orientation of the shear-deformation bands is similar to the minor fault near Könnern and the Halle Fault (fault trace according to Martiklos et al. 2001).

In this study, we also analyzed an E-W-trending fault north of the Halle Fault near Könnern. This fault is located in the eastern prolongation of the Harz Boundary Fault. Based on the available literature, we are not able to decide whether this fault belongs to the Harz Boundary Fault or represents a single feature.

In two pits (24 Könnern and 27 Morl), shear-deformation bands with NW-SE and W-E orientation occur with the same orientation as the Halle Fault and a smaller E-W trending basement fault near Könnern (Fig. 30). The shear-deformation bands in the Middle Pleistocene meltwater deposits near Könnern are therefore very likely to be related to movements along a basement fault (Fig. 31) and thus imply neotectonic activity in this area. The exposed shear-deformation band in the pit near Morl is isolated and restricted to the Paleogene sand. We therefore rule out a glaciotectonic origin. This is supported by the lack of contractional deformation structures.

Several historic earthquakes with intensities of 4.0 – 4.5 have been described in the Halle area (see Table 15; Leydecker, 2011). In addition, recent seismic activity along the Halle Fault system has manifested itself as two earthquakes in the last 4 years. On 16 April 2015, a M_w 3.2 earthquake was located near Röglitz 15 km SW of Halle at a depth of 19 km (Dahm et al., 2018). The second earthquake in this area took place on 29 April 2017 west of Leipzig between Dölzig und Schkeuditz. The epicentre of this earthquake with a magnitude (M_w) 2.8 was located at a depth of 25 km (Dahm et al., 2018). Recent paleoseismic studies (Brandes et al., 2012; Brandes and Winsemann, 2013) show that the Osning Thrust at the southern margin of the Lower Saxony Basin was reactivated due to stress changes caused by the decay of the Late Pleistocene Weichselian ice sheet. The historic earthquakes at the Osning Thrust might be related to a reactivation of the basement fault (Brandes et al., 2012; Brandes and Winsemann, 2013; Brandes et al., 2015). A similar situation might also have occurred along the Halle Fault where young historic earthquakes and neotectonic activity was identified. These might be triggered by glacial-isostatic adjustment.



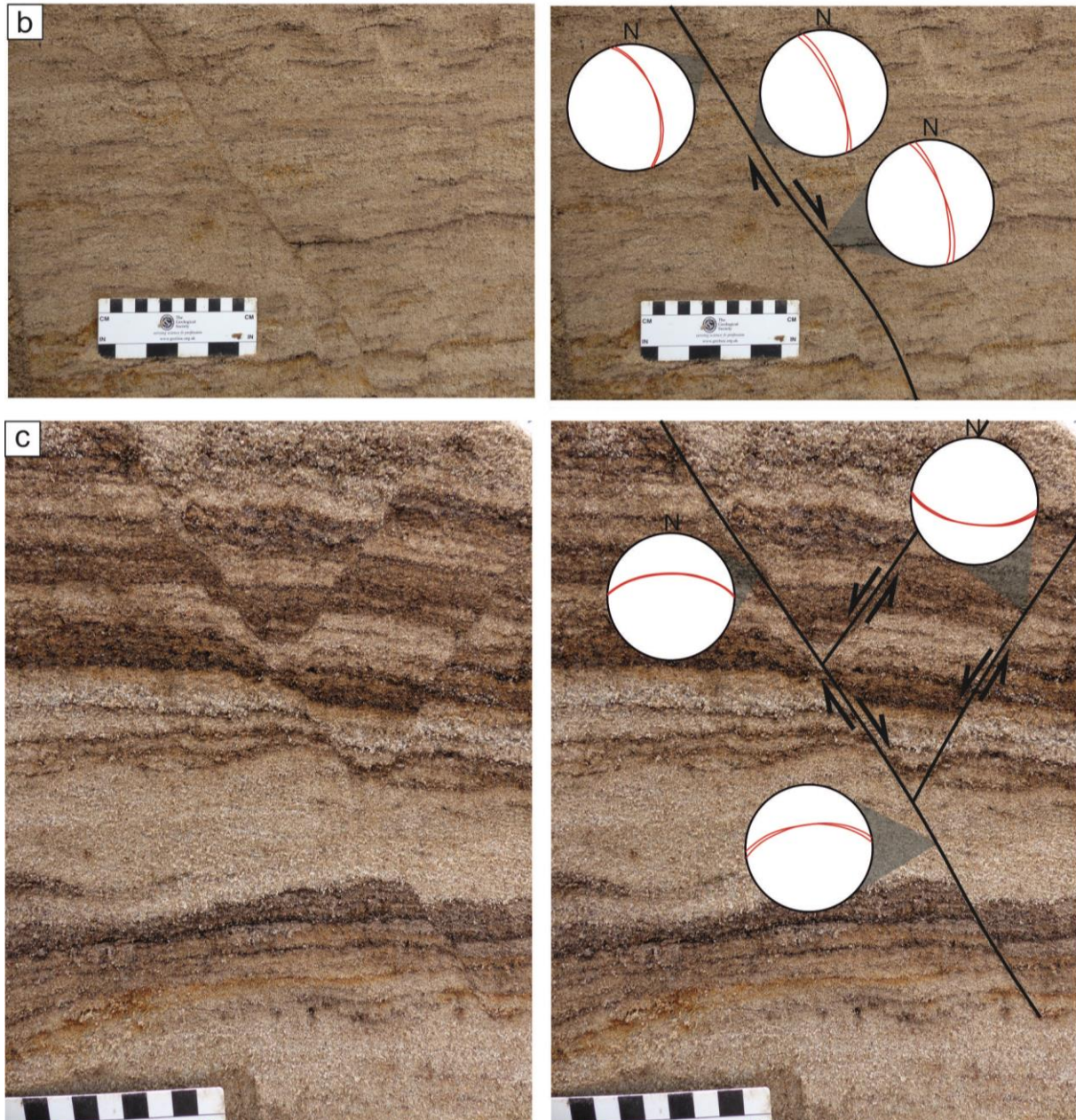


Fig. 31: Shear-deformation bands in meltwater deposits in pit 25 near Könnern. a) Shear-deformation band and interpreted trace together with stereographic projections of the deformation band orientation (n=14); b) shear-deformation band with normal displacement (n=6); c) conjugate shear-deformation bands with interpreted trace and stereographic projections (n=9).

6.4. Aller Valley Fault

36 sand pits were identified at the Aller Valley Fault using geological maps and GoogleEarth images. 17 of these pits were abandoned and refilled. The exposed sediments are undeformed in two pits. Deformation structures were observed in 17 pits (see Table 8 and Fig. 24, 32). A detailed analysis of all outcrops is given in Interim Report 5 (Müller et al., 2018b).

Table 8: Sand pits with deformation structures and the uncertainty of the interpretation at the Aller Valley Fault.

Pit Nr.	Location	Glaciotec. features	Neotec. features	Cryo. features	Uncertainties	Age of deposits
35	Am Aschenberg1	X			Low	Middle Pleistocene Saalian
38	Bahrdorf 2	X		X	Low	Middle Pleistocene Saalian
39	Bissen			X	Low	Middle Pleistocene Saalian
41	Eggestedt	X			High	Middle Pleistocene Elsterian
42	Eitze		X		Low	Middle Pleistocene Saalian
44	Filterberg	X			Low	Middle Pleistocene Saalian
45	Garßen			X	Low	Middle Pleistocene Saalian
48	Groß Eilstorf	X		X	Low	Middle Pleistocene
49	Groß Hehlen			X	High	Middle Pleistocene Saalian
52	Hinter dem Horn	X			High	Middle Pleistocene
54	Hülseberg	X		X	High	Middle Pleistocene
57	Langwedelermoor	X			Low	Middle Pleistocene Saalian
59	Meinkot			X	Low	Middle Pleistocene Saalian
63	Sassenburg	X		X	High	Middle Pleistocene Saalian
64	Scheuen	X			High	Middle Pleistocene Saalian
65	Schmede	X			High	Middle Pleistocene
68	Wesendorf			X	Low	Middle Pleistocene Saalian

The sand pits analyzed in the vicinity of the Aller Valley Fault expose Middle Pleistocene Elsterian and Saalian meltwater deposits and till partly overlain by Late Pleistocene Weichselian paraglacial deposits. Small-scale extensional deformation bands with normal displacement and contractional deformation structures such as thrust sheets, folds, compaction bands and deformation bands with reverse displacement occur within these sediments. Soft-sediment deformation structures include sand volcanoes, ice wedge casts and involutions. In some of the pits the deformation structures were inaccessible due to safety reasons (high and steep walls) so that a detailed analysis was not possible.

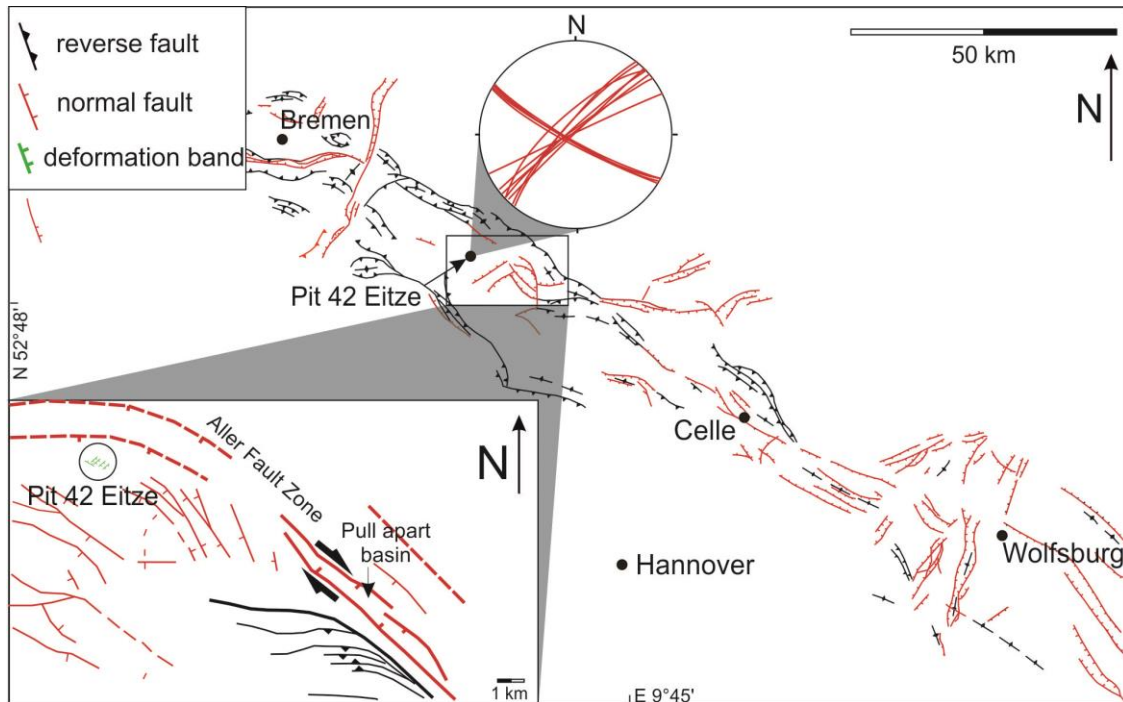


Fig. 32: Aller Fault zone. Shear-deformation bands with normal displacement in meltwater sand in pit 42 near Eitze with stereographic projection of the deformation band orientation. Small map based on Lohr et al. (2007); fault traces modified according to Baldschuhn and Kockel (1996).

The orientation and spatial and temporal framework of many of the deformation features imply that these structures evolved as near-surface glaciotectonic features during the Middle Pleistocene Elsterian and/or Saalian glaciations. Many outcrops (35-41 and 43-70) show the standard structural elements (thrusts, fault-propagation folds) of glaciotectonic complexes (cf. Brandes and Le Heron, 2010). The deposits in pit 44 in particular show the characteristic deformation sequence of low-angle thrust faults that developed in front of an advancing glacier and were later offset by normal faults that developed due to loading and shearing when the glacier transgressed these deposits (described in Interim Report 5 Müller et al., 2018b; cf. Feeser, 1988). The faults in this case have developed as shear-deformation bands.

The pattern of the deformation bands in pit 42 Eitze is different to deformation bands found in the meltwater deposits of the other pits (Fig. 32, 33). The lateral extent of these bands is larger and they partly show the same orientation as the Aller Valley Fault zone in this area (Fig. 32). This points to neotectonic activity and probably a fault reactivation due to lithospheric ice sheet interactions. Two sets of deformation bands exist with different orientations. The first set of deformation bands has a NW-SE orientation that follows the trend of the Aller Valley Fault zone in this area. A second

set of deformation bands strikes roughly perpendicular to the first set of the bands with a NE-SW orientation.

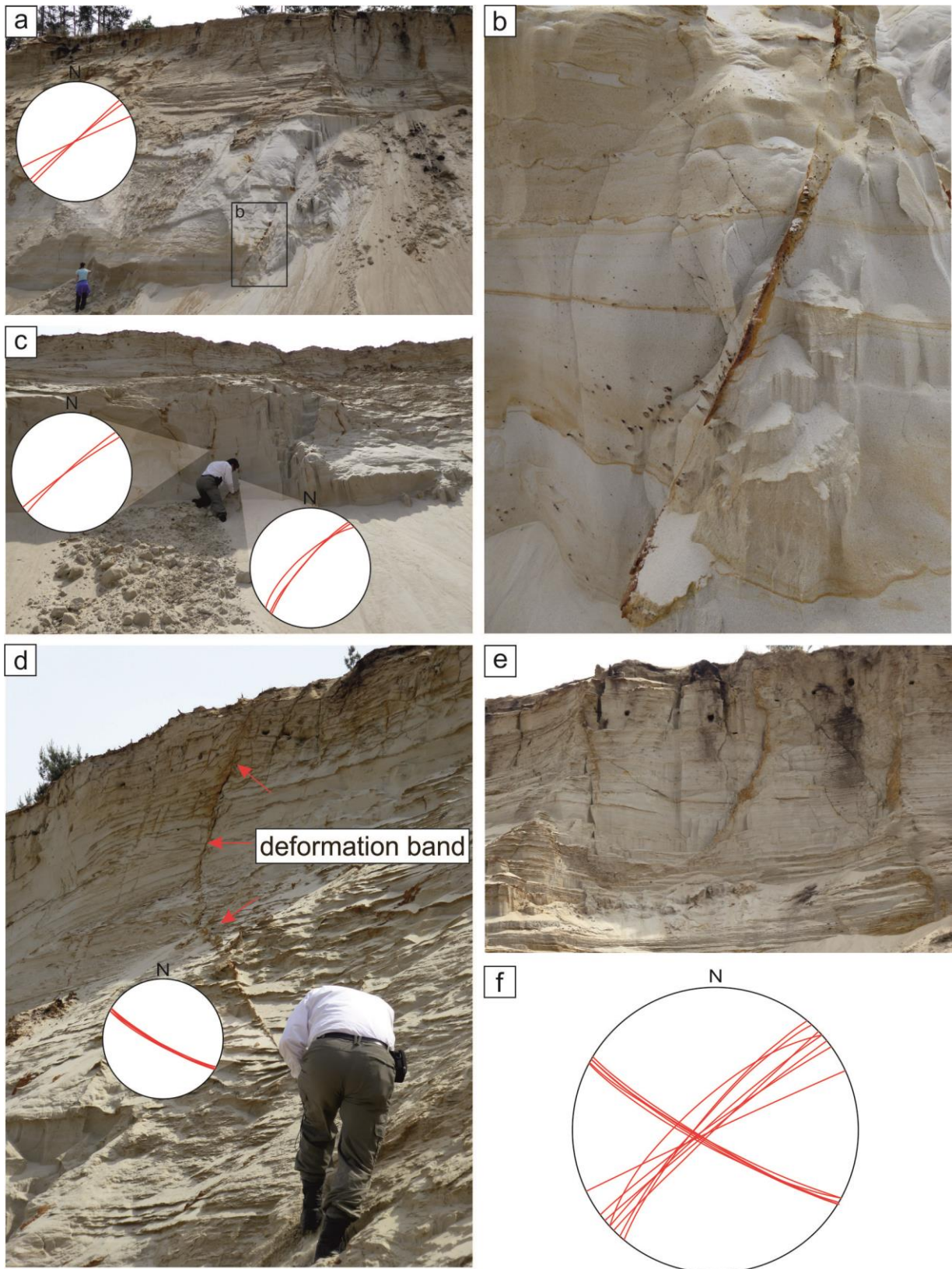


Fig. 33: Deformation structures in Middle Pleistocene Saalian meltwater deposits near Eitze. a) Overview image of the pit near Eitze. The deformation bands penetrate the entire succession. A stereographic projection shows the orientation of the deformation bands ($n=3$); b) close-up view of a

cemented deformation band in the lower part of the succession; c) close-up view of two deformation bands with stereographic projection of the orientation of the deformation bands in the lower part of the succession (n=2 and n=3); d) close-up view of a 0.5-cm-thick deformation band with the related stereographic projection of the band orientation (n=5); e) close-up view of deformation bands in the upper part of the succession; f) stereographic projection showing the orientation of all deformation bands (n=13).

These sets of deformation bands can be best explained with a strike-slip model similar to that described in Brandes et al. (2018a). The stress field in this area is roughly N-S oriented (Heidbach et al., 2016) and would allow strike-slip movements along the fault plane. A pull-apart structure probably developed between two NW-SE trending fault segments of the Aller Valley Fault (Fig. 32, 33, 34). This structure underwent NW-SE extension, which caused the NE-SW trending deformation bands. Further analyses are necessary to verify this assumption.

The work of Lohr et al. (2007) and Kley et al. (2008) shows potential strike-slip movements along the Aller Valley Fault zone in Jurassic times. Based on a 3D seismic data set, normal faults could be detected that formed during the Jurassic. These faults probably developed due to transtension and formed a pull-apart structure due to strike-slip movements (Lohr et al., 2007).

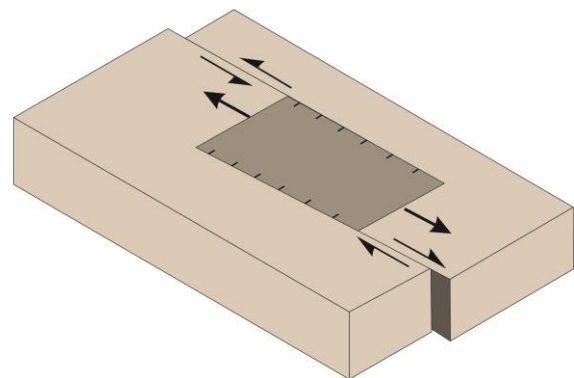


Fig. 34: Schematic model of a pull-apart basin.

It is therefore likely that neotectonic movements may have occurred along the Aller Valley Fault zone, which triggered the reactivation of these pull-apart structures. Shear-deformation bands in the pit near Eitze are the best indicator for potential neotectonic movements along the Aller Valley Fault zone.

Historic seismicity along the Aller Valley Fault zone also occurred in the year 997 with an estimated intensity of 6 in the area of the Altmark. In the years 1298, 1409 and 1576 historic seismicity with estimated intensities of 4 and 6 occurred in the area of Magdeburg (Leydecker, 2011). Also, recent seismic activity was instrumentally detected in the years 1977 M_L 4.0 near Soltau (Dahm et al., 2007), 2004 M_w 4.4 near Rotenburg (Dahm et al., 2007), 2014 M_L 1.3 near Walsrode (Brandes et al., 2019) and 2018 M_L 2.0 near Rethem (Brandes et al., 2019). The Wittenburg and Soltau events are more than 20 km away from a fault but are listed because of their high magnitude

and the resulting importance for the hazard assessment. The Rotenburg 2004 event has yet to be unequivocally classified as natural or triggered. The 2014 and 2018 earthquakes near Walsrode and Rethem were most likely too deep to be related to the Aller Valley Fault but are listed because of the close location to the fault zone. The occurrence of several earthquakes close to the fault underpins the assumption that the Aller Valley Fault displays neotectonic activity.

6.5. Gardelegen Fault

Five sand pits were identified at the Gardelegen Fault using geological maps and GoogleEarth images. Two of the five pits were abandoned and refilled. Deformation structures were observed in three pits (see Table 9 and Fig. 24). A detailed analysis of all outcrops is given in Interim Report 4 (Müller et al., 2018a).

Table 9: Sand pits with deformation structures and the uncertainty of the interpretation at the Gardelegen Fault.

Pit Nr.	Location	Glaciotec. features	Neotec. features	Cryo. features	Uncertainties	Age of deposits
72	Dolle	X			Low	Middle Pleistocene Saalian
73	Gardelegen	X			High	Middle Pleistocene Saalian
74	Hottendorf	X			Low	Middle Pleistocene Saalian

The pits expose Middle Pleistocene Saalian meltwater sand partly with overlying till beds. A few small-scale extensional and some contractional deformation structures occur within these sediments. The extensional structures are shear-deformation bands with normal displacement. Contractional features include fold structures and shear-deformation bands with reverse displacement. The random orientation of the deformation bands and their temporal framework makes analysis difficult, but based on their random orientation and the observation that there is no clear match with the trend of the Gardelegen Fault, it seems more likely that these structures evolved as near-surface glaciotectonic features during the Middle Pleistocene Saalian glaciations.

Several earthquakes with intensities of 4.0 – 6.0 occurred in the vicinity of the Gardelegen Fault in historic times (see Table 15; Leydecker, 2011). However, the sand

pits analyzed in the vicinity of the Gardelegen Fault do not show evidence of neotectonic movements with respect to the current exposure situation.

6.6. Steinhuder Meer Fault

Nine sand pits altogether were identified at the Steinhuder Meer Fault using geological maps and GoogleEarth images. Three of these nine pits were abandoned and refilled. The sediments are undeformed in one pit. Deformation structures were observed in five pits (see Table 10 and Fig. 24, 35). A detailed analysis of all outcrops is given in Interim Report 4 (Müller et al., 2018a).

Table 10: Sand pits with deformation structures and the uncertainty of the interpretation at the Steinhuder Meer Fault.* Note that the ages of pit 89 show luminescence ages at the time of fault movement.

Pit Nr.	Location	Glaciotec. features	Neotec. features	Cryo. features	Uncertainties	Age of deposits
89	Altenhagen		X		Low	Middle Pleistocene *IRSL189±5 ka to 158±4 ka
90	Bolsehle		X	X	High	Middle Pleistocene Saalian
91	Eilvese	X		X	Low	Middle Pleistocene Saalian
93	Rehburg			X	Low	Middle Pleistocene Saalian
95	Schneeren	X			Low	Middle Pleistocene Saalian

The sand pits analyzed in the vicinity of the Steinhuder Meer Fault expose Middle Pleistocene Saalian meltwater deposits, partly overlain by till beds. A number of small-scale extensional and very few contractional deformation structures have developed within these sediments. The extensional structures are represented by shear-deformation bands with normal displacement. Contractional structures include thrust sheets and shear-deformation bands with reverse displacement. Cryoturbation features are ice wedge casts and involutions. Deformation structures are exposed in four pits implying that these structures evolved as near-surface glaciotectonic features during the Middle Pleistocene Saalian glaciations.

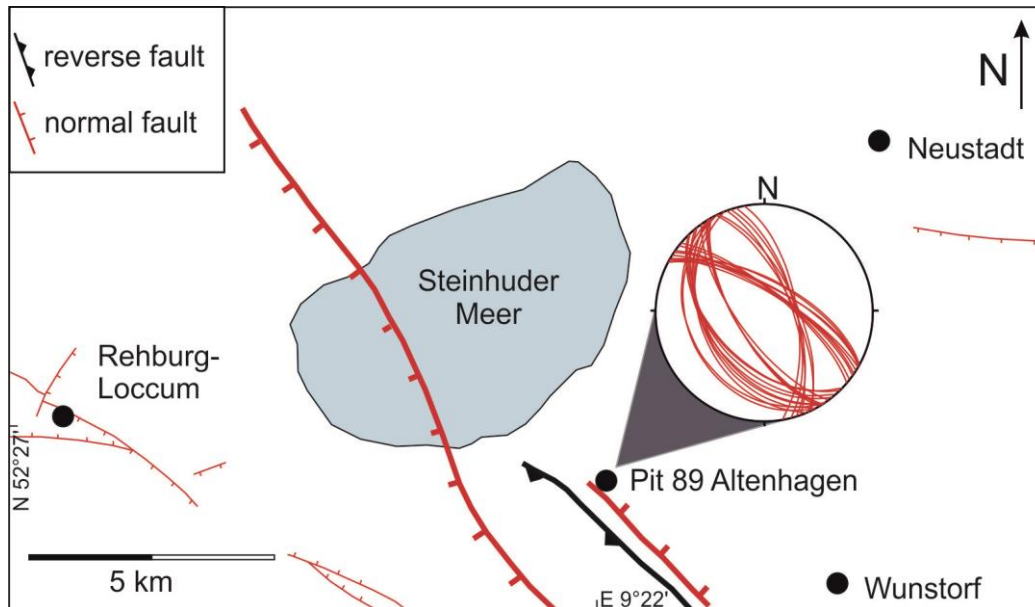


Fig. 35: Steinhuder Meer Fault. Shear-deformation bands with normal displacement in pit 89 near Altenhagen with stereographic projection of the deformation band orientation (fault traces after Baldschuhn and Kockel, 1987).

In one sand pit (89 Altenhagen) along the Steinhuder Meer Fault, a dense fault array of deformation bands with a NW-SE strike occurs with the same orientation as the Steinhuder Meer Fault. These shear-deformation bands have developed in Middle Pleistocene meltwater sediments. The orientation of the deformation bands is parallel to the Steinhuder Meer Fault implying that they are very likely to be related to movements along this fault and thus provide evidence for neotectonic activity. This probably implies fault reactivation due to lithospheric ice-sheet interactions (Fig. 35). In pit 90 at Bolsehle very few deformation bands with the orientation parallel to the Steinhuder Meer Fault occur. Uncertainty in this sand pit is therefore higher compared to the Altenhagen pit.

We analyzed several deformation structures in the pit near Altenhagen and they mostly show the same orientation (Fig. 36). Nearly all shear-deformation bands have a dip angle of 65 - 80°. According to Voss (1979), the normal fault at the SW edge of the Steinhuder Meer anticline structure has a dip angle of 70 - 75° in the upper part and a dip angle of 60 - 65 ° at a depth of 800 m. These fault angles have the same trend as the shear-deformation bands measured in the glaciolacustrine Middle Pleistocene sediments and imply a connection to the basement fault and small-scale deformation

structures. The shear-deformation bands, which have developed in unconsolidated ice-marginal glaciolacustrine deposits, all show normal displacements.

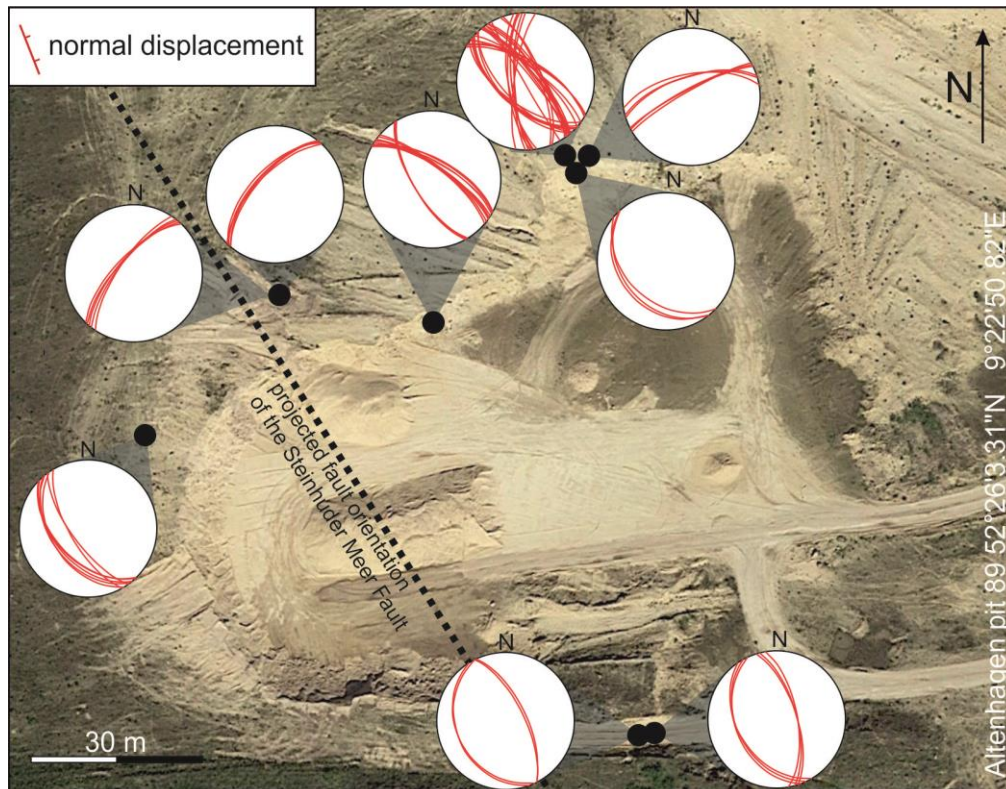


Fig. 36: Sand pit near Altenhagen with stereographic projections of the deformation band and fault orientation. The dotted line shows the orientation of the Steinhuder Meer Fault.

A growth-strata package indicative of sedimentation during deformation has developed at one shear-deformation band with a large offset (Fig. 37, see Interim Report 4, Müller et al., 2018a). Luminescence dating of the growth-strata package was carried out to estimate the timing of fault movement. The estimated IRSL ages (189 ± 5 ka to 158 ± 4 ka; Table 12) indicate Middle Pleistocene Saalian fault activity. This implies that the shear-deformation bands most likely developed during the Middle Pleistocene Saalian glaciations. The results of the luminescence measurements are described below.

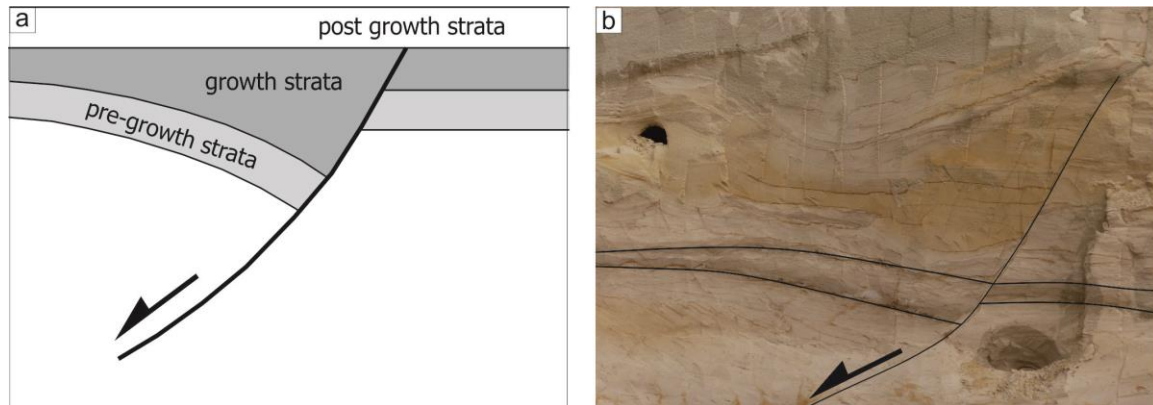


Fig. 37: Growth strata. a) Schematic model of growth strata (modified according to Williams et al. 1989); b) growth strata in the Altenhagen pit. Growth strata are sediment packages with thickness-variations caused by fault movement.

Coarse-grained samples were taken close to the Steinhuder Meer Fault in a sand pit near Altenhagen (pit 89) (see Interim Report 4, Müller et al., 2018a) and measured using the IRSL method.

Results of the luminescence dating

Sample Alt-1 provided reliable luminescence ages. The dose recovery ratios Alt-1 0.81 ± 0.01 for the pulsed IR_{50} signal and for sample Alt-2 0.84 ± 0.02 confirm that the applied SAR protocols were suitable for the D_e measurements. However, the value 0.9 - 1.1 (Wintle and Murray, 2006) was not achieved. Further analysis represented nearly the same dose recovery ratio.

The pulsed IR_{50} signal of the fine grain fraction yielded a recycling ratio of 1.01 ± 0.03 . This value is within 10% of unity (cf. Wintle and Murray, 2006) and confirms that the SAR protocol corrected sensitivity changes successfully during the measurements.

The fading test gave a mean g-value of 2.82 ± 0.19 %. The pulsed IR_{50} ages (Alt-1 118 ± 1.5 ka) and (Alt-2 141 ± 1.5 ka) was fading corrected using the R-software (R version 3.3.2.) based on Huntley and Lamothe (2001).

The estimated dosimetry results and dose rates from the samples from Altenhagen (pit 89) are listed in Table 11. The estimated luminescence ages are 158 ± 4 for Alt-1 and 189 ± 5 ka for Alt-2. The fading corrected feldspar ages are listed in Table 12.

Table 11: Dosimetry results and dose rates for the samples from Altenhagen (pit 89). An a-value of 0.09 ± 0.02 was used for the feldspar samples.

Sample	Water content (%)	Depth (m)	Radionuclide concentrations				Dose rate			
			Potassium (%)	Thorium (ppm)	Uranium (ppm)	D_{α} (mGy a ⁻¹)	D_{β} (mGy a ⁻¹)	D_{γ} (mGy a ⁻¹)	D_{cosmic} (mGy a ⁻¹)	Feldspar (mGy a ⁻¹)
Alt-1	3±1	2.4	1.03±0.01	1.46±0.02	0.46±0.01	0.16±0.02	0.36±0.09	1.43±0.0	0.21±0.2	1.53±0.3
Alt-2	3±1	2	1.00±0.01	1.50±0.02	0.46±0.01	0.16±0.02	1.64±0.12	0.35±0.0	0.21±0.2	1.50±0.3

Table 12: Feldspar luminescence ages from Altenhagen (pit 89).

Sample	feldspar	uncorr.	corr.
	D _e (Gy)	Age (ka)	Age (ka) corr
Alt-1	180.37±4.34	118±1.5	158±4
Alt-2	211.07±15	141±1.5	189±5

6.7. Elbe Lineament

13 sand pits were identified at the Elbe Lineament using geological maps and GoogleEarth images. Altogether seven of the 13 pits were abandoned and refilled. Deformation structures were observed in six pits (see Table 13 and Fig. 24). A detailed analysis of all outcrops is given in Interim Report 6 (Müller et al., 2018c).

Table 13: Sand pits with deformation structures and the uncertainty of the interpretation at the Elbe Lineament.

Pit Nr.	Location	Glaciotec. features	Neotec. features	Cryo. features	Uncertainties	Age of deposits
76	Alt Garge	X			Low	Middle Pleistocene Saalian
77	Bendelin	X			Low	Middle Pleistocene Saalian
80	Ferbitz	X			Low	Middle Pleistocene Saalian
81	Gusborn	X			Low	Middle Pleistocene Saalian
82	Meudelfitz	X			Low	Middle Pleistocene Saalian
86	Tramm	X			Low	Middle Pleistocene Saalian

The sand pits analyzed in the vicinity of the Elbe Lineament expose Middle Pleistocene Saalian meltwater sand partly with intercalated or overlying till beds. Several small-scale extensional and a few contractional deformation structures occur within these sediments. Extensional structures include deformation bands with normal displacement. Structures that were formed in a compressional stress regime are shear-deformation bands with reverse displacement, low-angle reverse faults and fold structures. Their orientation and temporal framework imply that these structures evolved as near-surface glaciotectionic features during the Middle Pleistocene Elsterian or Saalian glaciations. All outcrops display the standard structural elements of glaciotectionic complexes that developed in front of the glacier due to contraction and subsequent loading and shearing when the glacier transgressed these deposits.

No indications of neotectonic movements could be found in the sand pits analyzed along the Elbe Lineament (see Table 15).

6.8. Summary of results

97 sand and gravel pits altogether were analyzed in northern Germany. The selected sand and gravel pits are located within an area of up to 20 km around the major basement faults. 17 pits were analyzed at the Harz Boundary Fault, five pits at the Osning Thrust, 12 pits at the Halle Fault system, 36 pits at the Aller Valley Fault, five pits at the Gardelegen Fault, 13 pits at the Elbe Lineament and nine pits at the Steinhuder Meer Fault. Middle and Late Pleistocene fluvial deposits, meltwater deposits, paraglacial deposits and Holocene aeolian deposits are exposed in these pits. In 58 sand and gravel pits deformation structures occur, which are interpreted as glaciotectonic, neotectonic or cryoturbation features.

Reliable evidence of neotectonic deformation was found in six outcrops (Fig. 38): pit 42 in Eitze at the Aller Valley Fault, pit 25 in Könnern near the Halle Fault, outcrop 5 in Benzingerode at the Harz Boundary Fault and pit 89 in Altenhagen at the Steinhuder Meer Fault. Two outcrops at the Osning Thrust, pit 19 in Augustdorf and pit 22 in Oerlinghausen expose structures that indicate neotectonic activity. These two outcrops were already discussed in Brandes et al. (2012) and Brandes and Winsemann (2013). The results are summarized in Table 14. Indicators for neotectonic activity are shear-deformation bands and faults in Pleistocene sediments. Evidence for paleo-earthquakes in form of seismites was only found in the pits at the Osning Thrust. In case of the Aller Valley Fault, the Harz Boundary Fault, the Halle Fault system and the Steinhuder Meer Fault, it was only possible to identify shear-deformation bands, which are also indicative of fault movements, but not for earthquakes. The fault movement could therefore have taken place in form of creep.

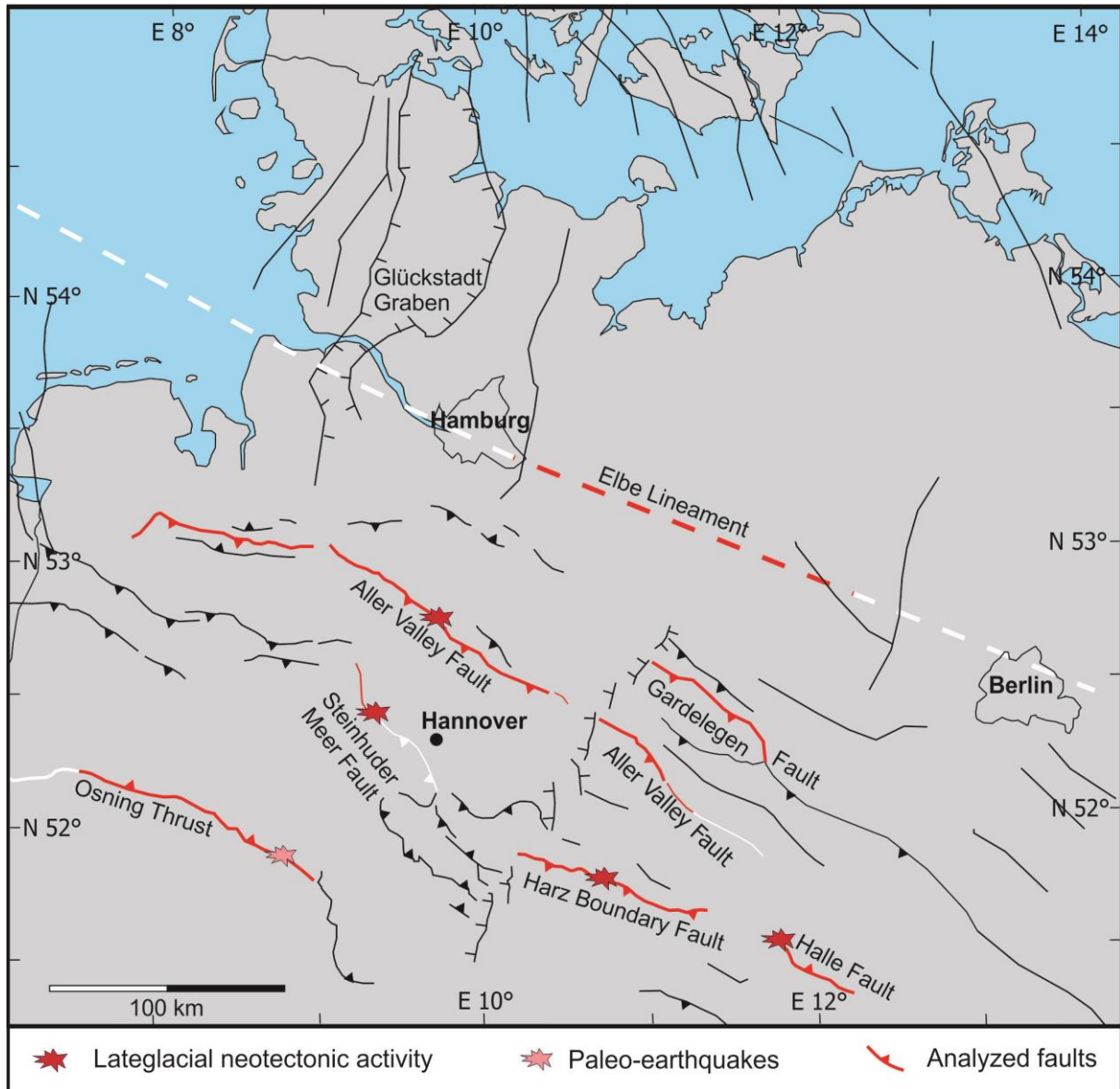


Fig. 38: Major basement faults revealing neotectonic activity. The major basement faults analyzed are shown in red. (Faults are based on Kley and Voigt 2008).

Table 14: Major basement faults in northern Germany where this study found evidence of neotectonic movements. The numbers represent the pit numbers shown in Fig. 24.

Major basement Fault	Locations	Indicators	Neotectonic movements	Paleo-earthquakes	Age of fault movement
Aller Valley Fault	Eitze (pit 42)	Shear-deformation bands (normal displacement)	Yes	Uncertain	Post Middle Pleistocene Saalian
Halle Fault system	Könnern (pit 25)	Shear-deformation bands (normal displacement)	Yes	Uncertain	Post Middle Pleistocene Saalian
Harz Boundary Fault	Benzingerode (outcrop 5)	Fault (normal and reverse displacement)	Yes	Uncertain	Late Pleistocene Weichselian After ~15 ka OSL 15.2 ± 0.8 ka IRSL 14.2 ± 0.8 ka
Osning Thrust	Augustdorf (pit 19) Oerlinghausen (pit 22)	Shear-deformation bands (normal displacement) Seismites	Yes	Yes	Late Pleistocene Weichselian OSL 15.9 ± 1.6 to 13.1 ± 1.5 ka
Steinhuder Meer Fault	Altenhagen (pit 89)	Shear-deformation bands (normal displacement)	Yes	Uncertain	Middle Pleistocene Saalian IRSL 158 ± 4 ka to 189 ± 5 ka

7. Discussion

7.1. Synthesis of the tectonic structures and the distribution of fault activity

The tectonic structure of northern Germany is the result of the Paleozoic Caledonian and Variscan orogenies (Krawczyk et al., 2008), Late Paleozoic to Mesozoic lithospheric extension (Betz et al., 1987) and a distinct Late Mesozoic to Paleogene inversion phase (Kley and Voigt, 2008). Different studies have shown that the inherited structural grain is the governing factor for young tectonic activity (e.g. Sykes, 1978). Brandes et al. (2012) show that neotectonic activity has occurred at the Osning Thrust, and the study of Müller et al. (*in press a*) found evidence for neotectonic activity at the Harz Boundary Fault. The Osning Thrust and the Harz Boundary Fault both formed during the Late Cretaceous inversion phase. Historic seismicity with intensities of up to 6 also concentrated at Late Cretaceous reverse faults such as the Osning Thrust, the Gardelegen Fault and the Haldensleben Fault (Brandes et al., 2012). Recent natural earthquakes that have been instrumentally detected in the last 18 years point to deep-seated seismicity in northern Germany. These earthquakes have reached a magnitude of M_L 3.1 and are partly concentrated at the Thor Suture, which is the remnant of a Silurian subduction zone (Brandes et al., 2019). Further deep earthquakes are located at the Moho at a depth of up to 30 km. This seismicity implies that the Moho acts as a regional detachment that compensates recent shortening (Fig. 39; Brandes et al., 2019).

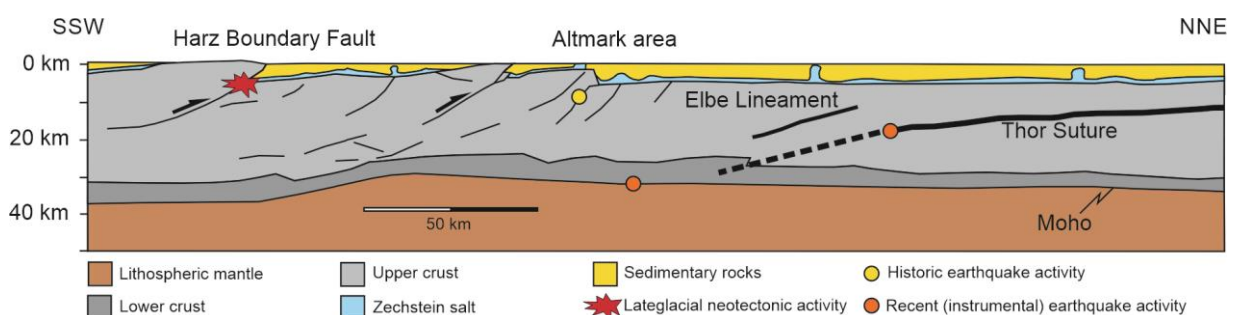


Fig. 39: Tectonic activity in northern Germany. The cross-section shows Lateglacial neotectonic activity, historic earthquake activity and recent (instrumental) earthquake activity at several fault systems in northern Germany (based on Brandes et al. 2019; Leydecker 2011; Müller et al. *in press a*). Unlike the other faults, the Elbe Lineament and the Thor Suture are terrane boundaries. The dashed line represents the uncertain location of the Thor Suture. Cross-section modified according to Kley et al. (2008), (Müller et al., *in press b*)

7.2. The Soltau 1977 and Rotenburg 2004 earthquakes

More than 70 earthquakes (excluding quarry blasts) have affected northern Germany over the last few decades (Uta, 2017). Many of these earthquakes are located in the vicinity of natural gas fields (Bischoff et al., 2013, 2014, 2015; Uta, 2017). Two outstanding seismic events that were instrumentally recorded in northern Germany are the Soltau earthquake in 1977 with a magnitude of M_L 4.0 and the Rotenburg earthquake in 2004 with a magnitude of M_W 4.4 (Leydecker et al., 1980; Dahm et al., 2007, 2015). The Rotenburg main shock was followed by three aftershocks with magnitudes up to M_L 2.2. Due to their relatively high magnitude, the Soltau and the Rotenburg earthquake are key events that play a major role in the seismic hazard assessment of northern Germany.

An analysis of the Soltau earthquake was published by Leydecker et al. (1980). The earthquake had an epicentral intensity of 5 - 6 and was located at a depth between 4 - 13 km (Leydecker et al., 1980). The Rotenburg earthquake was analyzed by Leydecker et al. (2006) and Dahm et al. (2007, 2015). The Rotenburg event in particular became a focus for research because of its vicinity to the Söhlingen hydrocarbon field. The hypocentre of the Rotenburg earthquake was located at a depth of about 5 - 7 km and the fault plane solution indicates normal fault kinematics (Dahm et al., 2007, 2015). The study of Leydecker et al. (2006) presents a deeper hypocentre than the results of Dahm et al. (2007) with a depth of 10 ± 3 km.

Dahm et al. (2007) state that the Rotenburg 2004 earthquake and the Soltau 1977 earthquake should be treated together because of the small distance of about 20 km between the two epicentres. The data base for the Soltau event is rather small. However, Dahm et al. (2007) interpret the Soltau earthquake as a result of hydrocarbon extraction. Their main arguments for classifying both the Soltau 1977 and the Rotenburg 2004 earthquakes as nontectonic events are their shallow depth, their location in the vicinity of gas fields (Soltau: Munster field, Rotenburg: Söhlingen field) and the lack of clear tectonic earthquakes with a comparable magnitude in this region during the last 100 years. The normal fault kinematics of the Rotenburg event also supports the interpretation of a hydrocarbon extraction related earthquake (Dahm et al., 2007).

A re-evaluation of the Rotenburg 2004 mainshock was carried out as part of a DGMK (Deutsche wissenschaftliche Gesellschaft für Erdöl, Erdgas und Kohle) project in 2017-18. The waveform database for this earthquake was significantly increased in this study by including several data sets from seismic stations that had not been included in the previous studies. The results imply a deeper hypocentre than in the study of Dahm et al. (2007). However, due to the lack of near seismic stations and the absence of an accurate S-wave velocity model, the hypocentre is less well-constrained with ranges at depths between 8 and 18 km and strongly influenced by the v_p/v_s -ratio. Focal depth uncertainties are in the range of $\pm 1 - 3$ km (Uta et al., 2018).

A clear classification (purely tectonic or triggered) of the Soltau 1977 and Rotenburg 2004 earthquake has not been possible until now. A thorough re-evaluation of the available waveforms for the Soltau 1977 earthquake is necessary followed by a relocalisation of the hypocentre and a new calculation of the fault plane solution to better quantify the earthquake parameters. This was successfully done for the Rotenburg 2004 earthquake (Uta et al., 2018). However, the newly derived hypocentre location from Uta et al. (2018) should be used as a basis for slip tendency simulations to test the impact of pressure changes and related stress-field changes on the reactivation potential for faults below the reservoir in order to better constrain the effects of hydrocarbon extraction at greater depth.

7.3. Limitations of the sand and gravel pit analysis

All accessible outcrops along the seven major basement faults were analyzed during this two-year project. Due to their limited size, the sand and gravel pits only enable access to a small portion of the Pleistocene sediments. However, the distribution of the outcrops sufficiently covers the fault traces and delivers reliable results. Several sand pits are located directly above the faults or are at least within a distance of 10 – 20 km (Fig. 24). Only trenching would allow a more comprehensive insight into the near-subsurface fault structure. This would require significantly higher effort in terms of costs and time and could be carried out in future studies.

Seismogenic faults may creep between earthquakes or move with small amounts of slip during small earthquakes, and thus do not leave SSDS indicative of earthquake

activity (McCalpin and Nelson, 2009). Seismites and SSDS such as sand volcanoes are produced by the passage of seismic waves resulting in the explosive expulsion of pore water. Aseismic creep by contrast does not produce such structures and is therefore difficult to detect.

7.4. Limitations of soft-sediment deformation structures for identifying paleo-earthquakes

SSDS can be an indicator for seismic shaking (e.g. Obermeier et al., 1990; Obermeier, 1996; Rossetti, 1999; Wheeler, 2002; Moretti et al., 2014). SSDS have therefore been used as indicators for paleo-earthquakes in northern Central Europe (e.g. Brandes et al., 2012; Hoffmann and Reicherter, 2012; Brandes and Winsemann, 2013; Pisarska-Jamroży et al., 2018; Grube, 2019a, 2019b; Pisarska-Jamroży and Woźniak, 2019), although it must be kept in mind that SSDS can be also induced by different non-seismic processes (see Chapter 3) and it is often challenging to derive the related drivers, especially in areas that were affected by glaciations and/or by periglacial processes. Furthermore, not all earthquakes trigger liquefaction and fluidization processes and SSDS are only likely to be formed in susceptible deposits. Such SSDS commonly develop in fine- to medium-grained saturated sand with loose packing (high porosity). Permeability barriers such as mud laminae or matrix-rich impermeable beds that support the increase in pore water pressure must be present. Liquefaction mostly develops in sediments that were buried less than 5 m (Owen and Moretti, 2011).

Based on the literature and field examples, Owen and Moretti (2011) defined six criteria for recognising seismites in the field: (1) a large areal extent, (2) lateral continuity, (3) vertical repetition, (4) a comparable morphology with structures described from earthquakes, (5) proximity to active faults and (6) the complexity and frequency of SSDS are dependent on their distance to the triggering fault.

According to Van Loon et al. (2016) the most important criterion for the recognition of a seismite is the vertical repetition of beds with SSDS. However, many applied criteria are not diagnostic and do not rule out other trigger mechanisms (Owen and Moretti, 2011; Brandes and Winsemann, 2013).

Periglacial environments, e.g. seasonal freeze and thaw cycles, can lead to the formation of vertically stacked beds with SSDS that are produced by loading or diapirism (Vandenberghe, 2013). Wet, low-lying and flat areas without lateral drainage that are underlain by fine-grained sediments are most prone to cryoturbation (Vandenberghe, 2013). In non-glacigenic settings, fast depositional loading of water saturated sediments may lead to the formation of all styles of liquefaction and fluidization structures if the overburden and pore pressure is high enough (Owen, 2003; Rodríguez et al., 2009). These SSDS may also appear at different levels, but are not the result of earthquakes.

However, finding evidence for many of these criteria is difficult. Identifying a large areal extent of seismites presents a challenge because the outcrops in northern Germany are isolated sand and gravel pits. Nevertheless, many analyzed pits are reasonably large with a lateral extent that allows observation of potential seismites. Although many outcrops are located above the tip line of the basement faults or at least in their vicinity, we did not find any SSDS in the pits that show a distinct continuity or vertical repetition.

SSDS not fulfilling the criteria mentioned above and lacking deformation bands in the vicinity make an earthquake origin unlikely. Seismites by contrast can develop in a larger area around the epicentre of the earthquake, however, a magnitude of ($M \geq 5$) is necessary (e.g. Atkinson et al., 1984; Rodríguez-Pascua et al., 2000).

Recent studies of seismically induced SSDS in northern Germany were carried out by Grube (2019a, b).

The recent study of Grube (2019b) proposed neotectonic deformation and strong Holocene to Late Holocene (<300 a ^{14}C cal BP) (<300 calibrated radiocarbon years before present) earthquakes ($M \geq 5.5$). According to Grube (2019b) the very young deformation may be related to earthquakes in 1959 and 1760 in Hamburg and Schleswig-Holstein. The assumption is based on normal and reverse faults, growth faults, graben and horst structures, folds, sand blows and infill structures in mainly Middle Pleistocene Saalian glaciofluvial and Late Pleistocene Weichselian periglacial sediments.

The study of (Grube, 2019a) has proposed strong Late Pleistocene Weichselian (~ 31.350 , ~ 26.850 , ~ 18.980 ^{14}C cal a BP) and Holocene and Late Holocene (4900,

1200 ¹⁴C cal a BP) earthquakes ($M \geq 6$) near Hamburg. This assumption is based on the occurrence of normal faults, folds, bowls, sand volcanoes and large clastic dykes as well as compressional structures in Middle Pleistocene Saalian glaciofluvial and glaciolacustrine sand and silt, Late Pleistocene Weichselian periglacial sediments and Holocene peats (Grube, 2019b). Lauenburg clay (Elsterian) and Holsteinian clays occur at the surface of the pits due to glaciotectonic disturbance of the sediments.

However, in this complex geological setting this interpretation should be viewed with caution (see also Bertran et al., 2019b). Grube (2019a, b) described compressional structures in the glaciolacustrine deposits as being due to ice push. The association of folds, normal and reverse faults and SSDS is also typical for glaciotectonic deformation and it remains unclear whether earthquakes have caused these structures. Faults and graben structures commonly occur in the Late Pleistocene Weichselian periglacial deposits, and also here it remains unclear whether these structures have not been formed by freeze and thaw cycles. Bertran et al. (2019b) imply that the earthquake-induced sand blows may rather correspond to thermal contraction in the permafrost or be caused by large floods (Li et al., 1996). The main argument supporting the claim that earthquakes caused the structures is that organic material was found in bowls. However, there are problems with the dating approach. The material was disturbed by subrecent *Alnus* roots (Grube, 2019b).

Another problem with the study of Grube (2019b) is that the structures observed cannot be connected to a major fault system. Grube (2019b) writes that “faults can be assumed in this area but no geophysical proof is available yet”. The supposed high magnitude ($M6$) earthquake (Grube, 2019a) must however be regarded with caution because glaciotectonic and periglacial processes cannot be ruled out in both studies.

7.5. Indicators for neotectonic movements

Shear-deformation bands are suitable indicators for neotectonic movements along the basement faults and fault activity can be identified on the basis of shear-deformation bands (Brandes et al., 2018a, b). Shear-deformation bands develop in the so-called process zone of an active fault (Fig. 40; Ballas et al., 2015). The spatial extent of neotectonically induced shear-deformation bands along the major basement faults observed in this study can be best explained by the geometry of the process zone. However, it is not possible to decide whether the fault activity was accompanied by earthquakes or whether it was aseismic creep. It is only possible to derive earthquake activity from SSDS, e.g. sand volcanoes or clastic dykes

(see Fig. 18), that were caused by the passage of seismic waves. However, these structures alone are not unambiguous and therefore it makes sense to use them in combination with shear-deformation bands, which reflect the trend of the underlying basement faults. Observing SSDS in combination with shear-deformation bands, e.g. Brandes and Winsemann (2013) in mixed alluvial-aeolian Late Pleniglacial deposits near the Osning Thrust, is the most reliable method for establishing the prior existence of paleo-earthquakes.

More research on deformation bands and their formation processes has to be carried out to better understand their relationship to faults. This study provides evidence of neotectonic activity at the Aller Valley Fault, the Steinhuder Meer Fault, the Harz Boundary Fault and the Halle Fault system. The outcrops exhibit deformation bands indicating fault activity. However, the lack of SSDS at these locations means it is not possible to confirm whether neotectonic activity was accompanied by earthquakes.

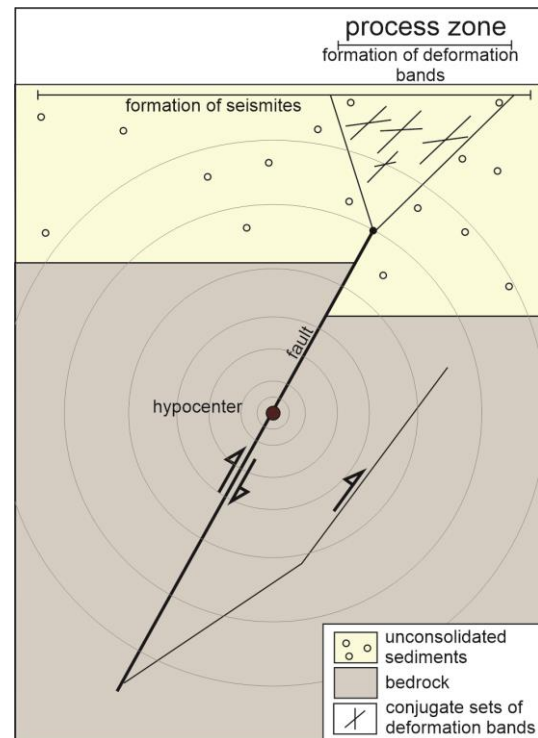


Fig 40: Schematic model of the formation and distribution of deformation bands in the process zone of a reverse fault (modified according to Ballas et al., 2015).

7.6. Characterization of deformation structures with the ESI scale and the PalSeisDB

It is not possible to correlate the deformation structures observed in this study with the ESI scale in most cases. Primary effects like surface rupture, tectonic uplift and subsidence have not been recorded in the study area so far. Surface ruptures in particular were destroyed by erosion (e.g. Kaiser, 2005) or anthropogenic activity. Secondary effects like ground cracks, slope movements, anomalous waves and tsunamis, hydrological anomalies or tree shaking cannot be applied in this study, which is based on geological/sedimentological indicators. Only liquefaction and fluidization structures (SSDS) provide an indication for the magnitude of the earthquake.

SSDS that can be correlated with the ESI scale were only observed at the Osning Thrust. As previously described in Brandes and Winsemann (2013), the association of the SSDS implies that the inferred earthquake at the Osning Thrust had a magnitude of at least 5.5. Correlated with the ESI scale, the size of the SSDS implies an earthquake intensity of ~8.

Out of seven investigated locations, this study identified four with new evidence for neotectonic - but not necessarily seismic - activity that can be included in the PalSeisDB. These are the outcrops at the locations Benzingerode (outcrop 5), Könnern (pit 25), Eitze (pit 42) and Altenhagen (pit 89). Although the indicators for neotectonic activity (deformation bands) are solid, there is no indication for earthquakes (SSDS) and thus the ESI scale cannot be applied. Tables based on PalSeisDB are inserted in the Appendix. Major basement faults and related deformation features are shown in the tables (Table A8-A11).

The offset along the fault at Benzingerode is at least 1.5 m. However, it is not clear, if this offset is the product of one single rupture event (that would lead to the estimation of a rather high intensity) or the result of a series of smaller events (with lower intensities). Neither can aseismic creep be ruled out. The neotectonic evidence for all other outcrops is based on shear-deformation bands. As discussed in section 7.5, it is not possible to determine whether these structures formed during seismogenic rupture processes or during aseismic creep.

7.7. Summary of evidence for movement at the basement faults

This study provided evidence of neotectonic activity. The neotectonic activity in northern Germany is a consequence of the regional lithospheric stress field, which is governed by the push of the mid-Atlantic ridge and the continuing Alpine orogeny. The work of Brandes et al. (2011), Brandes et al. (2012), Brandes and Winsemann (2013), Brandes et al. (2015) has shown that additional stress field changes due to glacial-istostatic adjustment might have induced Middle Pleistocene to Lateglacial and historic seismicity. The study area was also affected by these stress field changes. WNW-ESE trending faults in northern Germany have the highest reactivation potential because they trend parallel to the former ice margin (Brandes et al., 2015). The maximum horizontal components of the ice sheet-induced stress for these faults are in line with the paleo-stress field (Stewart et al., 2000).

The knowledge of the seismic activity in northern Germany is incomplete due to the infrequent occurrence of earthquakes and the short period of instrumental observation which started around 1900. Table 15 and Fig. 41 present a compilation of neotectonic activity, historic and recent earthquakes which is probably incomplete. The results of this two-year project do not exclude neotectonic movements and paleo-earthquakes at faults where no geological evidence like SSDS or deformation bands was found in the sand and gravel pits studied. The present study was conceived with the sole aim of detecting positive features. This does not mean that faults along which no evidence of neotectonic movement was found are inactive. However, it does reveal clear evidence for neotectonic activity at five faults, and provides a valuable contribution to the seismic hazard assessment in northern Germany. The orientation of these faults makes them prone to reactivation under GIA stress and they could also be reactivated by the current stress field.

Historic earthquakes in a 20-km-wide zone around the major faults were chosen and are listed in Table 15. It is necessary to bear in mind that the assignment of earthquakes to faults is rarely unambiguous. The epicentres of historic earthquakes often have an inaccuracy of 10-30 km (personal com. D. Kaiser, 2019). In this report, we have used the term “*historic earthquakes*” for events from 800 – 1900 and the term “*recent earthquakes*” for earthquakes since 1900.

Evidence of neotectonic movement at the **Aller Valley Fault** was found near **Eitze in pit 42** as shear-deformation bands with normal displacement, which probably developed in the process zone of the fault. Indications of seismogenic fault ruptures were not found in the Pleistocene sediments but cannot be excluded. The neotectonic movements must have occurred post Saalian because the sediments date from the Saalian. The results of this study imply that the Aller Valley Fault has been active since the Middle Pleistocene Saalian that may have continued in historic times. Historic earthquakes in Magdeburg occurred with intensities of 4.0 – 6.0 (Leydecker, 2011, Table 15, Fig. 41). The events are probably related to the Aller Valley Fault. Two of those earthquakes (in the years 1298 and 1567) are also assigned to the Gardelegen Fault, because the accuracy of the epicenter location is low. Recent earthquakes were detected in the year 1977 near Soltau with a magnitude of M_L 4.0, in 2004 near Rotenburg with a magnitude of M_L 4.5 (Dahm et al., 2007), in 2014 close to Walsrode with a magnitude of M_L 1.3 at a depth of 25.5 km and in 2018 close to Rethem with a magnitude of M_L 2.0 at a depth of 28.5 km (Brandes et al., 2019). However, these earthquakes are most likely too deep to be related to the Aller Valley Fault.

No evidence of neotectonic movement was found in sand and gravel pits at the **Elbe Lineament**. A historic earthquake with an intensity of 5 occurred near Lüneburg (Table 15, Fig. 41). However, this event is questionable (Leydecker, 2011). Recent earthquakes were detected in 2000 near Wittenburg with a magnitude M_L of 3.2 (Leydecker, 2011), in 2012 near Hitzacker with a magnitude of M_L 2.0 at a depth of 31.4 km and in 2012 near Perleberg with a magnitude of M_L 1.9 at a depth of 24.5 km. These earthquakes are located between the Elbe Lineament and the Thor Suture (Brandes et al., 2019). However, Brandes et al. (2019) shows that the hypocentre of the M_L 2.0 earthquake which occurred in 2012 near Hitzacker, is located below the Elbe Lineament and likely in the prolongation of the Thor Suture.

No evidence of neotectonic movement was found in sand and gravel pits at the **Gardelegen Fault**. Historic earthquakes with an intensity of 4.0 – 6.0 occurred in the Altmark area and in the vicinity of Magdeburg (Leydecker, 2011; Table 15, Fig. 41).

Evidence of neotectonic movement at the **Halle Fault system** was found near **Könnern in pit 25** as indicated by shear-deformation bands with normal displacement above a blind fault north of the Halle Fault. Indications of fault rupture were not found

in Middle Pleistocene sediments but cannot be excluded. The neotectonic movements occurred post Saalian because the sediments date from the Middle Pleistocene Saalian (cf. Knoth, 1992). The Halle Fault and related faults have been active since the Middle Pleistocene Saalian and there have been repeated events in historic times (Leydecker, 2011). Historic earthquakes with intensities of 3.5 - 4.5 occurred near Merseburg, Halle, Halle/Weißenfels (Leydecker, 2011; Table 15, Fig. 41). Recent earthquakes were detected in 1908 near Halle/Weißenfels with an intensity of 3.0, in 1987 near Gröbzig with a magnitude of M_L 2.4, in 2015 near Röglitz with a magnitude of M_W 3.2 and M_L 2 (Dahm et al., 2018; BGR, 2019) and in 2017 near Schkeuditz with a magnitude M_W of 2.8 (Dahm et al., 2018; Fig. 41). Several historic earthquakes with intensities of 3.0 – 4.5 and recent earthquakes with intensities of 3.0 – 6.0 and magnitudes of M_L 2.8 to 4.1 have occurred near Leipzig, but are most likely linked to the Leipzig fault system and located outside the study area.

Evidence of neotectonic movement at the **Harz Boundary Fault** was found near **Benzingerode in outcrop 5**. A fault exposed in a sinkhole close to the Harz Boundary Fault exhibits polyphase tectonic evolution with initial normal fault movements and a later reactivation as an oblique reverse fault. Luminescence dating of the deposits indicates fault movement after ~15 ka (Müller et al., *in press a*). A recent earthquake with an intensity of 4 occurred near Quedlinburg (Leydecker, 2011; Table 15, Fig. 41).

Evidence of neotectonic movement associated with paleo-earthquakes at the **Osning Thrust** was found near **Augustdorf in pit 19** and **Oerlinghausen in pit 22**. Indicators are shear-deformation bands with normal displacement, which most likely developed in the process zone of the active fault, and seismites that include clastic dykes and a sand volcano. Luminescence dating revealed the neotectonic movement to have occurred in the Lateglacial between 16 to 13 ka (Brandes et al., 2012; Roskosch et al., 2012; Brandes and Winsemann, 2013). Historic earthquakes occurred in the area of Bielefeld and near Oerlinghausen with an intensity of 6 (Leydecker, 2011; Table 15, Fig. 41). A recent earthquake was detected in 2019 NE of Paderborn with a magnitude of M_L 2.1 (BGR, 2019).

Evidence of neotectonic movement at the **Steinhuder Meer Fault** was found in **Altenhagen pit 89**. Indicators are shear-deformation bands with normal displacement that probably developed above the Steinhuder Meer Fault (Table 15, Fig. 41).

Indications of fault rupture such as seismites were not found in the Middle Pleistocene sediments but cannot be excluded. The neotectonic movement occurred post Saalian because luminescence dating reveals the growth strata to date back to the Middle Pleistocene Saalian (189 ± 4 ka to 189 ± 5 ka).

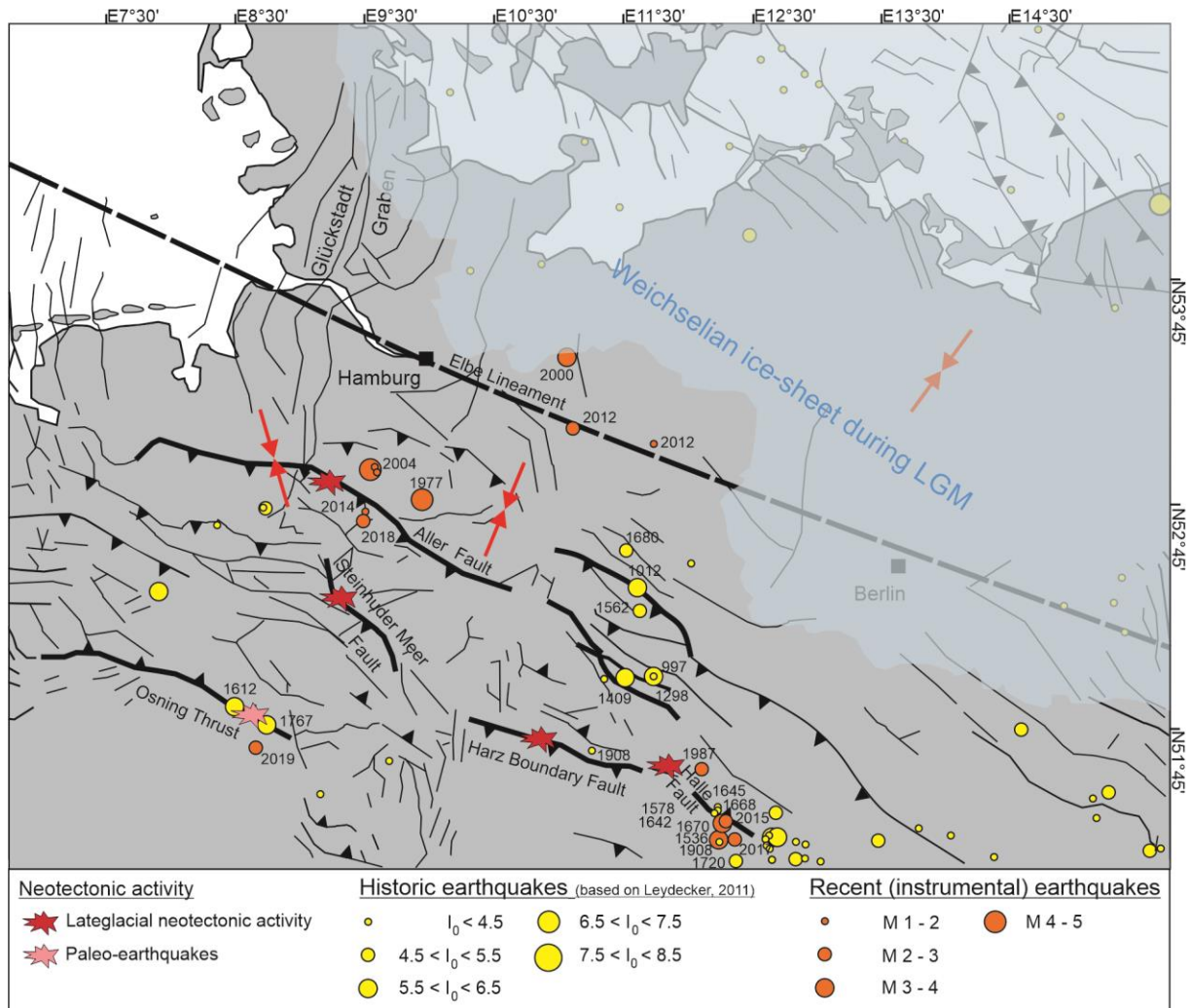


Fig. 41: Tectonic activity along seven major basement faults in northern Germany analyzed in this study. The figure shows neotectonic activity, historic earthquakes and recent earthquakes (modified according to Brandes et al., 2015, Müller et al., *in press b*). The red arrows show the recent stress field in northern Germany. The numbers represent the year of each earthquake listed in Table 15. The faults analyzed in this study are shown in bold; the Elbe Lineament is shown as dashed line because it represents a terrane boundary; LGM: Last Glacial Maximum; the shaded area represents the ice sheet expansion during the Weichselian LGM.

Table 15: Tectonic activity along seven major basement faults in northern Germany analyzed in this study. Neotectonic activity, paleo-earthquakes, historic earthquakes and recent earthquakes with the timing of each tectonic event are listed. The selected historic earthquakes are located up to 20 km away from the fault. The Wittenburg and Soltau events are more than 20 km away from a fault but are listed because of their high magnitude and the resulting importance for the hazard assessment. The Rotenburg 2004 event has yet to be unequivocally classified as natural or triggered. The numbers (X*) are related to the study of Brandes et al. (2019) and have been adopted for a better assignment. However, the 2014 and 2018 earthquakes near Walsrode and Rethem were most likely too deep to be related to the Aller Valley Fault. Some of the historic earthquakes are assigned to different major faults because the accuracy of the epicenter is low. * M_w was calculated using the equation $M_w = 0.682 I_0 + 0.16$ according to Grünthal et al. (2009).

Major basement fault	Neotectonic activity post-Miocene (this study)	Paleo-earthquakes post-Miocene (this study)	Historic earthquakes 800 - 1900 (Leydecker, 2011)	Recent earthquakes Since 1900
Aller Valley Fault	Eitze (pit 42) (post Middle Pleistocene Saalian)	Uncertain	997 (I ₀ 6.0) Altmark 1298 (I ₀ 4.0) Magdeburg 1409 (I ₀ 6.0) Magdeburg 1576 (I ₀ 4.0) Magdeburg (questioned)	1977 M _L 4.0 near Soltau (Dahm et al., 2007) 2004 M _w 4.4 near Rotenburg (Dahm et al., 2007) 2014 M _L 1.3 (5*) near Walsrode (Brandes et al., 2019) 2018 M _L 2.0 (7*) near Rethem (Brandes et al., 2019)
Elbe Lineament	No evidence found	No evidence found	1323 (I ₀ 5.0) Lüneburg (questioned)	2000 M _L 3.2 near Wittenburg (Leydecker, 2011) 2012 M _L 2.0 (2*) near Hitzacker (Brandes et al., 2019) 2012 M _L 1.9 (3*) near Perleberg (Brandes et al., 2019)
Gardelegen Fault	No evidence found	No evidence found	997 (I ₀ 6.0) Altmark 1012 (I ₀ 5.5) Altmark 1298 (I ₀ 4.0) Magdeburg 1562 (I ₀ 4.5) Altmark 1576 (I ₀ 4.0) Magdeburg (questioned) 1680 (I ₀ 4.5) Altmark	No
Halle Fault system	Könnern (pit 25) (post Middle Pleistocene Saalian)	Uncertain	1536 (I ₀ 3.5) Merseburg 1578 (I ₀ 3.5) Halle 1642 (I ₀ 3.5) Halle 1645 (I ₀ 4.0) Halle / Weißenfels 1668 (I ₀ 4.0) Halle / Weißenfels	1908 (I ₀ 3.0/M _w 2.2*) Halle / Weißenfels (Leydecker, 2011) 1987 M _L 2.4 Gröbzig (BGR, 2019) 2015 M _w 3.2 near Röglitz (Dahm et al., 2018) 2015 M _L 2 near Röglitz (BGR, 2019) 2017 M _w 2.8 near Schkeuditz (Dahm et al., 2018)

1670 (I_o 4.0) Halle / Weißenfels
1720 (I_o 4.5) Halle / Weißenfels

Harz Bounday Fault	Benzingerode (outcrop 5) (Late Pleistocene) (after ~15 ka)	Uncertain	No	1908 (I _o 3.0 / M _w 2.2*) Quedlinburg
Osning Thrust	Augustdorf (pit 19) Oerlinghausen (pit 22) (Late Pleistocene) (between ~16 – 13 ka)	Yes	1612 (I _o 6.0) Bielefeld 1767 (I _o 6.0) Oerlinghausen	2019 M _L 2.1 NE of Paderborn (BGR, 2019)
Steinhuder Meer Fault	Altenhagen (pit 89) (Middle Pleistocene) (between ~158 – 189 ka)	Uncertain	No	No

8. Conclusions

1. Five of the seven investigated major basement faults in northern Germany (Aller Valley Fault, Harz Boundary Fault, Halle Fault system, Osning Thrust and Steinhuder Meer Fault) reveal evidence of neotectonic activity.
2. The Osning Thrust is the only fault with clear evidence of paleo-earthquakes.
3. Shear-deformation bands in Middle Pleistocene sediments indicate neotectonic movement at the Aller Valley Fault, Halle Fault system and Steinhuder Meer Fault, which developed in the process zone of the faults. Seismic and aseismic creep, both may have occurred along these faults.
4. A fault with a young polyphase evolution (normal and reverse fault movement) exposed in a sinkhole close to the Harz Boundary Fault indicates neotectonic activity at this location. The date of the fault activity (Lateglacial) confirms observations made at the Osning Thrust and Sorgenfrei Tornquist Zone (Brandes et al., 2012; Brandes and Winsemann, 2013; Brandes et al., 2018b).
5. The seismicity is most likely induced by varying lithospheric stress conditions related to glacial-isostatic adjustment. Lateglacial, historic and recent earthquakes have occurred in this region. Thus, the most likely driver for fault activity since the Middle Pleistocene is the glacial-isostatic adjustment (GIA).
6. Northern Germany was repeatedly overridden by ice sheets. This strongly limits the standard use of SSDS to determine paleoseismic activity because these structures are likely to be the result of glaciotectionics.
7. Shear-deformation bands are potentially a good indicator for neotectonic fault activity but they cannot provide any clear evidence of earthquakes. However, SSDS in combination with shear-deformation bands indicate that the neotectonic activity was accompanied by earthquakes.

9. Outlook

The aim of this study was to find paleoseismic evidence at seven major fault zones in northern Germany. This study was initiated by the publications of Brandes et al. (2012) and Brandes and Winsemann (2013), which provide evidence of paleoseismic events at the Osning Thrust. We could not find further evidence of paleo-earthquakes, however, it was possible to find evidence of neotectonic activity at the Harz Boundary Fault, Aller Valley Fault, the Halle Fault system and the Steinhuder Meer Fault. It is not possible to ascertain whether earthquakes accompanied these events because seismites could not be identified.

Trenching of Pleistocene to Holocene sediments above the tip line of these faults could provide more information on neotectonic movement and potential earthquakes and thus verify the occurrence of neotectonic activity. Requirements are that 1) the faults reach near to the Earth's surface, 2) the tip line of the fault is covered by sediments and 3) it is possible to date these sediments. Faults that fulfil these requirements represent promising targets for near-surface geophysical surveys such as shear wave seismic profiles, georadar or ERT. These methods should be applied in order to better understand fault structure and to identify potential displacements in near-surface sediments that point to young fault activity.

It is important to bear in mind that this study relies on artificial outcrops in the form of sand and gravel pits that provide insight into the near-surface sediments and related deformation structures in the vicinity of the seven major basement faults. The results are strongly influenced by the current state of the outcrops. This situation may change in the future due to ongoing mining activity. Additional information might therefore be derived from these outcrops in the future that changes the current interpretation.

Further research has to be carried out on deformation bands to better understand their relationship to active faults and analyse their potential as indicator for paleoseismic activity (with the possibility of including them as features in the ESI scale). Estimating the magnitude of earthquakes using deformation bands has so far been difficult because no categorization for a magnitude assessment exists. The processes involved and factors governing the formation of deformation bands are not yet fully understood. Some initial results indicate a relationship between the occurrence of cataclastic deformation bands and rupturing faults (Cashman et al., 2007). More research needs

to be carried out on the interplay between fault activity and deformation band formation. Apart from the analysis of natural deformation bands, this should include experimental studies on deformation band evolution. A systematic study of deformation bands at active and fossil faults in different tectonic settings should also be carried out to collect a larger data set and test the hypothesis about deformation bands that was presented in this report.

We recommend further analyses of faults that are optimally oriented for a reactivation under GIA stress like the Haldensleben Fault and the Wittenberge Fault. These faults are due for further paleoseismic analyses in northern Germany.

Appendix

Table A1: All sand and gravel pits and sinkholes along the Harz Boundary Fault in the Subhercynian Basin.

Nr.	Location	Coordinates	Geological map 1:25000	Geological map 1:50000	Deposits	References	Deformation structures	References
1	Abbenrode	51°56'21.77"N 10°37'6.96"E	4029 Vienenburg	L4128 Goslar	Fluvial gravel overlain by meltwater deposits	(Weymann, 2004); Field observation	Glaciotectonic features; Normal faults;	(Weymann, 2004); Field observation
2	Aschersleben 1	51°45'56.83"N 11°25'30.48"E	4234 Aschersleben	L4334 Aschersleben	Meltwater deposits overlain by fluvial sand and gravel and loess	(Weymann, 2004); Field observation	Cryoturbation	Field observation
3	Aschersleben 2	51°46'32.72"N 11°24'34.09"E	4234 Aschersleben	L4334 Aschersleben	Boulder clay overlain by meltwater deposits, fluvial sand and gravel and loess	(Weymann, 2004); Field observation	Glaciotectonic features	(Weymann, 2004)
4	Badeborn	51°45'55.94"N 11°16'23.59"E	4233 Ballenstedt	L4332 Quedlinburg	Loess	(Weissermel et al., 1926)		
5	Benzingerode	51°49'33.02"N 10°52'33.01"E	4131 Derenburg	L4130 Werningerode	Debris-flow deposits	(Schröder et al., 1927); Field observation	Sinkholes with normal and reverse faults	(Franzke et al., 2015); Field observation
6	Beuchte	51°59'11.92"N 10°30'35.01"E	4029 Vienenburg	L4128 Goslar	Fluvial gravel	(Schroeder et al., 1931); Field observation	Cryoturbation	Field observation
7	Halberstadt	51°54'25.00"N 11° 5'29.35"E	4032 Schwanebeck	L4132 Halberstadt	Meltwater deposits overlain by loess	(Schröder et al., 1929a); Field observation		
8	Hoym	51°46'48.30"N 11°20'20.25"E	4234 Aschersleben	L4334 Aschersleben	Meltwater deposits overlain by fluvial sand and gravel, till and loess	(Weymann, 2004)	Recumbent fold	Field observation
9	Lengde	51°59'31.54"N 10°32'56.42"E	4029 Vienenburg	L4128 Goslar	Fluvial gravel	(Schröder et al., 1931)		
10	Palandsmühle	51°57'42.89"N 10°21'9.40"E	4028 Goslar	L4128 Goslar	Fluvial gravel	(Bode et al., 1926)		
11	Quedlinburg	51°47'8.52"N 11°10'35.85"E	4232 Quedlinburg	L4332 Quedlinburg	Fluvial gravel overlain by loess	(Weymann, 2004); Field observation	Cryoturbation	Field observation
12	Reinstedt	51°45'53.97"N 11°21'49.91"E	4234 Aschersleben	L4334 Aschersleben	Fluvial gravel overlain by loess	(Weymann, 2004)		
13	Ströbeck	51°54'46.04"N 10°57'25.75"E	4031 Dingelstedt am Huy	L4130 Werningerode	Meltwater deposits overlain by fluvial sand and gravel, till and loess	(Schröder et al., 1929b)		
14	Suderode	51°58'53.25"N 10°37'40.86"E	4029 Vienenburg	L4128 Goslar	Fluvial gravel overlain by loess	(Weymann, 2004); Field observation		
15	Warnstedt	51°47'6.07"N 11° 2'5.24"E	4232 Quedlinburg	L4332 Quedlinburg	Meltwater deposits	(Weymann, 2004); Field observation	Glaciotectonic features; Normal faults, open fold;	(Weymann, 2004); Field observation
16	Westdorf	51°43'48.54"N 11°25'45.69"E	4234 Aschersleben	L4334 Aschersleben	Meltwater deposits overlain by fluvial gravel	(Weymann, 2004); Field observation	Cryoturbation	(Weymann, 2004)
17	Wiedelah	51°58'20.93"N 10°34'46.28"E	4029 Vienenburg	L4128 Goslar	Fluvial gravel overlain by loess	(Schröder et al., 1931); Field observation	Cryoturbation	Field observation

Table A2: All sand pits along the Osning Thrust.

Nr.	Location	Coordinates	Geological map 1:25000	Geological map 1:50000	Deposits	References	Deformation structures	References
18	Am Ellenberg	52°11'17.47"N 8° 0'0.93"E	3814 Bad Iburg	L3914 Bad Iburg	Meltwater deposits	(Haack et al., 1930)		
19	Augustdorf 1	51°55'12.72"N 8°44'38.43"E	4018 Lage	L4118 Detmold	Alluvial-fan deposits overlain by mixed alluvial-aeolian and aeolian sand-sheet deposits	(Meinsen, et al., 2014)	Irregular branched and stepped dykes, normal faults/joints, deformation bands: normal displacement;	Brandes & Winsemann, 2013
20	Augustdorf 2	51°54'49.13"N 8°42'55.69"E	4018 Lage	L4118 Detmold	Aeolian dune sand	(Keilhack et al., 1917)		
21	Müssen	51°57'22.31"N 8°46'52.64"E	4018 Lage	L4118 Detmold	Meltwater deposits overlain by subglacial till	(Keilhack et al., 1917)		Brandes & Winsemann, 2013
22	Oerlinghausen	51°56'30.14"N 8°40'25.64"E	4018 Lage	L4118 Detmold	Alluvial-fan deposits, overlain by mixed alluvial-aeolian and aeolian sand-sheet deposits	(Meinsen, et al., 2014)	Sand volcano, sharp-sided dykes, intrusive sedimentary bodies, flame structures, ball-and-pillow structures, small-scale inversion structures;	

Table A3: All sand and gravel pits along the Halle Fault system.

Nr.	Location	Coordinates	Geological map 1:25000	Geological map 1:50000	Deposits	References	Deformation structures	References
23	Gutenberg	51°33'2.04"N 12° 0'10.63"E	4438 Landsberg	L4538 Landsberg	Meltwater deposits	(Weissermel et al., 1909); Field observation	Glaciotectonic	Field observation
24	Köchstedt	51°28'29.42"N 11°47'39.24"E	4536 Teutschenthal	L4536 Halle (Saale)	Fluvial deposits	(Radzinski et al., 1962); Field observation	Cryoturbation	Field observation
25	Könnern	51°41'0.52"N 11°44'31.18"E	4336 Könnern	L4226 Bernburg (Saale)	Glaciolacustrine subaquous fan and glaciofluvial delta deposits overlain by loess	(Kunert et al., 1963), (Knoth, 1992); Field observation	Deformation bands	Field observation
26	Landsberg	51°30'48.67"N 12° 8'21.54"E	4438 Landsberg	L4538 Landsberg	Meltwater deposits	(Weissermel et al., 1909); Field observation		
27	Morl	51°32'43.00"N 11°54'12.05"E	4437 Halle (Saale) Nord	L4536 Halle (Saale)	Paleogene deposits overlain by Pleistocene deposits	(Kraiß et al., 1922); Field observation	Deformation band	Field observation
28	Nehlitz	51°34'40.38"N 11°58'25.50"E	4437 Halle (Saale) Nord	L4536 Halle (Saale)	Meltwater deposits and loess	(Kraiß et al., 1922); Field observation		
29	Nellschütz 1	51°12'53.47"N 12° 1'10.28"E	4738 Bad Dürrenberg	L4738 Leipzig West	Fluvial deposits	(Siegert, 1909b), (Knoth, 1992); Field observation	Cryoturbation	Field observation
30	Nellschütz 2	51°12'40.60"N 12° 2'34.36"E	4738 Bad Dürrenberg	L4738 Leipzig West	Fluvial deposits	(Siegert, 1909b), (Knoth, 1992); Field observation		
31	Niederwünsch	51°21'32.26"N 11°48'8.70"E	4636 Müncheln	L4736 Merseburg	Glaciofluvial Gilbert-typ delta overlain by subglacial till	(Wansa et al., 2004)	Cryoturbation, normal faults	(Wansa et al., 2004)
32	Schkeitbar	51°14'53.44"N 12°13'9.17"E	4739 Zwenkau	L4738 Leipzig West	Terminal moraine deposits overlain by paraglacial deposits	(Hazard, 1924), (Knoth, 1992); Field observation		
33	Schladebach 1	51°18'27.01"N 12° 6'23.52"E	4638 Leuna	L4738 Leipzig West	Fluvial deposits	(Siegert et al., 1909a); Field observation		
34	Schladebach 2	51°19'38.10"N 12° 5'55.43"E	4638 Leuna	L4738 Leipzig West	Fluvial deposits	(Siegert et al., 1909a); Field observation	Cryoturbation, reverse faults	Field observation

Table A4: All sand pits along the Aller Valley Fault.

Nr.	Location	Coordinates	Geological map 1:25000	Geological map 1:50000	Deposits	References	Deformation structures	References
35	Am Aschenberg 1	52°42'14.82"N 10°15'45.77"E	3227 Eschede	L3326 Celle	Meltwater deposits overlain by paraglacial deposits (Geschiebedecksand)	(Stoller et al., 1915)	Deformation bands with reverse displacement; fault-propagation fold	Field observation
36	Am Aschenberg 2	52°41'44.79"N 10°16'40.61"E	3327 Lachendorf	L3326 Celle	Meltwater deposits overlain by paraglacial deposits (Geschiebedecksand)	(Harbort et al., 1916c)		
37	Bahrdorf 1	52°23'23.81"N 10°59'14.76"E	3631 Groß Twülpstedt	L3730 Königslutter am Elm	Meltwater deposits	(Mestwerdt et al., 1914)		
38	Bahrdorf 2	52°23'26.55"N 10°59'31.64"E	3631 Groß Twülpstedt	L3730 Königslutter am Elm	Meltwater deposits	(Mestwerdt et al., 1914)	Deformation and compaction bands; ice wedge casts	Field observation
39	Bissen	53° 3'35.90"N 8°32'55.97"E	2917 Delmenhorst	L2916 Delmenhorst	Meltwater deposits overlain by paraglacial deposits (Geschiebedecksand)	Field observation	Cryoturbation: ice wedge casts	Field observation
40	Celle	52°37'4.70"N 10° 2'20.44"E	3326 Celle	L3326 Celle	Meltwater deposits	Field observation		
41	Eggestedt	53°14'8.67"N 8°37'38.96"E	2717 Schwanewede	L2716 Brake (Unterweser)	Glaciolacustrine sand overlain by paraglacial deposits (Geschiebedecksand)	(Höfle et al., 1976)	Cryoturbation, deformation bands with normal displacement	(Höfle et al., 1976); Field observation
42	Eitze	52°54'27.62"N 9°18'10.45"E	3021 Verden (Aller)	L3120 Verden (Aller)	Meltwater deposits	Field observation	Deformation bands with normal displacement, conjugate systems	Field observation
43	Fallersleben-Sülfeld	52°25'38.53"N 10°43'4.06"E	3530 Wolfsburg	L3530 Wolfsburg	Fluvial sand	(Woldstedt et al., 1929)		
44	Filterberg	52°29'50.02"N 10°38'25.72"E	3529 Gifhorn	L3528 Gifhorn	Meltwater deposits	Field observation	Deformation bands with normal and reverse displacement	Field observation
45	Garßen	52°41'27.86"N 10° 8'59.95"E	3326 Celle	L3326 Celle	Meltwater deposits overlain by paraglacial deposits (Geschiebedecksand)	(Harbort et al., 1916a)	Cryoturbation: convolute bedding	Field observation
46	Giersberg	53° 0'19.39"N 9° 6'35.93"E	2920 Achim	L2920 Achim	Meltwater deposits overlain by aeolian sand	Field observation		
47	Groß Eicklingen	52°33'34.26"N 10°11'45.61"E	3427 Wienhausen	L3526 Burgdorf	Aeolian dune sand	(Harbort et al., 1916b)		
48	Groß Eilstorf	52°49'36.11"N 9°26'16.27"E	3122 Häuslingen	L3122 Walsrode	Till overlain by paraglacial deposits (Geschiebedecksand)	Field observation	Deformation bands with normal and reverse displacement, ice wedge casts, folds, remnants of sand volcanoes	Field observation

49	Groß Hehlen	52°39'50.75"N 10° 2'10.84"E	3326 Celle	L3326 Celle	Meltwater deposits overlain by paraglacial deposits (Geschiebedecksand)	(Harbort et al., 1916a)	Deformation bands with normal displacement, fault-propagation fold	Field observation
50	Hassel	52°47'46.52"N 9°13'29.59"E	3221 Eystrup	L3320 Nienburg (Weser)	Aeolian dune sand			Field observation
51	Hinter dem Forde	52°58'43.31"N 8° 3'26.42"E	3014 Garrel	L3114 Cloppenburg	Fluvial sand			Field observation
52	Hinter dem Horn	53°15'42.09"N 8°42'2.56"E	2718 Osterholz-Scharmbeck	L2718 Osterholz-Scharmbeck	Meltwater deposits		Folds	Field observation
53	Hohnsleben	52° 9'41.35"N 11° 3'54.89"E	3832 Welfensleben	L3932 Oschersleben (Bode)	Meltwater deposits	(Koert et al., 1927)		
54	Hülseberg	53°16'27.87"N 8°44'46.09"E	2718 Osterholz-Scharmbeck	L2718 Osterholz-Scharmbeck	Meltwater deposits overlain by paraglacial deposits (Geschiebedecksand)		Deformation bands, cryoturbation: convolute bedding	Field observation
55	Kästorf	52°32'22.50"N 10°29'51.19"E	3428 Müden/3429 Wesendorf	L3528 Gifhorn	Meltwater deposits overlain by paraglacial deposits (Geschiebedecksand)			Field observation
56	Kreienmoor	53°12'50.84"N 8°36'8.10"E	2717 Schwanewede	L2716 Brake (Unterweser)	Glaciolacustrine sand overlain by paraglacial deposits (Geschiebedecksand)	(Höfle et al., 1976)	Cryoturbation, deformation bands	(Höfle et al., 1976)
57	Langwedelermoor	52°59'59.59"N 9°10'17.23"E	2921 Ahausen	L2920 Achim	Meltwater deposits		Deformation bands with normal displacement, conjugate systems, thrust sheets	Field observation
58	Lunsen	52°58'6.60"N 9° 3'48.79"E	3020 Thedinghausen	L3120 Verden (Aller)	Fluvial sand overlain by floodplain deposits			Field observation
59	Meinkot	52°23'13.34"N 10°58'23.37"E	3631 Groß Twülpstedt	L3730 Königslutter am Elm	Meltwater deposits	(Mestwerdt et al., 1914)	Cryoturbation: ice wedge casts	Field observation
60	Meißendorf	52°45'10.03"N 9°48'11.43"E	3224 Westenholz	L3324 Wietze	Meltwater deposits overlain by paraglacial deposits (Geschiebedecksand)	(Lang et al., 1980)		
61	Nordkampen	52°51'44.05"N 9°24'48.82"E	3122 Häuslingen	L3122 Walsrode	Meltwater deposits			Field observation
62	Ostenholz	52°46'0.90"N 9°43'38.07"E	3224 Westenholz	L3324 Wietze	Meltwater deposits overlain by paraglacial deposits (Geschiebedecksand)	(Lang et al., 1980)		
63	Sassenburg	52°30'58.13"N 10°38'42.05"E	3429 Wesendorf	L3528 Gifhorn	Meltwater deposits overlain by paraglacial deposits (Geschiebedecksand)		Cryoturbation: ice wedge casts, deformation bands	Field observation
64	Scheuen	52°40'18.21"N 10° 3'55.91"E	3326 Celle	L3326 Celle	Meltwater deposits overlain by paraglacial deposits (Geschiebedecksand)	(Harbort et al., 1916a)	Deformation bands with normal displacement, thrust sheets	Field observation
65	Schmede	53° 1'53.31"N 8°23'23.50"E	2916 Hatten	L2916 Delmenhorst	Till overlain by aeolian sand		Deformation bands with normal displacement, thrusts, folds, cryoturbation: convolute bedding	Field observation

66	Tappenbeck	52°28'16.07"N 10°43'18.78"E	3530 Wolfsburg	L3520 Wolfsburg	Meltwater deposits overlain by paraglacial deposits (Geschiebedecksand)	(Woldstedt et al., 1929)		
67	Walle	52°44'36.01"N 9°54'50.06"E	3225 Offen	L3324 Wietze	Meltwater deposits	(Lang et al., 1983)		
68	Wesendorf	52°35'26.95"N 10°30'58.82"E	3429 Wesendorf	L3528 Gifhorn	Meltwater deposits overlain by paraglacial deposits (Geschiebedecksand)	Field observation	Cryoturbation: ice wedge casts	Field observation
69	Westenholz	52°46'12.35"N 9°42'25.21"E	3224 Westenholz	L3324 Wietze	Meltwater deposits overlain by paraglacial deposits (Geschiebedecksand)	(Lang et al., 1980)		
70	Wilsche	52°31'41.73"N 10°28'29.73"E	3428 Müden (Aller)	L3528 Gifhorn	Meltwater deposits overlain by paraglacial deposits (Geschiebedecksand)	Field observation		

Table A5: All sand and gravel pits along the Gardelegen Fault.

Nr.	Location	Coordinates	Geological map 1:25000	Geological map 1:50000	Deposits	References	Deformation structures	References
71	Born	52°22'33.18"N 11°27'28.02"E	3634 Bülstringen	L3734 Haldensleben	Meltwater deposits	(Picard et al., 1908)		
72	Dolle	52°23'57.24"N 11°37'45.89"E	3535 Dolle	L3534 Hansestadt Gardelegen	Meltwater deposits and till	(Wieggers, 1914); Field observation	Normal faults, reverse faults, folds	Field observation
73	Gardelegen	52°32'35.43"N 11°25'9.19"E	3434 Gardelegen	L3534 Hansestadt Gardelegen	Meltwater deposits	(Scholz, 1887a)	Deformation bands	Field observation
74	Hottendorf	52°32'2.49"N 11°32'42.23"E	3435 Lindstedt (Uchtsprunge)	L3534 Hansestadt Gardelegen	Meltwater deposits overlain by till	(Scholz, 1887b)	Normal faults	Field observation
75	Niegripp	52°15'20.76"N 11°46'6.60"E	3736 Zielitz	L3736 Burg	Fluvial deposits	(Korn et al., 1923)		

Table A6: All sand pits along the Elbe Lineament.

Nr.	Location	Coordinates	Geological map 1:25000	Geological map 1:50000	Deposits	References	Deformation structures	References
76	Alt Garge	53°15'9.36"N 10°48'14.25"E	2730 Bleckede	L2730 Boizenburg (Elbe)	Meltwater deposits overlain by paraglacial deposits (Geschiebedecksand)	(Meyer et al., 2004)	Deformation bands: normal displacement, folds	Field observation
77	Bendelin	52°54'33.14"N 12° 7'48.09"E	3038 Glöwen	L3138 Havelberg	Meltwater deposits overlain by till	(Grunder, 1896)	Deformation bands: normal displacement	Field observation
78	Boizenburg	53°22'33.20"N 10°40'34.08"E	2630 Boizenburg (Elbe)	L2730 Boizenburg (Elbe)	Aeolian dune sand	(Krienke et al., 2001)		
79	Breetze	53°15'48.27"N 10°43'24.24"E	2730 Bleckede	L2730 Boizenburg (Elbe)	Meltwater deposits overlain by paraglacial deposits (Geschiebedecksand)	(Meyer et al., 2004)		
80	Ferbitz	53° 5'17.09"N 11°34'37.74"E	2935 Schnackenburg	L2943 Lenzen (Elbe)	Meltwater deposits	(Weissermel, 1901)	Folds	Field observation
81	Gusborn	53° 5'15.08"N 11°13'5.86"E	2933 Gusborn	L2932 Dannenberg (Elbe)	Meltwater deposits	(Reuter, 1975b)	Deformation bands: normal displacement	Field observation
82	Meudelfitz	53° 9'46.30"N 11° 0'40.06"E	2832 Dannenberg Elbe/Nord	L2932 Dannenberg (Elbe)	Meltwater deposits	(Reuter, 1975a)	Deformation bands: normal displacement	Field observation
83	Niendorf	53°15'59.31"N 10°43'52.48"E	2730 Bleckede	L2730 Boizenburg (Elbe)	Meltwater deposits overlain by paraglacial deposits (Geschiebedecksand)	(Meyer et al., 2004)		
84	Riskau	53° 5'58.53"N 11° 2'2.23"E	2932 Dannenberg Elbe/Süd	L2932 Dannenberg (Elbe)	Meltwater deposits	(Lepper & Tüxen, 1975)		
85	Tießau	53°11'27.30"N 10°58'12.12"E	2831 Göhrde	L2930 Dahlenburg	Meltwater deposits	(Höfle, 1977)		
86	Tramm	53° 3'29.69"N 11° 4'5.85"E	2932 Dannenberg Elbe/Süd	L2932 Dannenberg (Elbe)	Meltwater deposits	(Lepper & Tüxen, 1975)		
87	Wiershop	53°26'2.14"N 10°26'6.24"E	2528 Geesthacht	L2528 Geesthacht	Meltwater deposits overlain by till	(Gagel et al., 1911)		
88	Zweedorf	53°26'29.00"N 10°38'43.38"E	2529 Büchen	L2528 Geesthacht	Meltwater deposits	(Gagel et al., 1914)		

Table A7: All sand and gravel pits along the Steinhuder Meer Fault.

Nr.	Location	Coordinates	Geological map 1:25000	Geological map 1:50000	Deposits	References	Deformation structures	References
89	Altenhagen	52°26'3.31"N 9°22'50.82"E	3522 Wunstorf	L3522 Garbsen	Meltwater deposits overlain by loess and paraglacial deposits	(Voss et al., 1979)	Conjugate normal faults, reverse faults	Field observation
90	Bolsehle	52°33'52.58"N 9°17'42.03"E	3421 Husum	L3520 Rehburg-Loccum	Meltwater deposits	(Voss et al., 1982)	Normal faults, ice wedge casts	Field observation
91	Eilvese	52°32'27.86"N 9°23'19.38"E	3422 Neustadt am Rübenberge	L3522 Garbsen	Meltwater deposits overlain by paraglacial deposits (Geschiebedecksand)	(Jordan et al., 1980)	Conjugate normal faults, ice wedge casts, cryoturbation	Field observation
92	Poggenhagen	52°27'50.71"N 9°26'36.39"E	3522 Wunstorf	L3522 Garbsen	Meltwater deposits	(Voss et al., 1979)		
93	Rehburg	52°29'22.68"N 9°14'4.07"E	3521 Rehburg	L3520 Rehburg-Loccum	Meltwater deposits overlain by paraglacial deposits (Geschiebedecksand)	(Jordan et al., 1979)	Ice wedge casts, cryoturbation	Field observation
94	Schneeren 1	52°31'9.21"N 9°19'33.95"E	3421 Husum	L3520 Rehburg-Loccum	Meltwater deposits	(Voss et al., 1982)		
95	Schneeren 2	52°32'45.43"N 9°20'29.12"E	3422 Neustadt am Rübenberge	L3522 Garbsen	Meltwater deposits overlain by paraglacial deposits (Geschiebedecksand)	(Jordan et al., 1980)	Normal faults	Field observation
96	Schneeren 3	52°33'18.91"N 9°20'50.42"E	3422 Neustadt am Rübenberge	L3522 Garbsen	Meltwater deposits overlain by till	(Jordan et al., 1980)		
97	Vehrenheide	52°29'31.34"N 9°14'45.99"E	3521 Rehburg	L3520 Rehburg-Loccum	Meltwater deposits overlain by paraglacial deposits (Geschiebedecksand)	(Jordan et al., 1979)		

Table A8: PalSeisDB. Fault in a sinkhole near Benzingerode (outcrop 5) (Harz Boundary Fault).

PSE: Faults Benzingerode

Location	Northern Germany		Country.	DE		Comments 1 Striations on the fault plane indicate initial normal fault movements and a later reactivation of the fault as oblique reverse fault.
Lon.	10.875861	Coord GPS coordinates of the sinkhole, where a fault is exposed	Observation type	sinkhole		
Lat.	51.825889		Feature type	Trench ID		
			fault (normal and reverse)			
Short description	Fault with normal and reverse displacement that developed in Late Pleistocene debris-flow deposits. The fault trends NNE-ward.					Comments 2 There is no evidence of an earthquake.
Feature reference	Exposed in a sinkhole near the city Benzingerode.					Comments 3
thickness (cm)	width (cm)	length (cm)	width (cm)	thickness (cm)		
		150				
Dimension reference						
Preferred age estimate			Comments / references			
Estimated	14.4 - 15.2 ka		Luminescence ages (IRSL, OSL) of the reddish debris-flow points to a fault reactivation after 14.4 - 15.2 ka.			
Range	0.9 - 0.8 ka					
Qualifier						
Age determined from stratigraphic relationships + references						
Degree of weathering + reference						
Related fault	Harz Boundary Fault	Fault ID		Rel.EQ I		
List of most relevant references	Franzke et al., 2015					

Table A9: PalSeisDB. Deformation bands near Könnern (pit 25) (Halle Fault system).

PSE: Deformation bands Könnern

Location	Northern Germany		Country	DE	Comments 1	The shear-deformation bands show normal displacement and often occur as conjugated systems. They follow the trend of the Halle basement fault and a smaller fault near Könnern.	
Lon.	11.740472	Coord	<small>general coordinates for the open pit (Könnern), not the coordinates of the specific feature</small>	Observation type			open pit
Lat.	51.683806			Feature type	shear-deformation bands	Trench ID	
Short description					Comments 3		
Shear-deformation bands that developed in Middle Pleistocene, unconsolidated meltwater sediments. All have displacements in a scale of cm, mostly trend NW-SE and W-E, with the same orientation as the Halle Fault and a smaller basement fault near Könnern.							
Feature reference							
exposed in Könnern pit							
thickness (cm)	width (cm)	length (cm)	width (cm)	thickness (cm)			
2 - 3							
Dimension reference							
Preferred age estimate		Comments / references					
Estimated							
Range							
Qualifier							
Age determined from stratigraphic relationships + references							
The deformation bands developed in meltwater deposits that are Saalian in age (Knoth, 1992). Therefore, fault movements occur in post Middle Pleistocene Saalian times.							
Degree of weathering + reference							
Related fault	Halle Fault system	Fault ID		Rel.EQ 1			
List of most relevant references							

Table A10: PalSeisDB. Deformation bands near Eitze (pit 42) (Aller Valley Fault).

PSE: Deformation bands Eitze

Location	Northern Germany		Country	DE	Comments 1	The shear-deformation bands show normal displacement and occur as conjugated systems. They follow the trend of the Aller Valley Fault and show that strike-slip movements along the Aller Valley Fault occur.	
Lon.	9.302472	Coord	general coordinates for the open pit (Eitze), not the coordinates of the specific feature	Observation type	open pit	Comments 2	The shear-deformation bands are cemented by iron oxides (goethite)
Lat.	52.907861			Feature type	shear-deformation bands		Trench ID
Short description					Comments 3	There is no evidence of an earthquake.	
Shear-deformation bands that developed in Middle Pleistocene, unconsolidated meltwater sediments. All have displacements in a scale of cm, mostly trend NW-SE and NE-SW							
Feature reference							
exposed in Eitze pit							
thickness (cm)	width (cm)	length (cm)	width (cm)	thickness (cm)			
0.2-0.5							
Dimension reference							
Preferred age estimate		Comments / references					
Estimated							
Range							
Qualifier							
Age determined from stratigraphic relationships + references							
The deformation bands developed in meltwater deposits that are Saalian in age (NiBis Kartenserver). Therefore, fault movements occur in post Middle Pleistocene Saalian times.							
Degree of weathering + reference							
Related fault	Aller Valley Fault	Fault ID		Rel.EQ 1			
List of most relevant references							

Table A11: PalSeisDB. Deformation bands near Altenhagen (pit 89) (Steinhuder Meer Fault).

PSE: Deformation bands Altenhagen

Location	Northern Germany	
Lon.	9.379778	Coord general coordinates for the open pit (Altenhagen), not the coordinates of the specific feature
Lat.	52.434083	
Country.	DE	
Observation type	open pit	
Feature type	shear-deformation bands	
Trench ID		

Comments 1 The shear-deformation bands show normal displacement and follows the trend of the Steinhuder Meer basement fault.

Comments 2 Growth strata points to a Middle Pleistocene (Saalian) time of fault reactivation.

Comments 3 There is no evidence for an earthquake.

Short description
Shear-deformation bands that developed in Middle Pleistocene, unconsolidated meltwater sediments, all have displacements in a scale of cm, mostly trend NW-SE.

Feature reference
exposed in Altenhagen pit

thickness (cm)	width (cm)	length (cm)	width (cm)	thickness (cm)
0.3 - 1				

Dimension reference

Preferred age estimate	Comments / references
Estimated	158±4 ka - 189±5 ka
Range	Luminescence dating (IRSL) of growth strata pointing to a Saalian age of reactivation.
Qualifier	

Age determined from stratigraphic relationships + references
Fault movements occurred between ~158 - 189 ka. This time of fault reactivation is based on luminescence ages of growth strata.

Degree of weathering + reference

Related fault	Steinhuder Meer Fault	Fault ID		Rel.EQ 1	
----------------------	-----------------------	-----------------	--	-----------------	--

List of most relevant references

References

- Aber, J.S., Ber, A. (2007).** Glaciotectonism. *In: Van der Meer, J.J.M. (Ed.), Developments in Quaternary Science, 6, Elsevier, Amsterdam, pp.1-246.*
- Abramovitz, T., Thybo, H. (2000).** Seismic images of Caledonian, lithosphere-scale collision structures in the southeastern North Sea along Mona Lisa Profile 2. *Tectonophysics, 317, 27-54.*
- AGI, Glossary of geology (2009).** American Geological Institute, Washington, D.C., online version, www.agiweb.org. Accessed May 2019.
- Alfaro, P., Delgado, J., Estévez, A., Molina, J., Moretti, M., Soria, J. (2002).** Liquefaction and fluidization structures in Messinian storm deposits (Bajo Segura Basin, Betic Cordillera, southern Spain). *International Journal of Earth Sciences, 91, 505-513.*
- Åmark, M. (1986).** Clastic dykes formed beneath an active glacier. *Geologiska Föreningen i Stockholm Föreläsningar, 108, 13-20.*
- Anketell, J.M., Cegła, J., Dżułyński, S. (1970).** On the deformational structures in systems with reverse density gradients. *Annales de la Societe Geologique de Pologne, 40, 3-30.*
- Aitken, M.J. (1985).** Thermoluminescence dating. *Academic Press, London, p. 551.*
- Aitken, M.J. (1998).** Introduction to optical dating: the dating of Quaternary sediments by the use of photon-stimulated luminescence. *Oxford University Press, Oxford, New York, p. 267.*
- Atkinson, G.M., Finn, W.L., Charlwood, R.G. (1984).** Simple computation of liquefaction probability for seismic hazard applications. *Earthquake Spectra, 1, 107-123.*
- Aydin, A. (1978).** Small faults formed as deformation bands in sandstone. *In: Byerlee, J.D., Wyss, M. (Eds.), Rock Friction and Earthquake Prediction, Contributions to Current Research in Geophysics (CCRG), 6, Birkhäuser, Basel, pp. 913-930.*
- Aydin, A., Johnson, A.M. (1978).** Development of faults as zones of deformation bands and as slip surfaces in sandstone. *Pure and Applied Geophysics, 116, 931-942.*
- Aydin, A., Borja, R.I., Eichhubl, P. (2006).** Geological and mathematical framework for failure modes in granular rock. *Journal of Structural Geology, 28, 83-98.*

Baldschuhn, R., Kockel, F. (1987). Geologische Karte von Hannover und Umgebung - Quartär und Tertiärabdeckung 1:100000. *Niedersächsisches Landesamt für Bodenforschung und Bundesanstalt für Geowissenschaften und Rohstoffe, Hannover.*

Baldschuhn, R., Best, G., Kockel, F. (1991). Inversion tectonics in the north-west German basin. In: *Spencer, A.M. (Ed.), Generation, Accumulation and Production of Europe's Hydrocarbons. Special Publication of the European Association of Petroleum Geoscientists, 1, Oxford University Press, pp. 149-159.*

Baldschuhn, R., Binot, F., Fleig, S., Kockel, F. (1996). Geotektonischer Atlas von Nordwest-Deutschland und dem deutschen Nordsee Sektor. *Geologisches Jahrbuch, A153, 3-95.*

Baldschuhn, R., Kockel, F. (1996). Strukturübersicht und Lage der geologischen Schnitte 1:500 000. In: *Baldschuhn, R., Binot, F., Fleig, S., Kockel, F. (Eds.), Geotektonischer Atlas von Nordwest-Deutschland - Teil 17. Bundesanstalt für Geowissenschaften und Rohstoffe, Hannover.*

Baldschuhn, R., Kockel, F. (1999). Das Osning-Lineament am Südrand des Niedersachsen-Beckens. *Zeitschrift der Deutschen Gesellschaft für Geowissenschaften, 150, 673-695.*

Ballas, G., Fossen, H., Soliva, R. (2015). Factors controlling permeability of cataclastic deformation bands and faults in porous sandstone reservoirs. *Journal of Structural Geology, 76, 1-21.*

Benediktsson, Í.Ö., Möller, P., Ingólfsson, Ó., Van der Meer, J.J., Kjær, K.H., Krüger, J. (2008). Instantaneous end moraine and sediment wedge formation during the 1890 glacier surge of Brúarjökull, Iceland. *Quaternary Science Reviews, 27, 209-234.*

Benn, D.I., Evans, D.J.A. (2013). Glaciers and Glaciation. *Routledge, New York, 2. Edition, p. 802.*

Bennett, M.R. (2001). The morphology, structural evolution and significance of push moraines. *Earth-Science Reviews, 53, 197-236.*

Bennett, M.R., Huddart, D., Waller, R.I., Midgley, N.G., Gonzalez, N., Tomio, N. (2004). Styles of ice-marginal deformation at Hagafellsjökull-Eystri, Iceland during the 1998/99 winter-spring surge. *Boreas, 33, 97-107.*

Best, G. (1996). Floßtektonik in Nordwestdeutschland. Erste Ergebnisse reflexionsseismischer Untersuchungen an der Salzstruktur "Oberes Allertal". *Zeitschrift der Deutschen Gesellschaft für Geowissenschaften, 147, 455-464.*

Best, G., Zirngast, M. (2002). Die strukturelle Entwicklung der exhumierten Salzstruktur "Oberes Allertal". *Geologisches Jahrbuch, Sonderheft A1*, 1-518.

Bertran, P. (1993). Deformation-induced microstructures in soils affected by mass movements. *Earth Surface Processes and Landforms*, 18, 645-660.

Bertran, P., Font, M., Giret, A., Manchuel, K., Sicilia, D. (2019a). Experimental soft-sediment deformation caused by fluidization and intrusive ice melt in sand. *Sedimentology*, 66, 1102-1117.

Bertran, P., Manchuel, K., Sicilia, D. (2019b). Discussion on 'Palaeoseismic structures in Quaternary sediments, related to an assumed fault zone north of the Permian Peissen-Gnutz salt structure (NW Germany) - Neotectonic activity and earthquakes from the Saalian to the Holocene' (Grube, 2019). *Geomorphology*. doi: 10.1016/j.geomorph.2019.03.010.

Betz, D., Führer, F., Greiner, G., Plein, E. (1987). Evolution of the Lower Saxony Basin. *Tectonophysics*, 137, 127-170.

BGR (2012). Salzgeologische Bewertung des Einflusses von „kryogenen Klüften“ und halokinetischen Deformationsprozessen auf die Integrität der geologischen Barriere des Salzstocks Gorleben. *Bericht zum Arbeitspaket 2 Vorläufige Sicherheitsanalyse für den Standort Gorleben*. GRS, 273, p.86.

BGR (2019). Der Geodatendienst GERSEIS innerhalb der interaktiven Kartenanwendung Geoviewer der BGR.
https://geoviewer.bgr.de/mapapps4/resources/apps/geoviewer/index.html?lang=de&ab=geophysik&cover=geophysik_gerseis_ag_s_wms (October, 2019)

Bischoff, M., Bönnemann, C., Fritz, J., Gestermann, N., Plenefisch, T. (2013). Untersuchungsergebnis zum Erdbeben bei Völkersen (Landkreis Verden) am 22.11.2012; *Report, LBEG / BGR, Hannover*, p. 60.

Bischoff, M., Ceranna, L., Fritz, J., Gestermann, N., Plenefisch, T. (2014). Untersuchungsergebnisse zum Erdbeben bei Syke (Landkreis Diepholz) am 01.05.2014 – Seismologische Auswertung. *Report, Hannover*, p. 33.

Bischoff, M., Bönnemann, C., Ceranna, L., Fritz, J., Gestermann, N., Pasternak, M., Plenefisch, T. (2015). Kurzbericht zum Erdbeben bei Emstek (Landkreis Cloppenburg) am 19.12.2014 – Seismologische Auswertung. *Report, Hannover*, p. 24.

Bockheim, J.G., Tarnocai, C. (1998). Recognition of cryoturbation for classifying permafrost-affected soils. *Geoderma*, 81, 281-293.

Bode, A., Schroeder, H. (1926). Erläuterungen zu Blatt 4028 Goslar, Geologische Karte von Preußen und benachbarten deutschen Ländern 1:25000. *Preußische Geologische Landesanstalt, Berlin, p.107.*

Boulton, G.S., Slot, T., Blessing, K., Glasbergen, P., Leijnse, T., Van Gijssel, K. (1993). Deep circulation of groundwater in overpressured subglacial aquifers and its geological consequences. *Quaternary Science Reviews, 12, 739-745.*

Boulton, G.S., Caban, P. (1995). Groundwater flow beneath ice sheets: part II - its impact on glacier tectonic structures and moraine formation. *Quaternary Science Reviews, 14, 563-587.*

Böse, M., Lüthgens, C., Lee, J.R., Rose, J. (2012). Quaternary glaciations of northern Europe. *Quaternary Science Reviews, 44, 1-25.*

Brandes, C., Le Heron, D.P. (2010). The glaciotectonic deformation of Quaternary sediments by fault-propagation folding. *Proceedings of the Geologists' Association, 121, 270-280.*

Brandes, C., Polom, U., Winsemann, J. (2011). Reactivation of basement faults: interplay of ice sheet advance, glacial lake formation and sediment loading. *Basin Research, 23, 53-64.*

Brandes, C., Tanner, D.C. (2012). Three-dimensional geometry and fabric of shear deformation bands in unconsolidated Pleistocene sediments. *Tectonophysics, 518, 84-92.*

Brandes, C., Winsemann, J., Roskosch, J., Meinsen, J., Tanner, D.C., Frechen, M., Steffen, H., Wu, P. (2012). Activity along the Osning Thrust in Central Europe during the Lateglacial: ice sheet and lithosphere interactions. *Quaternary Science Reviews, 38, 49-62.*

Brandes, C., Winsemann, J. (2013). Soft-sediment deformation structures in NW Germany caused by Late Pleistocene seismicity. *International Journal of Earth Sciences, 102, 2255-2274.*

Brandes, C., Schmidt, C., Tanner, D.C., Winsemann, J. (2013) Paleostress pattern and salt tectonics within a developing foreland basin (northwestern Subhercynian Basin, northern Germany). *International Journal of Earth Sciences, 102, 2239-2254.*

Brandes, C., Steffen, H., Steffen, R., Wu, P. (2015). Intraplate seismicity in northern Central Europe is induced by the last glaciation. *Geology, 43, 611-614.*

Brandes, C., Igel, J., Loewer, M., Tanner, D.C., Lang, J., Müller, K., Winsemann, J. (2018a). Visualization and analysis of shear deformation bands in unconsolidated Pleistocene sand using ground-penetrating radar: Implications for paleoseismological studies. *Sedimentary Geology*, 367, 135-145.

Brandes, C., Steffen, H., Sandersen, P.B.E., Wu, P., Winsemann, J. (2018b). Glacially induced faulting along the NW segment of the Sorgenfrei-Tornquist Zone, northern Denmark: implications for neotectonics and Lateglacial fault-bound basin formation. *Quaternary Science Reviews*, 189, 149-168.

Brandes, C., Plenefisch, T., Tanner, D.C., Gestermann, N., Steffen, H. (2019). Evaluation of deep crustal earthquakes in northern Germany - Possible tectonic causes. *Terra Nova*, 31, 83-93.

Brinckmeier, G. (1925). Geologische Untersuchungen am Allertalgraben. *Abhandlungen der Preußischen Geologischen Landesanstalt*, 95, 1-31.

Bryan, K. (1946). Cryopedology, the study of frozen ground and intensive frost action, with suggestions on nomenclature. *American Journal of Science*, 244, 622-642.

Burke, H., Phillips, E., Lee, J.R., Wilkinson, I.P. (2009). Imbricate thrust stack model for the formation of glaciotectionic rafts: an example from the Middle Pleistocene of north Norfolk, UK. *Boreas*, 38, 620-637.

Busschers, F.S., Van Balen, R.T., Cohen, K.M., Kasse, C., Weerts, H.J.T., Wallinga, J., Bunnik, F.P.M. (2008). Response of the Rhine-Meuse fluvial system to Saalian ice sheet dynamics. *Boreas*, 37, 377-398.

Cashman, S.M., Baldwin, J.N., Cashman, K.V., Swanson, K., Crawford, R. (2007). Microstructures developed by coseismic and aseismic faulting in near-surface sediments, San Andreas fault, California. *Geology*, 35, 611-614.

Chamley, H. (1990). Sedimentology. *Springer Verlag, Berlin Heidelberg*, 1. Edition, p. 285.

Chapot, M.S., Roberts, H.M., Duller, G.A.T., Lai, Z.P. (2012). A comparison of natural and laboratory-generated dose response curves for quartz optically stimulated luminescence signals from Chinese Loess. *Radiation Measurements*, 47, 1045-1052.

Cheel, R.J., Rust, B.R. (1986). A sequence of soft-sediment deformation (dewatering) structures in Late Quaternary subaqueous outwash near Ottawa, Canada. *Sedimentary Geology*, 47, 77-93.

- Chen, J., Lee, H.S. (2013).** Soft-sediment deformation structures in Cambrian siliciclastic and carbonate storm deposits (Shandong Province, China): Differential liquefaction and fluidization triggered by storm-wave loading. *Sedimentary Geology*, 288, 81-94.
- Cobbold, P.R., Rodríguez, N. (2007).** Seepage forces, important factors in the formation of horizontal hydraulic fractures and bedding parallel fibrous veins (“beef” and “cone-in-cone”). *Geofluids*, 7, 313-332.
- Cohen, K.M., Harper, D.A.T., Gibbard, P.L. (2016).** International Chronostratigraphic Chart <http://stratigraphy.org/ICSchart>. *ChronostratChart2016-12.jpg*. Accessed June 2019.
- Collinson, J.D. Thompson, D.B. (1982).** Sedimentary Structures. *George Allen & Unwin, London*, p. 186.
- Collinson, J.D. (1994).** Sedimentary deformational structures. In: *Maltman, A. (Ed.), The geological deformation of sediments. Chapman & Hall, London*, pp. 95-125.
- Collinson, D., Mountney, N.P., Thompson, D.B. (2006).** Sedimentary Structures. *Terra Publishing, England*, 3. Edition, p. 292.
- Croot, D.G. (1988).** Morphological, structural and mechanical analysis of neoglacial ice-pushed ridges in Iceland. In: *Croot, D.G. (Ed.), Glaciotectonics: Forms and Processes. Balkema, Rotterdam*, pp. 33-47.
- Dahm, T., Krüger, F., Stammler, K., Klinge, K., Kind, R., Wylegalla, K., Grasso, J.R. (2007).** The 2004 M_w 4.4 Rotenburg, northern Germany, earthquake and its possible relationship with gas recovery. *Bulletin of the Seismological Society of America*, 97, 691-704.
- Dahm, T., Cesca, S., Hainzl, S., Braun, T., Krüger, F. (2015).** Discrimination between induced, triggered and natural earthquakes close to hydrocarbon reservoirs: A probabilistic approach based on the modeling of depletion-induced stress changes and seismological source parameters. *Journal of Geophysical Research*, 120, 2491-2509.
- Dahm, T., Heimann, S., Funke, S., Wendt, S., Rappsilber, I., Bindi, D., Plenefisch, T., Cotton, F. (2018).** Seismicity in the block mountains between Halle and Leipzig, Central Germany: centroid moment tensors, ground motion simulation, and felt intensities of two $M \approx 3$ earthquakes in 2015 and 2017. *Journal of Seismology*, 22, 985-1003.
- DEKORP-BASIN and Group R. (1999).** Deep crustal structure of the Northeast German basin: new DEKORP-BASIN '96 deep profiling results. *Geology*, 27, 55-58.

Dobinski, W. (2011). Permafrost. *Earth-Science Reviews*, 108, 158-169.

Döhler, S., Terhorst, B., Frechen, M., Zhang, J., Damm, B. (2018). Chronostratigraphic interpretation of intermediate layer formation cycles based on OSL dates from intercalated slope wash sediments. *Catena*, 162, 278-290.

Dredge, L.A., Grant, D.R. (1987). Glacial deformation of bedrock and sediment, Magdalen Islands and Nova Scotia, Canada: Evidence for a regional grounded ice sheet. In: *Van der Meer, J.J.M. (Ed.), Tills and Glaciotectonics, Balkema, Rotterdam, pp. 183-195.*

Drozdowski, G. (1988). Die Wurzel der Osning-Überschiebung und der Mechanismus herzynischer Inversionsstörungen in Mitteleuropa. *Geologische Rundschau*, 77, 127-141.

Duller, G.A.T. (2008). Luminescence Dating: Guidelines on Using Luminescence Dating in Archaeology. *English Heritage, Swindon, p. 43.*

Edelman, C.H., Florschütz, F., Jeswiet, J. (1936). Über spätpleistozäne frühholozäne kryoturbate Ablagerungen in den östlichen Niederlanden. *Verhandelingen Geologische Serie*, 11, 301-336.

Ehlers, J., Grube, A., Stephan, H.J., Wansa, S. (2011). Pleistocene glaciations of North Germany – new results. In: *Ehlers, J., Gibbard, P.L., Hughes, P.D. (Eds.), Quaternary Glaciations: Extent and Chronology - A Closer Look: Developments in Quaternary Science*, 15, 149-162.

Eissmann, L. (2002). Quaternary geology of eastern Germany (Saxony, Saxon-Anhalt, south Brandenburg, Thüringia), type area of the Elsterian and Saalian stages in Europe. *Quaternary Science Reviews*, 21, 1275-1346.

Eybergen, F.A. (1987). Glacier snout dynamics and contemporary push moraine formation at the Turtmannglacier, Wallis, Switzerland. In: *Van der Meer, J.J.M. (Ed.), Tills and Glaciotectonics, Balkema, Rotterdam, pp. 217-231.*

Faulkner, D.R., Mitchell, T.M., Jensen, E., Cembrano, J. (2011). Scaling of fault damage zones with displacement and the implications for fault growth processes. *Journal of Geophysical Research*, 116, B05403.

Feeser, V. (1988). On the mechanics of glaciotectionic contortion of clays. In: *Croot, D.G. (Ed.), Glaciotectonics: Forms and Processes. Balkema, Rotterdam, pp. 63-76.*

Feldmann, L. (2002). Das Quartär zwischen Harz und Allertal mit einem Beitrag zur Landschaftsgeschichte im Tertiär. *Clausthaler Geowissenschaften*, 1, 1-178.

Fernlund, J.M.R. (1988). The Halland Coastal Moraines: are they end moraines or glaciotectonic ridges? In: Croot, D.G. (Ed.), *Glaciotectonics: Forms and Processes*, Balkema, Rotterdam, pp. 77-90.

Fitzsimons, S.J., Lorrain, R.D., Vandergoes, M.J. (2000). Behaviour of subglacial sediment and basal ice in a cold glacier. In: Maltman, A.J.; Hubbard, B., Hambrey, M.J. (Eds.), *Deformation of Glacial Materials. Geological Society London Special Publications*, 176, pp. 181-190.

Fossen, H., Schultz, R.A., Shipton, Z.K., Mair, K. (2007). Deformation bands in sandstone: a review. *Journal of the Geological Society*, 164, 755-769.

Fossen, H. (2010a). Deformation bands and fractures in porous rocks. In: Fossen, H. (Ed.), *Structural Geology*, Cambridge University Press, pp. 141-148.

Fossen, H. (2010b). Deformation bands formed during soft-sediment deformation: observations from SE Utah. *Marine and Petroleum Geology*, 27, 215-222.

Franke, D., Hoffmann, N. (1999a). Das Elbe-Lineament - bedeutende Geofraktur oder Phantomgebilde? - Teil 1: Die Referenzgebiete. *Zeitschrift für Geologische Wissenschaften*, 27, 279-318.

Franke, D., Hoffmann, N. (1999b). Das Elbe-Lineament - bedeutende Geofraktur oder Phantomgebilde? - Teil 2: Regionale Zusammenhänge. *Zeitschrift für Geologische Wissenschaften*, 27, 319-350.

Franzke, H.J., Schmidt, D. (1993). Die mesozoische Entwicklung der Harznordrandstörung - Makrogefügeuntersuchungen in der Aufrichtungszone. *Zentralblatt für Geologie und Paläontologie Teil I*, 1443-1457.

Franzke, H.J., Hauschke, N., Hellmund, M. (2015). Spätpleistozäne bis frühholozäne Tektonik in einem Karsttrichter im Bereich der Störungszone des Harznordrandes nahe Benzingerode (Sachsen-Anhalt). *Hallesches Jahrbuch für Geowissenschaften*, 37, 1-10.

French, H.M. (2017). The periglacial environment. *John Wiley and Sons. 4. Edition*, Chichester, p. 544.

Frey, S.E., Gingras, M.K., Dashtgard, S.E. (2009). Experimental studies of gas escape and water escape structures: mechanisms and morphologies. *Journal of Sedimentary Research*, 79, 808-816.

Frischbutter, A. (2001). Recent vertical movements (map 4). *Brandenburgische Geowissenschaftliche Beiträge*, 8, 27-31.

Fuchs, M., Straub, J., Zöller, L. (2005). Residual luminescence signals of recent river flood sediments: a comparison between quartz and feldspar of fine- and coarse-grain sediments. *Ancient TL*, 23, 25-30.

Fuchs, M., Owen, L.A. (2008). Luminescence dating of glacial and associated sediments: review, recommendations and future directions. *Boreas*, 37, 636-659.

Gagel, C., Schlunck, J. (1911). Erläuterungen zu Blatt 2528 Geesthacht (Hamwarde), Geologische Karte von Preußen und benachbarten Bundesstaaten, 1:25000. *Königliche Preussische Geologische Landesanstalt, Berlin*, p. 46.

Gagel, C., Schlunck, J. (1914). Erläuterungen zu Blatt 2529/2530 Büchen (Pötraugresse), Geologische Karten von Preußen und benachbarten Bundesstaaten, 1:25000. *Königliche Preussische Geologische Landesanstalt, Berlin*, p. 62.

Galli, P. (2000). New empirical relationships between magnitude and distance for liquefaction. *Tectonophysics*, 324, 169-187.

Gangopadhyay, A., Talwani, P. (2003). Symptomatic features of intraplate earthquakes. *Seismological Research Letters*, 74, 863-883.

Gast, R., Gundlach, T. (2006). Permian strike slip and extensional tectonics in Lower Saxony, Germany. *Zeitschrift der Deutschen Gesellschaft für Geowissenschaften*, 157, 41-56.

Gehrmann, A., Hüneke, H., Meschede, M., Phillips, E.R. (2017). 3D microstructural architecture of deformed glacial sediments associated with large-scale glacial tectonism, Jasmund Peninsula (NE Rügen), Germany. *Journal of Quaternary Science*, 32, 213-230.

Gehrmann, A., Harding, C. (2018). Geomorphological mapping and spatial analyses of an Upper Weichselian glacial tectonic complex based on LiDAR data, Jasmund Peninsula (NE Rügen), Germany. *Geosciences*, 8, 208.

Gibert, L., Alfaro, P., García-Tortosa, F.J., Scott, G., (2011). Superposed deformed beds produced by single earthquakes (Tecopa Basin, California): insights into paleoseismology. *Sedimentary Geology*, 235, 148-159.

Grollmund, B., Zoback, M.D. (2001). Did deglaciation trigger intraplate seismicity in the New Madrid Seismic Zone? *Geology*, 29, 175-178.

Grube, A. (2019a). Palaeoseismic structures in Quaternary sediments of Hamburg (NW Germany), earthquakes evidence during the younger Weichselian and Holocene. *International Journal of Earth Sciences*, 108, 845-861.

Grube, A. (2019b). Palaeoseismic structures in Quaternary sediments, related to an assumed fault zone north of the Permian Peissen-Gnutz salt structure (NW Germany) – Neotectonic activity and earthquakes from the Saalian to the Holocene. *Geomorphology*, 328, 15-27.

Grunder, H. (1896). Erläuterungen zu Blatt 3038 Glöwen, Geologische Spezialkarte von Preußen und den Thüringischen Staaten 1:25000. *Königliche Preußische Geologische Landesanstalt, Berlin*, p. 63.

Grünthal, G., Stromeyer, D. (1992). The recent crustal stress field in central Europe: trajectories and finite element modeling. *Journal of Geophysical Research*, 97, 11805-11820.

Grünthal, G., Stromeyer, D., Wahlström, R. (2009). Harmonization check of M_w within the central, northern, and northwestern European earthquake catalogue (CENEC). *Journal of Seismology*, 13, 613-632.

Guérin, G., Mercier, N., Adamiec, G. (2011). Dose-rate conversion factors: update. *Ancient TL*, 29, 5-8.

Haack, W., Görz, G. (1930). Erläuterungen zu Blatt 3814 Bad Iburg, Geologische Karte von Preußen und benachbarten deutschen Ländern 1:25000. *Preußische Geologische Landesanstalt, Berlin*, p.93.

Harbort, E., Monke, H., Schucht, F. (1916a). Erläuterungen zu Blatt 3326 Celle, Geologische Karte von Preußen und benachbarten Bundesstaaten 1:25000. *Königliche Preußische Geologische Landesanstalt, Berlin*, p. 56.

Harbort, E., Monke, H., Stoller, J. (1916b). Erläuterungen zu Blatt 3427 Wienhausen, Geologische Karte von Preußen und benachbarten Bundesstaaten 1:25000. *Königliche Preußische Geologische Landesanstalt, Berlin*, p. 52.

Harbort, E., Stoller, J. (1916c). Erläuterungen zu Blatt 3327 Lachendorf, Geologische Karte von Preußen und benachbarten Bundesstaaten 1:25000. *Königliche Preußische Geologische Landesanstalt, Berlin*, p. 69.

Hardt, J., Lüthgens, C., Hebenstreit, R., Böse, M. (2016). Geochronological (OSL) and geomorphological investigations at the presumed Frankfurt ice-marginal position in northeast Germany. *Quaternary Science Reviews*, 154, 85-99.

Hardt, J., Böse, M. (2018). The timing of the Weichselian Pomeranian ice marginal position south of the Baltic Sea: a critical review of morphological and geochronological results. *Quaternary International*, 478, 51-58.

- Harry, D.G. (1988).** Ground ice and permafrost. *In: Clark, M.J. (Ed.), Advances in Periglacial Geomorphology. Wiley, Chichester, pp. 113-149.*
- Hart, J.K., Boulton, G.S. (1991).** The interrelation of glaciotectonic and glacio-depositional processes within the glacial environment. *Quaternary Science Reviews, 10, 335-350.*
- Hazard, J. (1924).** Erläuterungen zu Blatt 4739 Zwenkau, Geologische Karte von Sachsen 1:25000. *Finanzministerium, Leipzig, p. 44.*
- Heidbach, O., Rajabi, M., Reiter, K., Ziegler, M. (2016).** World stress map 2016. *Science, 277, 1956-62.*
- Hiemstra, J.F., Rijdsdijk, K.F., Evans, D.J.A. Van der Meer, J.J.M. (2005).** Integrated micro- and macro-scale analyses of Last Glacial Maximum Irish Sea Diamicts from Abermawr and Traeth y Mwnt, Wales, UK. *Boreas, 34, 61-74.*
- Höfle, H.C., Deichmüller, J., Hofmann, W., Irrlitz, W., Komodromos, A., Preuss, H., Tüxen, J., Mengeling, H., Meyer, K.D., Schlenker, B. (1976).** Erläuterungen zu Blatt 2717 Schwanewede, Geologische Karte von Niedersachsen 1:25000. *Niedersächsisches Landesamt für Bodenforschung, Hannover, p. 72.*
- Höfle, H.C. (1977).** Manuskriptkarte und Legende zur geologischen Übersichtskartierung von Niedersachsen 2831 Gohrde 1:25000, *Niedersächsisches Landesamt für Bodenforschung, Hannover.*
- Hoffmann, G., Reicherter, K. (2012).** Soft-sediment deformation of Late Pleistocene sediments along the southwestern coast of the Baltic Sea (NE Germany). *International Journal of Earth Sciences, 101, 351-363.*
- Houmark-Nielsen, M. (1988).** Glaciotectonic unconformities in Pleistocene stratigraphy as evidence for the behaviour of former Scandinavian ice-sheets. *In: Croot, D.G. (Ed.), Glaciotectonics: Forms and Processes, Balkema, Rotterdam, pp. 91-99.*
- Hughes, A.L., Gyllencreutz, R., Lohne, Ø.S., Mangerud, J., Svendsen, J.I. (2016).** The last Eurasian ice sheets – a chronological database and time-slice reconstruction, DATED-1. *Boreas, 45, 1-45.*
- Huijzer, B., Vandenberghe, J. (1998).** Climatic reconstruction of the Weichselian Pleniglacial in northwestern and central Europe. *Journal of Quaternary Science: Published for the Quaternary Research Association, 13, 391-417.*

Huntley, D.J., Lamothe, M. (2001). Ubiquity of anomalous fading in K-feldspars and the measurement and correction for it in optical dating. *Canadian Journal of Earth Sciences*, 38, 1093-1106.

Hurst, A., Cartwright, J. (2007). Relevance of sand injectites to hydrocarbon exploration and production. In: Hurst A., Cartwright, J. (Eds.), *Sand injectites: implications for hydrocarbon exploration and production, AAPG Memoir 87, Tulsa*, pp. 1-19.

Hurst, A., Scott, A., Vigorito, M. (2011). Physical characteristics of sand injectites. *Earth-Science Reviews*, 106, 215-246.

Hübscher, C., Lykke-Andersen, H., Hansen, M.B., Reicherter, K. (2004). Investigating the structural evolution of the western Baltic. *Eos, Transactions American Geophysical Union*, 85, 115-115.

Hürtgen, J. (2017). The first paleoseismic database of Germany and adjacent regions PalSeisDB v1.0. *Dissertation RWTH Aachen University, Germany*, p.108.

Ingólfsson, O. (1988). Large-scale glaciotectonic deformation of soft sediments: a case study of a late Weichselian sequence in western Iceland. In: Croot, D.G. (Ed.), *Glaciotectonics: Forms and Processes. Balkema, Rotterdam*, pp. 101-107.

Jain, M., Buylaert, J.P., Thomsen, K.J., Murray, A.S. (2015). Further investigations on 'non-fading' in K-Feldspar. *Quaternary International*, 362, 3-7.

Jordan, H., Besenecker, H., Cosack, E., Dahms, E., Fauth, H., Gramann, F., Heinemann, B., Hofmeister, E., Kosmahl, W., Merkt, J., Schneekloth, H., Tüxen, J. (1979). Erläuterungen zu Blatt 3521 Rehburg, Geologische Karte von Niedersachsen 1:25000. *Niedersächsisches Landesamt für Bodenforschung, Hannover*, p.134.

Jordan, H., Cosack, E., Dahms, E., Eckelmann, W., Groba, E., Irrlitz, W., Kockel, F., Schneekloth, H., Tüxen, J. (1980). Erläuterungen zu Blatt 3422 Neustadt am Rübenberge, Geologische Karten von Niedersachsen 1:25000. *Niedersächsisches Landesamt für Bodenforschung, Hannover*, p. 88.

Jubitz, K.B., Beutler, G., Schwab, G., Stackebrandt, W. (1991). Zur Strukturentwicklung des Spaltendiapirs der Allertalzone (Subherzyne Senke). *Zeitschrift für geologische Wissenschaft*, 19, 421-409.

Kaiser, A. (2005). Neotectonic modelling of the North German Basin and adjacent areas – a tool to understand postglacial landscape evolution? *Zeitschrift der deutschen Gesellschaft für Geowissenschaften*, 156, 357-366.

Kaiser, A., Reicherter, K., Hübscher, C., Gajewski, D. (2005). Variation of the present-day stress field within the North German Basin - insights from thin shell FE modeling based on residual GPS velocities. *Tectonophysics*, 397, 55-72.

Kars, R.H., Wallinga, J., Cohen, K.M. (2008). A new approach towards anomalous fading correction for feldspar IRSL dating - tests on samples in field saturation. *Radiation Measurements*, 43, 786-790.

Katzung, G., Müller, U., Krienke, H.D., Krull, P., Strahl, U. (2004). Auflagerung des Quartärs und Glazialtektonik. In: *Katzung, G. (Ed.), Geologie von Mecklenburg Vorpommern, Schweizerbart'sche Verlagsbuchhandlung, Stuttgart, pp. 397-408.*

Keilhack, K., Kraiss, A., Renner, O., Harbort, E., Stoller, J. (1917). Erläuterungen zum Blatt 4018 Lage, Geologische Karte von Preußen und benachbarten Bundesstaaten 1:25000. *Königliche Preußische Geologische Landesamt, Berlin, p. 55.*

Keller, G. (1974). Die Fortsetzung der Osningzone auf dem Nordwestabschnitt des Teutoburger Waldes. *Neues Jahrbuch für Geologie und Paläontologie Monatshefte*, 2, 72-95.

Kenzler, M., Obst, K., Hüneke, H., Schütze, K. (2010). Glazitektonische Deformation der kretazischen und pleistozänen Sedimente an der Steilküste von Jasmund nördlich des Königsstuhls (Rügen). *Brandenburger Geowissenschaftliche Beiträge*, 17, 107-122.

Kiden, P., Denys, L., Johnston P. (2002). Late Quaternary sea-level change and isostatic and tectonic land movements along the Belgian-Dutch North Sea coast: geological data and model results. *Journal of Quaternary Science*, 17, 535-546.

Kierulf, H.P., Steffen, H., Simpson, M.J.R., Lidberg, M., Wu, P., Wang, H. (2014). A GPS velocity field for Fennoscandia and a consistent comparison to glacial isostatic adjustment models. *Journal of Geophysical Research*, 119, 6613-6629.

Kim, Y.S., Peacock, D.C., Sanderson, D.J. (2004). Fault damage zones. *Journal of Structural Geology*, 26, 503-517.

Kley, J., Franzke, H.J., Jähne, F., Krawczyk, C., Lohr, T., Reicherter, K., Scheck-Wenderoth, M., Sippel, J., Tanner, D., Van Gent, H. (2008). Strain and stress. In: *Littke, R., Bayer, U., Gajewski, D., Nelskamp, S. (Eds.), Dynamics of complex intracontinental basins: The Central European Basin System. Springer, Berlin, Heidelberg, pp. 97-124.*

Kley, J., Voigt, T. (2008). Late Cretaceous intraplate thrusting in Central Europe: effect of Africa-Iberia-Europe convergence, not Alpine collision. *Geology*, 36, 839-842.

- Kley, J. (2013).** Saxonische Tektonik im 21. Jahrhundert. *Zeitschrift der deutschen Gesellschaft für Geowissenschaften*, 164, 295-311.
- Knight, J. (2002).** Glacial sedimentary evidence supporting stick-slip basal ice flow. *Quaternary Science Reviews*, 21, 975-983.
- Knoth, W. (1992).** Geologische Übersichtskarte von Sachsen-Anhalt 1:400000, *Geologisches Landesamt Sachsen-Anhalt, Halle/Saale*, 1. Edition, Halle.
- Knoth, W. (1995).** Sachsen-Anhalt. In: Benda, L. (Ed.), *Das Quartär Deutschlands*, Gebrüder Bornträger, Berlin, pp. 148-170.
- Knoth, W., Kriebel, U., Radzinski, K.H., Thomae, M. (1998).** Die geologischen Verhältnisse von Halle und Umgebung. *Hallesches Jahrbuch für Geowissenschaften, Beiheft*, 4, 7-34.
- Kockel, F. (2003).** Inversion structures in Central Europe. Expressions and reasons, an open discussion. *Netherlands Journal of Geosciences*, 82, 367-382.
- Koert, W., Dienemann, W. (1927).** Erläuterungen zu Blatt 3832 Welfensleben (Hötensleben), Geologische Karte von Preußen und benachbarten deutschen Ländern 1:25000. *Preußische Geologische Landesanstalt, Berlin*, p. 88.
- Korn, J., Stoller, J., Zimmermann, I.E. (1923).** Erläuterungen zu Blatt 3736 Zielitz (Niegripp), Geologische Karte von Preußen und benachbarten Bundesstaaten 1:25000. *Preußische Geologische Landesanstalt, Berlin*, p. 55.
- Kossow, D., Krawczyk, C.M. (2002).** Structure and quantification of processes controlling the evolution of the inverted NE-German Basin. *Marine and Petroleum Geology*, 19, 601-618.
- Krawczyk, C.M., McCann, T., Cocks, L.R.M., England, R.W., McBride, J.H., Wybraniec, S. (2008).** Caledonian tectonics. In: McCann, T. (Ed.), *The Geology of Central Europe. Precambrian and Paleozoic*, 1, Geological Society London, pp. 303-381.
- Kraiß, A., Picard, E. (1922).** Erläuterungen zu Blatt 4437 Halle an der Saale (Nord), Geologische Karte von Preußen und benachbarten Bundesstaaten 1:25000. *Preußische Geologische Landesanstalt, Berlin*, p. 86.
- Krienke, H.-D., Nagel, D., Bremer, F., Heck, H.-L., Müller, U., Schulz, W. (2001).** Geologische Karte von Mecklenburg-Vorpommern 1:200000, *Geologisches Landesamt Mecklenburg-Vorpommern, Güstrow*.

- Kunert, R., Altermann, M., Schmidt, B., Schmidt, E. (1963).** Erläuterungen zu Blatt 4336 Könnern, Geologische Spezialkarte der Deutschen Demokratischen Republik 1:25000. *Zentrales Geologisches Institut, Berlin*, p. 205.
- Kuriger, E.M., Truffer, M., Motyka, R.J. Bucki, A. K. (2006).** Episodic reactivation of large-scale push moraine in front of the advancing Taku Glacier, Alaska. *Journal of Geophysical Research*, 111, F01009.
- Lang, H.D., Anrich, H., Baldschuhn, R., Heine, H.W., Heinemann, B., Irrlitz, W., Resch, M., Schneekloth, H. (1980).** Erläuterungen zu Blatt 3224 Westenholz, Geologische Karte von Niedersachsen 1:25000. *Niedersächsisches Landesamt für Bodenforschung, Hannover*, p. 98.
- Lang, J., Winsemann, J., Steinmetz, D., Polom, U., Pollok, L., Böhner, U., Serangeli, J., Brandes, C., Hampel, A., Winghart, S. (2012).** The Pleistocene of Schöningen, Germany: a complex tunnel valley fill revealed from 3D subsurface modelling and shear wave seismics. *Quaternary Science Reviews*, 39, 86-105.
- Lang, J., Lauer, T., Winsemann, J. (2018).** New age constraints for the Saalian glaciation in northern central Europe: implications for the extent of ice sheets and related proglacial lake systems. *Quaternary Science Reviews*, 180, 240-259.
- Lang, J., Alho, P., Kasvi, E., Goseberg, N., Winsemann, J. (2019).** Impact of Middle Pleistocene (Saalian) glacial lake-outburst floods on the meltwater-drainage pathways in northern central Europe: insights from 2D numerical flood simulation. *Quaternary Science Reviews*, 209, 82-99.
- Lee, J.R., Phillips, E.R. (2008).** Progressive soft-sediment deformation within a subglacial shear zone – a hybrid mosaic-pervasive deformation model for Middle Pleistocene glaciotectionised sediments from eastern England. *Quaternary Science Reviews*, 27, 1350-1362.
- Le Heron, D.P. Etienne, J.L. (2005).** A complex subglacial clastic dyke swarm, Solheimajokull, southern Iceland. *Sedimentary Geology*, 181, 25-37.
- Lehné, R., Sirocko, F. (2007).** Rezente Bodenbewegungspotenziale in Schleswig-Holstein (Deutschland) – Ursachen und ihr Einfluss auf die Entwicklung der rezenten Topografie. *Zeitschrift der Deutschen Gesellschaft für Geowissenschaften*, 158, 329-347.
- Lehné, R.J., Sirocko, F. (2010).** Recent vertical crustal movements and resulting surface deformation within the North German Basin (Schleswig-Holstein) derived by GIS-based analysis of repeated precise leveling data. *Zeitschrift der Deutschen Gesellschaft für Geowissenschaften*, 161, 175-188.

Lepper, J., Tüxen, J. (1975). Geologische Übersichtskartierung 2932 Dannenberg (Elbe) Süd 1:25000. *Niedersächsisches Landesverwaltungsamt, 8. Edition, Hannover.*

Leydecker, G., Steinwachs, M., Seidl, D., Kind, R., Klussmann, J., Zerna, W. (1980). Das Erdbeben vom 2. Juni 1977 in der Norddeutschen Tiefebene bei Soltau. *Geologisches Jahrbuch Reihe E, 18, 3-18.*

Leydecker, G., Kopera, J.R. (1999). Seismological hazard assessment for a site in Northern Germany, an area of low seismicity. *Engineering Geology, 52, 293-304.*

Leydecker, G., Kaiser, D., Busche, H., Schmitt, T. (2006) Makroseismische Bearbeitung des Erdbebens vom 20. Okt. 2004 östlich Rotenburg (Wümme) im Norddeutschen Tiefland.- Bundesanstalt für Geowissenschaften und Rohstoffe; Hannover, <http://www.bgr.bund.de/DE/Themen/Erdbeben-Gefaehrdungsanalysen/Seismologie/Downloads/Rotenburg.pdf>. Accessed November 2016.

Leydecker, G. (2011). Erdbebenkatalog für die Bundesrepublik Deutschland mit Randgebieten für die Jahre 800 bis 2008. *Geologisches Jahrbuch Reihe E, 59, pp.1-198.*

Li, Y., Craven, J., Schweig, E.S., Obermeier, S.F. (1996). Sand boils induced by the 1993 Mississippi River flood: could they one day be misinterpreted as earthquake-induced liquefaction? *Geology, 24, 171-174.*

Litt, T., Behre, K.E., Meyer, K.D., Stephan, H.J., Wansa, S. (2007). Stratigraphische Begriffe für das Quartär des norddeutschen Vereisungsgebietes. *E & G - Quaternary Science Journal, 56, 7-65.*

Lohr, T., Krawczyk, C.M., Tanner, D.C., Samiee, R., Endres, H., Oncken, O., Trappe, H., Kulka, P.A. (2007). Strain partitioning due to salt: insights from interpretation of a 3D seismic data set in the NW German Basin. *Basin Research, 19, 579-597.*

Lotze, F. (1929). Überschiebungs-, Abscherungs- und Zerrungstektonik bei der Osningfaltung. *Nachrichten der Gesellschaft der Wissenschaften zu Göttingen. Mathematisch-Physikalische Klasse, 1929, 231-239.*

Lowe, D.R. (1975). Water escape structures in coarse-grained sediments. *Sedimentology, 22, 157-204.*

Lowe, D.R., LoPiccolo, R.D. (1974). The characteristics and origins of dish and pillar structures. *Journal of Sedimentary Petrology, 44, 484-501.*

Ludwig, A.O. (2011). Zwei markante Stauchmoränen: Peski/Belarusland und Jasmund, Ostseeinsel Rügen/Nordostdeutschland - Gemeinsame Merkmale und Unterschiede. *E & G - Quaternary Science Journal*, 60, 464-487.

Lüthgens, C., Böse, M. (2011). Chronology of Weichselian main ice marginal positions in north-eastern Germany. *E & G - Quaternary Science Journal*, 60, 236-247.

Madsen, A.T., Murray, A.S. (2009). Optically stimulated luminescence dating of young sediments: a review. *Geomorphology*, 109, 3-16.

Marotta, A.M., Mitrovica, J.X., Sabadini, R., Milne, G. (2004). Combined effects of tectonics and glacial isostatic adjustment on intraplate deformation in central and northern Europe: applications to geodetic baseline analyses. *Journal of Geophysical Research*, 109, B01413.

Martiklos, G., Beutler, G., Ehling, B.C. (2001). Geologische Übersichtskarte von Sachsen-Anhalt 1:400000, *Geologisches Landesamt Sachsen-Anhalt, Halle*.

Mazur, S., Scheck-Wenderoth, M., Krzywiec, P. (2005). Different modes of the Late Cretaceous Early Tertiary inversion in the North German and Polish basins. *International Journal of Earth Sciences*, 94, 782-798.

McCalpin, J.P. (2003). Neotectonics of Bear Lake Valley, Utah and Idaho: a preliminary assessment. *Utah Geological Survey, Miscellaneous Publication 3-4, Salt Lake City, Utah*, p. 43.

McCalpin, J.P., Nelson, A.R. (2009). Introduction to paleoseismology. *International Geophysics*, 95, 1-27.

McCarroll, D., Rijdsdijk, K.F. (2003). Deformation styles as a key for interpreting glacial depositional environments. *Journal of Quaternary Science*, 18, 473-489.

McKenna, J., Stein, S., Stein, C.A., (2007). Is the New Madrid seismic zone hotter and weaker than its surroundings? In: Stein, S., Mazzotti, S. (Eds.), *Continental Intraplate Earthquakes: Science, Hazard, and Policy Issues: Geological Society of America, Special Paper 425*, pp. 167-175.

Meinsen, J., Winsemann, J., Weitkamp, A., Landmeyer, N., Lenz, A., Dölling, M. (2011). Middle Pleistocene (Saalian) lake outburst floods in the Münsterland Embayment (NW Germany): impacts and magnitudes. *Quaternary Science Reviews*, 30, 2597-2625.

Meinsen, J., Winsemann, J., Roskosch, J., Brandes, C., Frechen, M., Dultz, S., Böttcher, J. (2014). Climate control on the evolution of Late Pleistocene alluvial-fan and aeolian sand-sheet systems in NW Germany. *Boreas*, 43, 42-66.

Mejdahl, V. (1979). Thermoluminescence dating: beta-dose attenuation in quartz grains. *Archaeometry*, 21, 61-72.

Menzies, J. (2000). Micromorphological analyses of microfabrics and microstructures indicative of deformation processes in glacial sediments. In: Maltman, A.J., Hubbard, B., Hambrey, M.J. (Eds.), *Deformation of Glacial Materials*. Geological Society London Special Publications, 176, pp. 245-257.

Mestwerdt, A. (1914). Erläuterungen zu Blatt 3631 Groß-Twülpstedt, Geologische Karte von Preußen und benachbarten Bundesstaaten 1:25000. *Königliche Preußische Geologische Landesanstalt, Berlin*, p. 56.

Meyer, K.D. (1987). Ground and end moraines in Lower Saxony. In: Van der Meer, J.J.M. (Ed.), *Tills and Glaciotectonics*, Balkema, Rotterdam, pp. 197-204.

Meyer, K.D., Boess, J., Grimmelmann, W., Kuster, H., Resch, M., Röhling, H.-G., Tüxen, J. (2004). Erläuterungen zu Blatt 2730 Bleckede, Geologische Karte von Niedersachsen 1:250000. *Niedersächsisches Landesamt für Bodenforschung, Hannover*, p. 136.

Michetti, A.M., Esposito, E., Guerrieri, L., Porfido, S., Serva, L., Tatevossian, R., Vittori, E., Audemard, F., Azuma, T., Clague, J., Comerci, V., Gürpınar, A., McCalpin, J., Mohammadioun, B. (2007). Environmental seismic intensity scale-ESI 2007. *Memorie descrittive della carta geologica d'Italia*, 74, 41.

Molina, J.M., Alfaro, P., Moretti, M., Soria, J. M. (1998). Soft-sediment deformation structures induced by cyclic stress of storm waves in tempestites (Miocene, Guadalquivir Basin, Spain). *Terra Nova*, 10, 145-150.

Moretti, M., Miguel, J., Alfaro, P., Walsh, N. (2001). Asymmetrical soft-sediment deformation structures triggered by rapid sedimentation in turbiditic deposits (Late Miocene, Guadix Basin, Southern Spain). *Facies*, 44, 283-294.

Moretti, M., Van Loon, A.T., Liu, M., Wang, Y. (2014). Restrictions to the application of 'diagnostic' criteria for recognizing ancient seismites. *Journal of Palaeogeography*, 3, 162-173.

Moretti, M., Alfaro, P., Owen, G. (2016). The environmental significance of soft-sediment deformation structures: key signatures for sedimentary and tectonic processes. *Sedimentary Geology*, 344, 1-4.

Möbus, G. (1989). Tektonik. *VEB Deutscher Verlag für Grundstoffindustrie, Leipzig, 1. Edition, p. 472.*

Mörner, N.A. (1978). Faulting, fracturing, and seismic activity as a function of glacial isostasy in Fennoscandia. *Geology, 6, 41-45.*

Mörner, N.A. (2003). Paleoseismicity of Sweden – a novel paradigm. *A contribution to INQUA from its Sub-Commission of Paleoseismology, Reno 2003, Stockholm, p. 320.*

Mörz, T., Karlik, E.A., Kreiter, S., Kopf, A. (2007). An experiment setup for fluid venting in unconsolidated sediments: new insights to fluid mechanics and structures. *Sedimentary Geology, 196, 251-267.*

Murton, J.B., French, H.M. (1993). Thermokarst involutions, Summer Island, Pleistocene Mackenzie Delta, western Canadian Arctic. *Permafrost and Periglacial Processes, 4, 217-229.*

Murray, A.S., Wintle, A.G. (2000). Luminescence dating of quartz using an improved single-aliquot regenerative-dose protocol. *Radiation measurements, 32, 57-73.*

Müller, C., Jähne-Klingenberg, F., von Goerne, G., Binot, F., Röhling, H.G. (2016). Vom geotektonischen Atlas („Kockel-Atlas“) zu einem 3D-Gesamtmodell des Norddeutschen Beckens: Basisinformationen zum tieferen Untergrund von Norddeutschland. *Zeitschrift der deutschen Gesellschaft für Geowissenschaften, 167, 65-106.*

Müller, K., Brandes, C., Winsemann, J. (2016). Paleoseismic investigation of northern Germany - 1st Interim Report. *Leibniz Universität Hannover, p. 31.*

Müller, K., Brandes, C., Winsemann, J. (2017a). Paleoseismic investigation of northern Germany - Harz Boundary Fault - 2nd Interim Report. *Leibniz Universität Hannover, p. 29.*

Müller, K., Brandes, C., Winsemann, J. (2017b). Paleoseismic investigation of northern Germany - Halle Fault – 3rd Interim Report. *Leibniz Universität Hannover, p. 23.*

Müller, K., Brandes, C., Winsemann, J. (2018a). Paleoseismic investigation of northern Germany – Gardelegen and Steinhuder Meer Fault – 4th Interim Report. *Leibniz Universität Hannover, p. 29.*

Müller, K., Brandes, C., Winsemann, J. (2018b). Paleoseismic investigation of northern Germany – Aller Valley Fault – 5th Interim Report. *Leibniz Universität Hannover, p. 33.*

Müller, K., Brandes, C., Winsemann, J. (2018c). Paleoseismic investigation of northern Germany – Osning Thrust and Elbe Lineament – 6th Interim Report. *Leibniz Universität Hannover*, p. 28.

Müller, K., Polom, U., Winsemann, J., Steffen, H., Tsukamoto, S., Günther, T., Igel, J., Spies, T., Lege, T., Frechen, M., Franzke, H.-J., Brandes, C. (in press a). Structural style and neotectonic activity along the Harz Boundary Fault, northern Germany: A multimethod approach integrating geophysics, outcrop data and numerical simulations. *International Journal of Earth Sciences*.

Müller, K., Winsemann, J., Pisarska-Jamroży, M., Lege, T., Spies T., Brandes, C. (in press b). The challenge to distinguish soft-sediment deformation structures (SSDS) formed by glaciotectionic, periglacial and seismic processes in a formerly glaciated area: a review and synthesis. *In: Steffen, H., Olesen, O., Sutinen, R. (Eds.), Glacially-Triggered Faulting. Cambridge University Press.*

Müller, K., Winsemann, J., Tanner, D.C., Lege, T., Spies T., Brandes, C. (in press c). Glacially-Induced Faults in Germany. *In: Steffen, H., Olesen, O., Sutinen, R. (Eds.), Glacially-Triggered Faulting. Cambridge University Press.*

Nichols, R.J., Sparks, R.S.J., Wilson, C.J.N. (1994). Experimental studies of fluidization of layered sediments and the formation of fluid escape structures. *Sedimentology*, 41, 233-253.

Nichols, G. (2007). Sedimentology and Stratigraphy. *Blackwell Publishing, Oxford*, p. 328.

Nocquet, J.M., Calais, E., Parsons, B. (2005). Geodetic constraints on glacial isostatic adjustment in Europe. *Geophysical Research Letters*, 32, L06308.

Obermeier, S.F., Jacobson, R.B., Smoot, J.P., Weems, R.E., Gohn, G.S., Monroe, J.E., Powars, D.S. (1990). Earthquake-induced liquefaction features in the coastal setting of South Carolina and in the fluvial setting of the New Madrid seismic zone. *US Geological Survey Professional Paper*, 1536, p. 27.

Obermeier, S.F. (1996). Use of liquefaction-induced features for paleoseismic analysis - an overview of how seismic liquefaction features can be distinguished from other features and how their regional distribution and properties of source sediment can be used to infer the location and strength of Holocene paleo-earthquakes. *Engineering Geology*, 44, 1-76.

Obermeier, S.F. (2009) Using liquefaction-induced and other soft-sediment features for paleoseismic analysis. *In: McCalpin J.P. (Ed.), Paleoseismology. International Geophysics Series, 95, Elsevier, Amsterdam*, pp. 497-564.

- Ogino, Y., Matsuoka, N. (2007).** Involutions resulting from annual freeze-thaw cycles: a laboratory simulation based on observations in northeastern Japan. *Permafrost and Periglacial Processes*, 18, 323-335.
- Oliveira, C.M.M., Hodgson, D.M., Flint, S.S. (2009).** Aseismic controls on in situ soft-sediment deformation processes and products in submarine slope deposits of the Karoo Basin, South Africa. *Sedimentology*, 56, 1201-1225.
- Otto, V. (2003).** Inversion-related features along the southeastern margin of the North German Basin (Elbe Fault System). *Tectonophysics*, 373, 107-123.
- Owen, G. (2003).** Load structures: gravity-driven sediment mobilization in the shallow subsurface. *Geological Society London Special Publications*, 216, 21-34.
- Owen, G., Moretti, M. (2008).** Determining the origin of soft-sediment deformation structures: a case study from Upper Carboniferous delta deposits in south-west Wales, UK. *Terra Nova*, 20, 237-245.
- Owen, G., Moretti, M. (2011).** Identifying triggers for liquefaction-induced soft-sediment deformation in sands. *Sedimentary Geology*, 235, 141-147.
- Pavlidis, S.B. (1989).** Looking for a definition of neotectonics. *Terra Nova*, 1, 233-235.
- Pedersen, S.A.S. (2014).** Architecture of Glaciotectonic Complexes. *Geosciences*, 4, 269-296.
- Perucca, L.P., Godoy, E., Pantano, A. (2014).** Late Pleistocene-Holocene earthquake-induced slumps and soft-sediment deformation structures in the Acequion River valley, Central Precordillera, Argentina. *Geologos*, 20, 147-156.
- Péwé, T.L. (1973).** Ice wedge casts and past permafrost distribution in North America. *Geoforum*, 4, 15-26.
- Phillips, E.R., Evans, D.J.A., Auton, C.A. (2002).** Polyphase deformation at an oscillating ice margin following the Loch Lomond re-advance, central Scotland, UK. *Sedimentary Geology*, 149, 157-182.
- Phillips, E.R., Lee, J.R., Burke, H. (2008).** Progressive proglacial to subglacial deformation and syntectonic sedimentation at the margins of the Mid-Pleistocene British Ice Sheet: evidence from north Norfolk, UK. *Quaternary Science Reviews*, 27, 1848-1871.

- Phillips, E.R., Merritt, J. (2008).** Evidence for multiphase water escape during rafting of shelly marine sediments at Clava, Inverness-shire, NE Scotland. *Quaternary Science Reviews*, 27, 988-1011.
- Picard, E., Wiegers, F. (1908).** Erläuterungen zu Blatt 3634 Bülstringen (Uthmöden), Geologische Karte von Preußen und benachbarten Bundesstaaten 1:25000. *Königliche Preußische Geologische Landesanstalt, Berlin*, p. 22.
- Piotrowski, J.A., Larsen, N.K., Junge, F.W. (2004).** Reflections on soft subglacial beds as a mosaic of deforming and stable spots. *Quaternary Science Reviews*, 23, 993-1000.
- Pisarska-Jamroży, M. (2013).** Varves and megavarves in the Eberswalde Valley (NE Germany) - A key for the interpretation of glaciolimnic processes. *Sedimentary Geology*, 291, 84-96.
- Pisarska-Jamroży, M., Weckwerth, P. (2013).** Soft-sediment deformation structures in a Pleistocene glaciolacustrine delta and their implications for the recognition of subenvironments in delta deposits. *Sedimentology*, 60, 637-665.
- Pisarska-Jamroży, M., Belzyt, S., Börner, A., Hoffmann, G., Hüneke, H., Kenzler, M., Obst, K., Rother, H., Van Loon, A.T. (2018).** Evidence from seismites for glacio-isostatically induced crustal faulting in front of an advancing land-ice mass (Rügen Island, SW Baltic Sea). *Tectonophysics*, 745, 338-348.
- Pisarska-Jamroży, M., Woźniak, P.P. (2019).** Debris flow and glacio isostatic-induced soft-sediment deformation structures in a Pleistocene glaciolacustrine fan: the southern Baltic Sea coast, Poland. *Geomorphology*, 326, 225-238.
- Prasad, S. (2000).** HF treatment for the isolation of fine grain quartz for luminescence dating. *Ancient TL*, 18, 15-17.
- Prescott, J.R., Hutton, J.T. (1994).** Cosmic ray contributions to dose rates for luminescence and ESR dating: large depths and long-term time variations. *Radiation measurements*, 23, 497-500.
- Rabbel, W., Förste, K., Schulz, A., Bittner, R., Röhl, J., Reichert, J.C. (1995).** A high-velocity layer in the lower crust of the North German Basin. *Terra Nova*, 7, 327-337.
- Radzinski, K.-H., Hoyningen-Huene, E., Kriebel, U., Schulze, G. (1962).** Erläuterungen zum Blatt 4536 Teutschenthal. Geologische Spezialkarte der Deutschen Demokratischen Republik 1:25000. *Zentrales Geologisches Institut, Halle*, p. 287.

Rappol, M., Stoltenberg, H.M. (1985). Compositional variability of Saalian till in the Netherlands and its origin. *Boreas*, 14, 33-50.

Rappsilber, I. (2003). Struktur und Entwicklung des nördlichen Saale-Beckens (Sachsen-Anhalt): Geophysik und Geologie. *Dissertation, Martin-Luther-Universität Halle-Wittenberg*, p. 118.

Rappsilber, I., Schwab, M. (2006). Tektonische Vorgeschichte der Halle Störung. In: *Halle Störung. Rappsilber, I. (Ed.), Mitteilungen zur Geologie und Bergwesen in Sachsen-Anhalt*, 10, 137-142.

Rees-Jones, J. (1995). Optical dating of young sediments using fine-grain quartz. *Ancient TL*, 13, 9-14.

Reicherter, K., Kaiser, A., Stackebrandt, W. (2005). The post-glacial landscape evolution of the North German Basin: morphology, neotectonics and crustal deformation. *International Journal of Earth Science*, 94, 1083-1093.

Reinecke, V. (2006). Untersuchung zur jungpleistozänen Reliefentwicklung und Morphodynamik im nördlichen Harzvorland. *Aachener Geographische Arbeiten*, 43, 27.

Reinecker, J., Heidbach, O., Müller, B. (2004). World Stress Map (2004 release). *World Wide Web address: www.world-stress-map.org. Accessed 2019.*

Reuter, G. (1975a). Manuskriptkarte zur geologischen Übersichtskartierung auf 2832 Dannenberg (Elbe) 1:25000, *Niedersächsisches Landesverwaltungsamt, Hannover.*

Reuter, G. (1975b). Manuskriptkarte zur geologischen Übersichtskartierung auf 2933 Gusborn 1:25000, *Niedersächsisches Landesverwaltungsamt, Hannover.*

Reuther, C.D. (2012). Einmessung und graphische Darstellung von Flächen und Linearen. In: *Reuther, C.D. (Ed.), Grundlagen der Tektonik, Springer, Heidelberg*, pp. 237-249.

Rhodes, E.J. (2011). Optically stimulated luminescence dating of sediments over the past 200,000 years. *Annual Review of Earth and Planetary Sciences*, 39, 461-488.

Rijsdijk, K.F., Owen, G., Warren, W.P., McCarroll, D., Van der Meer, J.J. (1999). Clastic dykes in over-consolidated tills: evidence for subglacial hydrofracturing at Killiney Bay, eastern Ireland. *Sedimentary Geology*, 129, 111-126.

Rijsdijk, K.F. (2001). Density-driven deformation structures in glacially consolidated diamicts: examples from Traeth Y Mwnt, Cardiganshire, Wales, UK. *Journal of Sedimentary Research*, 71, 122-135.

Rittenour, T.M. (2008). Luminescence dating of fluvial deposits: applications to geomorphic, palaeoseismic and archaeological research. *Boreas*, 37, 613-635.

Roberts, D.H., Long, A.J., Schnabel, C., Freeman, S., Simpson, M.J.R. (2008). The deglacial history of the southeast sector of the Greenland ice sheet during the Last Glacial Maximum. *Quaternary Science Reviews*, 27, 1505-1516.

Rodríguez, N., Cobbold, P.R., Løseth, H. (2009). Physical modeling of sand injectites. *Tectonophysics*, 474, 610-632.

Rodríguez-Pascua, M.A., Calvo, J.P., De Vicente, G., Gómez-Gras, D. (2000). Soft-sediment deformation structures interpreted as seismites in lacustrine sediments of the Prebetic Zone, SE Spain, and their potential use as indicators of earthquake magnitudes during the Late Miocene. *Sedimentary Geology*, 135, 117-135.

Rosenfeld, U. (1983). Beobachtungen und Gedanken zur Osningtektonik. *Neues Jahrbuch für Geologie und Paläontologie*, 166, 72-95.

Roskosch, J., Tsukamoto, S., Meinsen, J., Frechen, M., Winsemann, J. (2012). Luminescence dating of an Upper Pleistocene alluvial fan and aeolian sand-sheet complex: The Senne in the Münsterland Embayment, NW Germany. *Quaternary Geochronology*, 10, 94-101.

Roskosch, J., Winsemann, J., Polom, U., Brandes, C., Tsukamoto, S., Weitkamp, A., Bartholomäus, W.A., Henningsen, D., Frechen, M. (2015). Luminescence dating of ice-marginal deposits in northern Germany: evidence for repeated glaciations during the Middle Pleistocene (MIS 12 to MIS 6). *Boreas*, 44, 103-126.

Ross, J.A., Peakall, J., Keevil, G.M. (2011). An integrated model of extrusive sand injectites in cohesionless sediments. *Sedimentology*, 58, 1693-1715.

Rossetti, D.D.F. (1999). Soft-sediment deformation structures in late Albian to Cenomanian deposits, São Luís Basin, northern Brazil: evidence for palaeoseismicity. *Sedimentology*, 46, 1065-1081.

Scheck, M., Bayer, U., Otto, V., Lamarche, J., Banka, D., Pharaoh, T. (2002). The Elbe Fault System in North Central Europe – a basement controlled zone of crustal weakness. *Tectonophysics*, 360, 281-299.

Scheck-Wenderoth, M., Lamarche, J. (2005). Crustal memory and basin evolution in the Central European Basin System - new insights from a 3D structural model. *Tectonophysics*, 397, 143-165.

Scholz, M. (1887a). Erläuterungen zu Blatt 3434 Gardelegen, Geologische Spezialkarte von Preussen und den Thüringischen Staaten 1:25000. *Königliche Preußische Geologische Landesanstalt, Berlin*, p. 31.

Scholz, M. (1887b). Erläuterungen zu Blatt 3435 Lindstedt (Uchtspringe), Geologische Spezialkarte von Preussen und den Thüringischen Staaten 1:25000. *Königliche Preußische Geologische Landesanstalt, Berlin*, p. 33.

Schröder, H., Fliegel, G., Dahlgrün, F., Beck, G. (1927). Geologische Karte von Preußen und benachbarten deutschen Ländern, 1:25000, Blatt 4131 Derenburg, *Preußische Geologische Landesanstalt, Berlin*.

Schröder, H., Behrend, F., Fulda, E. (1929a). Erläuterungen zu Blatt 4032 Schwanebeck, Geologische Karte von Preußen und benachbarten deutschen Ländern 1:250000. *Preußische Geologische Landesanstalt, Berlin*, p. 32.

Schröder, H., Behrend, F., Fulda, E. (1929b). Erläuterungen zu Blatt 4031 Dingelstedt am Huy, Geologische Karte von Preußen und benachbarten deutschen Ländern 1:25000. *Preußische Geologische Landesanstalt, Berlin*, p. 49.

Schröder, H., Behrend, F., Fulda, E. (1931). Erläuterungen zu Blatt 4029 Vienenburg, Geologische Karte von Preußen und benachbarten Ländern 1:25000. *Königliche Preußische Geologische Landesanstalt, Berlin*, p. 104.

Schwab, U., Herold, U., Rappsilber, I., Thomae, M. (2006). Geologischer Überblick zur Halle Störung. In: *Rappsilber, I. (Ed.), Halle Störung. Mitteilung zu Geologie und Bergwesen in Sachsen-Anhalt*, 10, 9-12.

Schwan, J., Van Loon, A.J., Steenbeek, R., Van der Gaauw, P. (1980). Intraformational clay diapirism and extrusion in Weichselian sediments at Ormehøj (Funen, Denmark). *Geologie en Mijnbouw*, 59, 241-250.

Seilacher, A. (1969). Fault-graded beds interpreted as seismites. *Sedimentology*, 13, 155-159.

Shipton, Z.K., Cowie, P.A. (2003). A conceptual model for the origin of fault damage zone structures in high-porosity sandstone. *Journal of Structural Geology*, 25, 333-344.

Siegert, L., Bärtling, R. (1909a). Erläuterungen zu Blatt 4638 Merseburg Ost (Leuna), Geologische Karten von Preußen und benachbarten Bundesstaaten 1:25000. *Königliche Preußische Geologische Landesanstalt, Berlin, p. 67.*

Siegert, L. (1909b). Erläuterungen zu Blatt 4738 Lützen (Bad Dürrenberg), Geologische Karte von Preußen und benachbarten Bundesstaaten 1:25000. *Königliche Preußische Geologische Landesanstalt, Berlin, p.75.*

Sirocko, F., Reicherter, K., Lehné, R., Hübscher, C., Winsemann, J., Stackebrandt, W. (2008). Glaciation, salt and the present landscape. In: *Littke, R., Bayer, U., Gajewski, D., Nelskamp, S. (Eds.), Dynamics of Complex Intracontinental Basins: The Central European Basin System. Springer Berlin, Heidelberg, pp. 97-124.*

Spooner, N.A. (1994). The anomalous fading of infrared-stimulated luminescence from feldspars. *Radiation Measurements, 23, 625-632.*

Stewart, I.S., Sauber, J., Rose, J. (2000). Glacio-seismotectonics: ice sheets, crustal deformation and seismicity. *Quaternary Science Reviews, 19, 1367-1389.*

Stille, H. (1924). Die Osning-Überschiebung. *Abhandlungen der preußischen geologischen Landesanstalt, 95, 32-56.*

Stille, H. (1953). Zur Geschichte der Osning-Forschung. *Geotektonische Forschung, 9, 1-6.*

Stoller, J. (1915). Erläuterungen zu Blatt 3227 Eschede, Geologische Karte von Preußen und benachbarten Bundesstaaten 1:25000. *Königliche Preußische Geologische Landesanstalt, Berlin, p. 54.*

Sullwood, H.H. (1959). Nomenclature of load deformation in turbidites. *Geological Society of America Bulletin, 70, 1247-1248.*

Suter, F., Martínez, J.I., Vélez, M.I. (2011). Holocene soft-sediment deformation of the Santa Fe - Sopetrán Basin, northern Colombian Andes: evidence for pre-Hispanic seismic activity? *Sedimentary Geology, 235, 188-199.*

Sykes, L.R. (1978). Intraplate seismicity, reactivation of preexisting zones of weakness, alkaline magmatism, and other tectonism postdating continental fragmentation: *Reviews of Geophysics and Space Physics, 16, pp. 621-688.*

Tanner, B., Meissner, R. (1996). Caledonian deformation upon southwest Baltica and its tectonic implications: alternatives and consequences. *Tectonics, 15, 803-312.*

- Tarnocai, C., Zoltai, S.C. (1978).** Earth Hummocks of the Canadian Arctic and Subarctic. *Arctic and Alpine Research*, 10, 581-594.
- Tesauro, M., Kaban, M.K., Cloetingh, S.A., Hardebol, N.J., Beekman, F. (2007).** 3D strength and gravity anomalies of the European lithosphere. *Earth and Planetary Science Letters*, 263, 56-73.
- Thomas, G.S.P., Chiverrell, R.C. (2007).** Structural and depositional evidence for repeated ice marginal oscillation along the eastern margin of the Late Devensian Irish Sea Ice Stream. *Quaternary Science Reviews*, 26, 2375-2405.
- Tsukamoto, S., Denby, P.M., Murray, A.S., Bøtter-Jensen, L. (2006).** Time-resolved luminescence from feldspars: new insight into fading. *Radiation Measurements*, 41, 790-795.
- Tsukamoto, S., Kondo, R., Lauer, T., Jain, M. (2017).** Pulsed IRSL: A stable and fast bleaching luminescence signal from feldspar for dating Quaternary sediments. *Quaternary Geochronology*, 41, 26-36.
- Uta, P. (2017).** Recent intraplate earthquakes in northwest Germany – Glacial isostatic adjustment and/or a consequence of hydrocarbon production? *Unpublished doctoral thesis. Leibniz Universität Hannover*, p.197.
- Uta, P., Brandes, C., Gestermann, N., Plenefisch, T., Kaiser, D., Bönnemann, C., Winsemann, J. (2018).** The re-evaluation of the 2004 Rotenburg MW 4.4 earthquake. *Geophysical Research Abstracts* Vol. 20, EGU2018-10627-1, 2018.
- Vandenberghe, J. (1988).** Cryoturbations. In: Clark, M.J. (Ed.), *Advances in Periglacial Geomorphology*, New York, Wiley, pp. 179-198.
- Vandenberghe, J. (2013).** Cryoturbation Structures. In: Elias, S.A. (Ed.), *The Encyclopedia of Quaternary Science*, 3, Elsevier, Amsterdam, pp. 430-435.
- Vandenberghe, J., Wang, X., Vandenberghe, D. (2016).** Very large cryoturbation structures of Last Permafrost Maximum age at the foot of the Qilian Mountains (NE Tibet Plateau, China). *Permafrost and Periglacial Processes*, 27, 138-143.
- Van Gijssel, K. (1987).** A lithostratigraphic and glaciotectonic reconstruction of the Lamstedt Moraine, Lower Saxony (FRG). In: Van der Meer, J.J.M. (Ed.), *Tills and Glaciotectonics*, Balkema, Rotterdam, pp. 145-156.
- Van Vliet-Lanoë, B., Magyar, I.A., Meilliez, F. (2004).** Distinguishing between tectonic and periglacial deformations of quaternary continental deposits in Europe. *Global and Planetary Change*, 43, 103-127.

Van der Wateren, F.M. (1981). Glacial tectonics at the Kwintelooijen sandpit, Rhenen, the Netherlands. *Mededelingen Rijks Geologische Dienst*, 35, 252-268.

Van der Wateren, F.M., Kluiving, S.J., Bartek, L.R. (2000). Kinematic indicators of subglacial shearing. In: *Maltman, A.J., Hubbard, B., Hambrey, M.J. (Eds.), Deformation of Glacial Materials. Geological Society London Special Publications*, 176, pp. 259-278.

Van Loon, A.J. (2009). Soft-sediment deformation structures in siliciclastic sediments: an overview. *Geologos*, 15, 3-55.

Van Loon, A.T., Pisarska-Jamroży, M. (2014). Sedimentological evidence of Pleistocene earthquakes in NW Poland induced by glacio-isostatic rebound. *Sedimentary Geology*, 300, 1-10.

Van Loon, A.T., Pisarska-Jamroży, M., Nartišs, M., Krievāns, M., Soms, J. (2016). Seismites resulting from high-frequency, high-magnitude earthquakes in Latvia caused by Late Glacial glacio-isostatic uplift. *Journal of Palaeogeography*, 5, 363-380.

Van Wees, J.D., Stephenson, R.A., Ziegler, P.A., Bayer, U., McCann, T., Dadlez, R., Gaupp, R., Narkiewicz, M., Bitzer, F., Scheck, M. (2000). On the origin of the southern Permian basin, central Europe. *Marine and Petroleum Geology*, 17, 43-59.

Vermilye, J.M., Scholz, C.H. (1998). The process zone: a microstructural view of fault growth. *Journal of Geophysical Research*, 103, 12223-12237.

Vittori, E., Labini, S.S., Serva, L. (1991). Palaeoseismology: review of the state-of-the-art. *Tectonophysics*, 193, 9-32.

von Eynatten, H., Voigt, T., Meier, A., Franzke, H.J., Gaupp, R. (2008). Provenance of the clastic Cretaceous Subhercynian Basin fill: constraints to exhumation of the Harz Mountains and the timing of inversion tectonics in the Central European Basin. *International Journal of Earth Science*, 97, 1315-1330.

von Raumer, J.F., Bussy, F., Schaltegger, U., Schulz, B., Stampfli, G.M. (2013). Pre-Mesozoic Alpine basements – Their place in the European Paleozoic framework. *Geological Society of America Bulletin*, 125, 89-108.

Vogt, J., Grünthal, G. (1994). Die Erdbebenfolge vom Herbst 1612 im Raum Bielefeld. *Geowissenschaften*, 12, 236-240.

Voigt, T., Wiese, F., von Eynatten, H., Franzke, H.J., Gaupp, R. (2006). Facies evolution of syntectonic Upper Cretaceous deposits in the Subhercynian Cretaceous

Basin and adjoining areas (Germany). *Zeitschrift der Deutschen Gesellschaft für Geowissenschaften*, 157, 203-244.

Voss, H.H., Bauer, G., Dahms, E., Gramann, F., Heine, H.W., Hofmeister, E., Irrlitz, W., Mayrhofer, H., Merkt, J., Scherler, P.C., Schneekloth, H., Tüxen, J. (1979). Erläuterungen zu Blatt 3522 Wunstorf, Geologische Karte von Niedersachsen 1:25000. *Niedersächsisches Landesamt für Bodenforschung, Hannover*, p. 102.

Voss, H.H., Fansa, M., Gramann, F., Hedemann, H.A., Irrlitz, W., Jaritz, W., Kosmahl, W., Plaumann, S., Roeschmann, G., Scherler, P.C., Schütte, H. (1982). Erläuterungen zu Blatt 3421 Husum, Geologische Karte von Niedersachsen 1:25000. *Niedersächsisches Landesamt für Bodenforschung, Hannover*, p.130.

Wansa, S., Radzinski, K.H., Berger, C., Blumenstengel, H., Friedel, C.H., Hartmann, K.J., Herold, U., Karpe, P., Kater, R., Müller, D.W., Rappsilber, I., Schroeter, A., Schumann, G., Sommerwerk, K., Thomae, M. (2004). Erläuterungen zu Blatt 4636 Müncheln, Geologische Karte von Sachsen-Anhalt 1:25000. *Landesamt für Geologie und Bergwesen Sachsen-Anhalt, Halle*, p. 143.

Washburn, A.L. (1980). Geocryology: a survey of periglacial processes and environments. *John Wiley and Sons, New York*, p. 406.

Wheeler, R.L., Etensohn, F.R., Rast, N., Brett, C.E. (2002). Distinguishing seismic from nonseismic soft-sediment structures: criteria from seismic hazard analysis. *Geological ociety of America, Special paper*, 359, 1-11.

Weise, O.R. (1983). Das Periglazial. Geomorphologie und Klima in gletscherfreien, kalten Regionen. *Gebrüder Bornstraeger, Berlin Stuttgart*, p.199.

Weissermel, W., Dahlgrün, F. (1926). Erläuterungen zu Blatt 4233 Ballenstedt, Geologische Karte von Preußen und benachbarten Ländern 1:25000. *Preußische Geologische Landesanstalt, Berlin*, p.78.

Weissermel, W., Picard, E., Quitzow, W., Kühn, B., Dammer, B. (1909). Erläuterungen zu Blatt 4438 Landsberg, Geologische Karte von Preußen und benachbarten Bundesstaaten 1:25000. *Königliche Preußische Geologische Landesanstalt, Berlin*, p.17.

Weissermel, W. (1901). Erläuterungen zu Blatt 2935 Schnackenburg, Geologische Karte von Preußen und den Thüringischen Staaten 1:25000. *Königliche Preußische Geologische Landesanstalt, Berlin*, p.19.

Wells, D.L., Coppersmith, K.J. (1994). New empirical relationships among magnitude, rupture length, rupture width, rupture area, and surface displacement. *Bulletin of the seismological Society of America*, 84, 974-1002.

Weymann, H.J. (2004). Die mittelpleistozäne Flußentwicklung im nord-östlichen Harzvorland. Petrographie, Terrassenstratigraphie. *Geologische Beiträge Hannover*, 6, 3-116.

Wieggers, F. (1914). Erläuterungen zu Blatt 3535 Dolle, Geologische Karte von Preußen und benachbarten Bundesstaaten 1:25000. *Berlin*, p. 27.

Williams, G.D., Powell, C.M., Cooper, M.A. (1989). Geometry and kinematics of inversion tectonics. In: Cooper, M.A., Williams, G.D. (Eds.), *Inversion Tectonics. Geological Society Special Publications*, 44, London, pp. 3-15.

Winsemann, J., Brandes, C., Polom, U., Weber, C. (2011). Depositional architecture and deformation pattern of Middle Pleistocene ice marginal deposits in north-western Germany: a synoptic overview. *E & G - Quaternary Science Journal*, 60, 212-235.

Winsemann, J., Lang, J., Roskosch, J., Polom, U., Böhner, U., Brandes, C., Glotzbach, C., Frechen, M. (2015). Terrace styles and timing of terrace formation in the Weser and Leine valleys, northern Germany: response of a fluvial system to climate change and glaciation. *Quaternary Science Reviews*, 123, 31-57.

Wintle, A.G. (1973). Anomalous fading of thermo-luminescence in mineral samples. *Nature*, 245, 143-144.

Wintle, A.G., Murray, A.S. (2006). A review of quartz optically stimulated luminescence characteristics and their relevance in single-aliquot regeneration dating protocols. *Radiation Measurements*, 41, 369-391.

Woltstedt, P. (1924). Die Störungszone des oberen Allertals. *Jahrbuch der Preußischen Geologischen Landesanstalt, Berlin*, pp. 89-97.

Woltstedt, P., Görz, G. (1929). Erläuterungen zu Blatt 3530 Wolfsburg, Geologische Karte von Preußen und benachbarten deutschen Ländern 1:25000. *Preußische Geologische Landesanstalt, Berlin*, p. 71.

Wrede, V. (1988). Der nördliche Harzrand - flache Abscherbahn oder wrench fault system. *Geologische Rundschau*, 77, 101-107.

Wrede, V. (2008). Nördliche Harzrandstörung: Diskussionsbeiträge zu Tiefenstruktur, Zeitlichkeit und Kinematik. *Zeitschrift der Deutschen Gesellschaft für Geowissenschaften*, 159, 293-316.

Wright, J.D. (2001). Paleo-oceanography: Cenozoic Climate – Oxygen Isotope Evidence. *In: Steele, J., Thorpe, S., Turekian, K. (Eds.), Encyclopedia of Ocean Sciences, Academic Press, pp. 415-426.*